

UNIVERSITY OF CALIFORNIA

Santa Barbara

High Resolution Laser Spectroscopy and Nanoscale Proximal Probe Desorption of
Historically Significant Molecules

A dissertation submitted in partial satisfaction of the
requirements for the degree Doctor of Philosophy
in Chemistry

by

Shawn Christopher Owens

Committee in charge:

Professor Mattanjah de Vries, Chair

Professor Michael Bowers

Professor Steve Buratto

Professor Trevor Hayton

June 2015

The dissertation of Shawn Christopher Owens is approved.

Michael Bowers

Steve Buratto

Trevor Hayton

Mattanjah de Vries, Committee Chair

June 2015

High Resolution Laser Spectroscopy and Nanoscale Proximal Probe Desorption of
Historically Significant Molecules

Copyright © 2015

by

Shawn Christopher Owens

VITA OF SHAWN CHRISTOPHER OWENS

June 2015

SKILLS AND TECHNIQUES

- Extensive knowledge of materials characterization via laser ablation/desorption, supersonic jet-cooled, resonant 2-photon ionization (R2PI) spectroscopy and time-of-flight mass spectrometry (TOF-MS) techniques.
- Proficiency in several additional analytical chemistry techniques (including UV-Vis, GC-MS, FTIR, Raman, SEM/EDS, MALDI and optical microscopy).
- Operated and resolved technical issues via electrical schematics on several laser systems (high power flash lamp Nd:YAG, deep UV excimer, tunable UV-Vis dye laser).
- Integrated LabVIEW software with new hardware and software applications, in addition to design and fabrication of hardware via CAD programs.
- Understanding and daily use of high vacuum systems, including diffusion pumps, turbo-molecular pumps, leak detection protocol and system design.
- Experience with relevant laser alignment tools, oscilloscopes, delay/pulse generators, digitizers, multi-meter, spatial filters, reflective objectives and other relevant optics.

RESEARCH EXPERIENCE

University of California Santa Barbara

Santa Barbara, CA

Doctoral Researcher with Dr. Mattanjah de Vries

2009 – 2015

Initiated projects to explore the R2PI spectroscopy of dyes, pigments, and other molecular markers- leading to the successful identification of trace amounts of chocolate residues in 1200 year-old pottery sherds.

Collaborated with two co-authors to develop a method for nanoscale desorption of material via heated atomic force microscope (AFM) tip, and subsequent chemical analysis with high resolution laser spectroscopy. Work led to the successful commercialization of AFM induced desorption instrument.

Managed a team of 3 lab assistants to modify a microscope laser mass spectrometer to incorporate highly accurate manual translation within a high vacuum chamber, including integration with LabVIEW software. This enabled surface analytical techniques and trace chemical detection while maintaining high spatial resolution.

Getty Conservation Institute at the Getty Center

Los Angeles, CA

Visiting Scientist with Dr. Catherine Schmidt Patterson

June 2013

Applied several analytical techniques (SEM-EDS, ATR-FTIR, visible and UV microscopy, Raman spectroscopy) to investigate structurally similar organic molecules in microscopic paint cross sections.

Santa Clara University Santa Clara, CA
Undergraduate Research Assistant with Dr. Michael Carrasco 2007-2009
Synthesized and studied the site-specific attachment of organic molecules to peptides, and how these alterations changed their function and structure, including analysis using GC-MS and NMR.

EDUCATION

University of California, Santa Barbara Santa Barbara, CA
Ph.D. Analytical/Physical Chemistry Expected April 2015
Santa Clara University Santa Clara, CA
B.A. Chemistry 2006-2009
University of Hawaii-Manoa Honolulu, HI
Chemistry 2004-2006

TEACHING EXPERIENCE

University of California Santa Barbara Santa Barbara, CA
Lead Teaching Assistant: General, Analytical and Photochemistry 2009-2010
Selected as Lead TA, overseeing and mentoring 30 graduate students.
Mentor 2013-2014
California Alliance for Minority Participation
Provided one-on-one training and support on a research projects for several undergraduate students.

PUBLICATIONS

S. Owens, M.R. Ligare, L.E. Gulian, F.M. Siouri, P.A. Mazzella, J.A. Berenbeim, J Leandro, S Tyson-Smith, A Ford, G Wilson, M.S. de Vries. New Method for the Direct Analysis of Xanthine Stimulants in Archaeological Vessels. *In Preparation*.
S. Owens, J.A. Berenbeim, C Schmidt Patterson, E.P. Dillon and M.S. de Vries. Sub-micron proximal probe thermal desorption and laser mass spectrometry on painting cross-sections. *Analytical Methods* **2014**; 6: 8940-8945.
J Sue, N Michaelian, **S. Owens**, S.T. Dashner, A.J. Wong, A.E. Barron, M.R. Carrasco. Chemoselective and Microwave-Assisted Synthesis of Glycopeptoids. *Organic Letters* **2009**; 11(22): 5210-5213.

ABSTRACT

Nanoscale Organic Molecule Analysis Using Proximal Probe Desorption and High-Resolution Laser Spectroscopy

by

Shawn Christopher Owens

A system combining laser desorption, jet-cooling, resonant 2-photon ionization (R2PI) spectroscopy, and time-of-flight mass spectrometry (TOF-MS) generates exceptionally well resolved vibronic spectroscopy and fragment free mass spectrometry for molecules within a complex matrix. Following laser desorption, gas-phase molecules are entrained in a supersonic molecular beam of argon. This causes extremely efficient jet-cooling of the internal degrees of freedom within the molecules and makes it possible to perform high resolution spectroscopy. The cold molecule is resonantly excited to the first electronic excited state by a tunable dye laser, and subsequently ionized by another photon before being detected in the TOF-MS. The result is the ability to selectively ionize a single target molecule within an extremely complex matrix.

The advantages of R2PI spectroscopy have been extended to include nanoscale proximal probe thermal desorption, allowing detection of organic paint pigments *in situ* within microscopic paint cross sections. These organic paints are often present as part of complex mixtures within thin layers, well below the spatial resolution of many instruments. We also report the first high resolution spectroscopy of chromophores within madder dye, an historically significant organic colorant, allowing for the unambiguous identification of the molecule within the intrinsically complex nature of ancient paintings.

Additionally, pottery sherds from Maya vessels (600-900 CE) and Mississippian vessels (1100-1200 CE) were examined for three molecular markers (theobromine, theophylline and caffeine) using R2PI spectroscopic techniques. The data obtained supports the existence of a previously unknown trade network between Mesoamerican and North American civilizations.

TABLE OF CONTENTS

Chapter I. Introduction.....	1
Chapter II. Instrumental Methods.....	3
A. Molecular Beam Machine.....	3
B. Microscope Mass Spectrometer	20
Chapter III. At the Interface of Chemistry and Art	28
A. High Spectral and Spatial Resolution	28
B. Ancient Organic Dye R2PI Spectroscopy.....	36
C. Modern Synthetic Organic Pigment R2PI Spectroscopy	42
D. Non-Resonant 2-Photon Ionization Mass Spectrometry	43
Chapter IV. Nanometer Scale Thermal Desorption.....	53
A. Chemical Analysis with High Spatial Resolution.....	53
B. Experimental	54
C. Results and Discussion.....	62
D. Summary	67
Chapter V. Organic Residue Analysis in Ancient Pottery.....	72
A. Chemistry, Archaeology, Archaeometry and Anthropology	72
B. El Pilar Pottery	82
C. Illinois River Sherds.....	91
B. Summary	92

Chapter I. Introduction

Works of artistic, historic and cultural significance are created of an immense collection of materials and can include a variety of both inorganic (e.g. ceramic, stone, glass, pigments, minerals, or metal) and organic (e.g. wood, paper, canvas, organic colorants, glues, waxes, oils, varnishes, polymers, or fibers) components, often within a single complex object. The effective preservation of works of art requires a fundamental understanding of the composition, and interactions between all the materials from which they are fabricated in order to help predict their behavior over long periods of time, responses to environmental stresses, and compatibility with current conservation treatment methods. Scientific research into materials and techniques additionally can assist archaeologists, anthropologists and art historians in their investigations into the relationships between an object and the historical and cultural environments in which it was created. An understanding of works of art at a molecular and microstructural level can elucidate historic geological sources, manufacturing processes and shed light on new trade routes. While a wealth of information may be gleaned from detailed analysis of cultural heritage materials, the complexity of those materials has proven challenging.

The following studies outline a new method which has been developed that is particularly well suited for the analysis of these material classes with high spatial and molecular specificity, through the combination of nanoscale atomic force microscopy (AFM) proximal probe thermal desorption and jet-cooled laser spectroscopy. This high-resolution spectroscopy affords highly resolved and unique vibronic spectra, allowing for the discrimination of structurally similar molecules. The new combination allows for AFM thermal desorption of organic pigments within microscopic paint cross-sections, followed by

analysis with laser spectroscopy. Importantly, it maintains the high molecular specificity required to unambiguously identify any molecule of interest within even highly complex mixtures. Additionally, the method has been extended to investigate trace beverage residues within ancient pottery sherds, possibly revealing evidence for a previously unknown trade network.

Chapter II. Instrumental Methods

The defining feature of the de Vries research laboratory is the ability to perform high resolution spectroscopy on organic molecules using an instrument that is colloquially known as the ‘beam machine’. Each of the experiments described in this dissertation were accomplished in this instrument using a unique combination of mass spectrometry and resonant 2 photon ionization (R2PI) spectroscopy techniques, which allows for isomer specific optical detection of mass selected molecules.

A. Molecular Beam Machine

A schematic for the beam machine can be seen in Figure 1. The instrument consists of (1) laser desorption, (2) supersonic jet-cooling (3) photo-ionization and (4) mass detection in time-of-flight mass spectrometer. Each component of these experiments serves a vital role in providing highly resolved spectra, and will be described in detail.

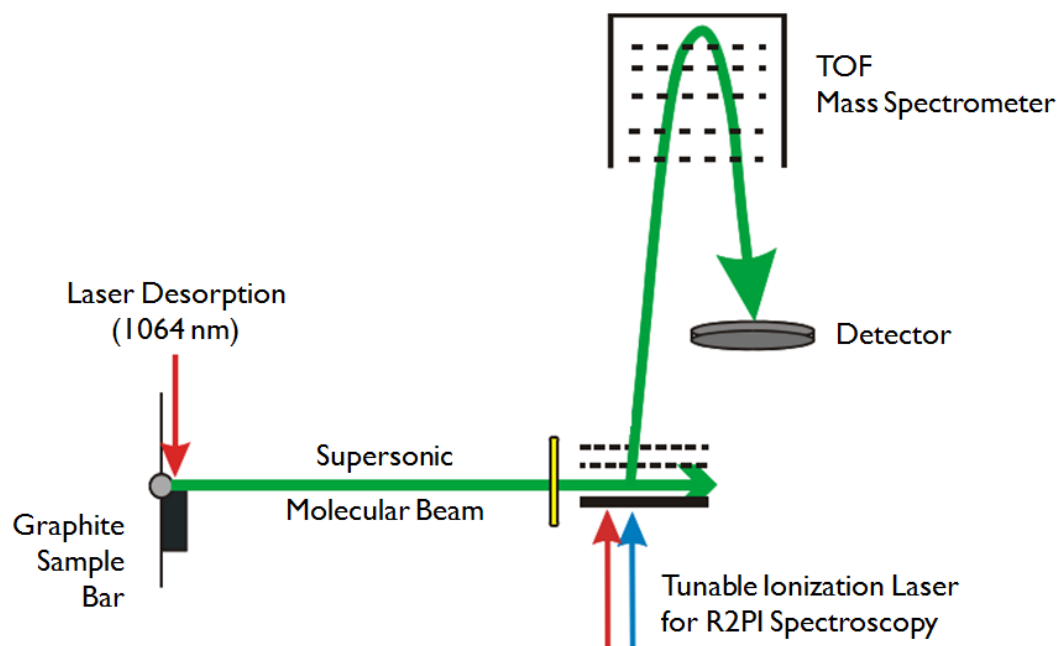


Figure 1: The ‘beam machine’ instrument schematic

The vacuum chamber housing the source of the mass spectrometer was maintained at 2×10^{-5} torr by a diffusion pump (Edwards Diffstak 250, 2000 L/s), and the time-of-flight region was held around 2×10^{-6} torr (Diffstak 100, 280 L/s) while running experiments.

A.1. Laser Desorption

All experiments conducted in the beam machine are done in the gas-phase, and therefore require a method for obtaining gas-phase neutral molecules from what are exclusively solid samples. There are a number of approaches to this, and much depends on the samples in questions- heating for example, is a simple and effective method for vaporizing volatile and thermally robust molecules. Unfortunately, many organic molecules with high molecular weights tend to be nonvolatile or thermally fragile and so require a different approach.

The first experiments using laser desorption were performed in the 1960s by Honig and Woolston, but it wasn't until the late 1970s that Posthumus et al. pioneered the method to induce desorption of large non-volatile organic biomolecules with a laser.^{1,2} Posthumus exposed a sample to a sub-microsecond laser pulse, and subsequently detected the cations produced with masses up to 1228 amu.³ Approximately a decade later, Hillenkamp and Karas used UV laser to desorb organic molecules as large as 10,000 amu.⁴ Perhaps the most notable achievement in laser desorption was the development of matrix assisted laser desorption ionization (MALDI) and electrospray ionization (ESI) by John Fenn and Koichi Tanaka, who were consequently awarded the 2002 Nobel Prize in chemistry for their work.⁵ The ability of laser desorption to produce fragment free, neutral gas-phase molecules has been heavily researched- with a commonly cited ratio of post desorption neutrals to ions on the order of 10,000:1.⁶⁻⁸

The mechanism of laser desorption is complicated by numerous measures, and in many respects is not clearly defined. Desorption initiated by IR lasers can in fact be described by relatively simple thermal models, where ion signal is highly correlated with surface temperatures from the laser pulse.⁹⁻¹¹ If the heating rate is sufficiently fast (i.e. faster than the time required than that of a vibrational excitation that could lead to thermal fragmentation), then it is possible to laser desorb thermally labile organic compounds that are unattainable with other methods.¹²⁻¹⁴ The heating rates necessary are on the order of 10^{11} K/s, or a 1000 K increase in a typical laser pulse length of 10 ns. It is assumed that the substrate absorbs the laser energy rather than the molecule and the bond to the surface that restricts the flow of energy into the molecule.¹⁵ Due to the high heating rates existing, desorption with relatively little internal energy will be preferred over a surface reaction.¹⁶ This is in contrast to UV laser desorption (e.g. 266 nm), which relies more heavily on parameters including wavelength, substrate, power density, pulse duration and sample preparation. Each of these can independently alter the ion signal, which likely suggests more than one possible mechanism for laser desorption.¹⁷

The substrate chosen as the matrix for desorption of each target sample is also important in determining the efficiency of laser desorption. The substrate containing our sample is normally graphite, chosen specifically to absorb the majority of the energy from the laser. Being a porous substrate, it has the added benefit of self-replenishing sample material via diffusion through the graphite between laser shots.¹⁸ This is particularly useful for molecules with high vapor pressures, as they are more mobile within the matrix and will diffuse particularly fast. Gold-plated copper sample bars are also used, primarily when analyzing liquid extraction samples.

All experiments described herein use a Continuum Minilite Nd:YAG operating at either its fundamental of 1064 nm, or 266 nm provided by its 4th harmonic. As discussed, laser desorption involves mainly the heating of the substrate rather than the adsorbate. It is therefore typical to match the desorption wavelength with the characteristics of the substrate, while also avoiding any possible overlap with the absorption spectrum of the adsorbate.¹⁹ Normally, 1064 nm is used with graphite substrates, and gold performs best with 266 nm. Sample bars measure 50 x 3.2 x 6.4 mm. An attenuator is used to reduce the intensity of the laser to appropriate levels based on sample and substrate characteristics, typically 20-150 μ J. The desorption beam is focused into a vertical slit by a lens, in order to maximize the spread of the beam on the graphite sample bar. The size of the beam on the sample bar is approximately 3 x 0.5 mm. The sample bar is translated with a motor to expose fresh sample between shots.

A.2. Supersonic Jet-Cooling

The majority of spectroscopy done on large organic molecules in the gas-phase is limited by broad, featurless spectra that often have limited value due mostly to the high density of states present in these systems. Solution-phase studies are equally challenging, as they are severely hindered by solvent-solute interactions, causing similarly featurless spectra. Further refining the ability to study large organic molecules required decreasing the amount of fragmentation seen in the desorption step, as well as lowering the number of rotational and vibrational states that are populated in the molecules of interest, prior to performing the spectroscopic studies. This was first accomplished by coupling laser desorption with supersonic jet-cooling, and was initially pioneered by Smalley, Warton, and Levy - it allowed highly resolved spectroscopy on aromatic molecules.²⁰

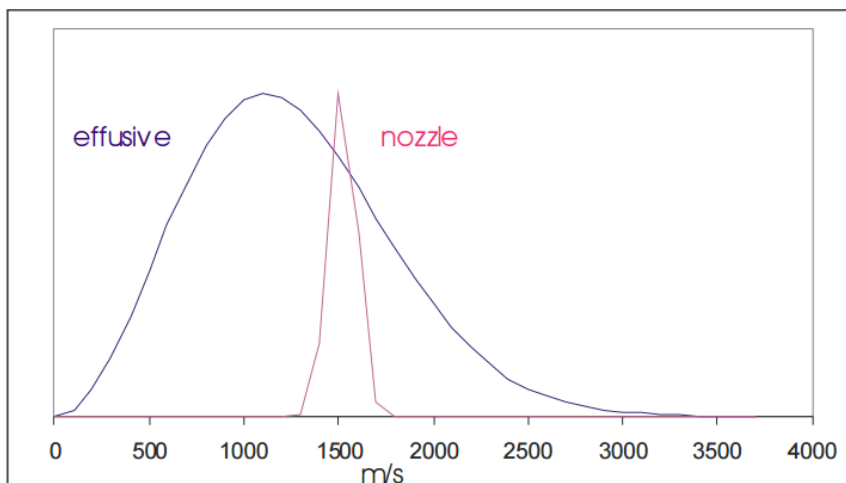


Figure 2: Velocity distribution in both effusive and pulsed nozzle.

By allowing a gas at relatively high pressure (6×10^3 torr) to expand through a small orifice into an area of low pressure (2×10^{-5} torr), a molecular beam is produced moving at supersonic velocities. The geometry of the instrument is designed in a way that allows for the desorption process to occur in the low pressure area, right outside of the valve opening the orifice (i.e. the valve is opened at a rate of 10 Hz). The laser desorbed molecules are entrained within this pulsed jet expansion, and their internal energy is transferred to the carrier gas through numerous collisions with the carrier gas (argon) in the molecular beam. The width of the velocity distribution of the molecular beam (see Figure 2, which compares an effusive beam with a molecular beam) is a direct measure of the translational temperature of the gas, and can be as low as 1 K in these experiments.²¹ Any of the molecules that have become entrained in this molecular beam will have energies consistent with those of the beam. In addition, even if a non-resonant ionization technique is used on these cooled molecules, it will still have the advantage of resulting in much less fragmentation following ionization.²²

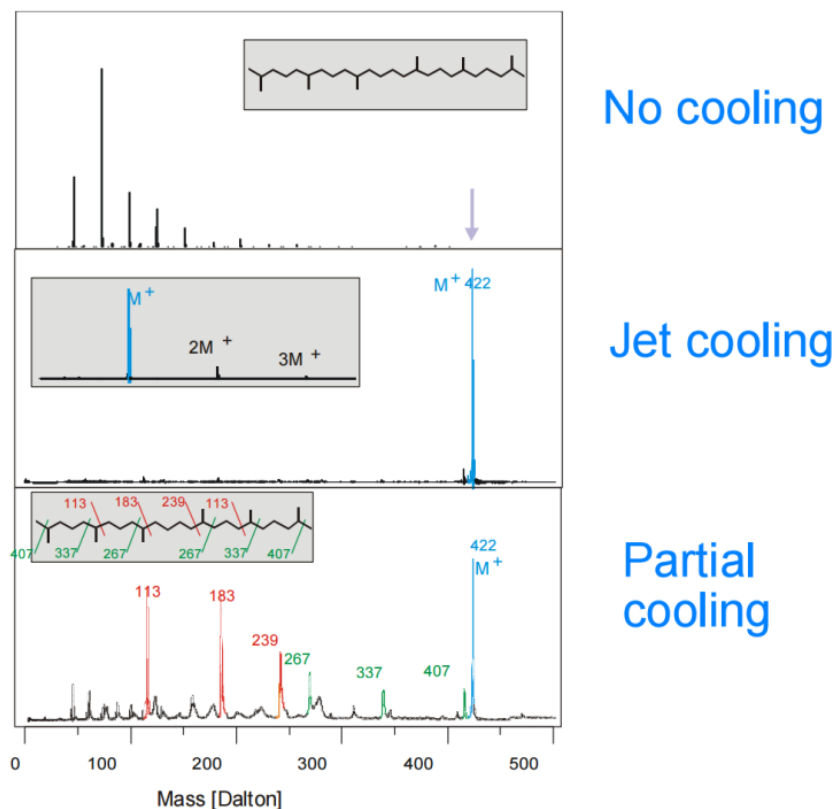


Figure 3 : Comparison of no jet-cooling, full jet-cooling, and partial jet-cooling.

The result of this cooling is a large reduction of the number of populated rotational and vibration modes within the molecules, and a large simplification of the spectra produced. Rotational temperatures as low as 5-10 K (estimated by the shape of the rotational contour) and 15 K vibrational temperatures (estimated by probing the ions formed from a jet-cooled, but vibrationally excited molecule) can be achieved with this method.¹⁸ The rate of energy transfer for vibrational modes is much smaller than that of rotation, due to the fact that the spacing of these modes is much larger than those of rotational modes and will therefore populate only the lowest energy level in comparison to the many rotational levels populated.¹⁸ This translates to spectra that no longer have the congestion produced by overlapping modes seen in room temperature and solution phase spectroscopy. Figure 3 shows the contrast of cooled and non-cooled methods.

A fraction of the entrained molecules and cooled molecules then pass through a 1 x 4 mm slit skimmer and into a differentially pumped ion source, prior to being intersected with ionization lasers 9.4 cm away from the nozzle. The beam is principally free of collisions at this point, and high resolution spectroscopic studies with very little fragmentation can be carried out on the molecules. Meijer et al. have explored the characteristics to optimize cooling and efficiency, and have obtained a detection efficiency of 10^{-6} .^{18, 23} It is in the collision free region that the molecular beam is probed with one or more lasers, and ions which are mass and wavelength selected can be detected.

The opening diameter of the nozzle is 250 μM , and is controlled by an ACPV2 pulsed supersonic piezovalve, opening at rate of 10 Hz.

A.3. Photoionization

Photoionization is the product of the collision between a photon and a molecule, resulting in the creation of an ion and an ejected photoelectron. Either one photon can be used to cross the ionization potential (IP), or several photons can be combined to cross this threshold. For instance, when a molecule absorbs an adequate amount of energy, a transition can occur from the ground state to an electronic excited state, and then can subsequently be ionized with another photon. Figure 4 shows a schematic representation of the photoionization processes that will be described here.

Single Photon Ionization

Single photon ionization requires the use of a photon source with sufficient energy to reach the IP of the target step in one step. Most aromatic compounds of interest to the de Vries Lab have IP's of around 7-8eV and so are accessible only using vacuum UV photon sources.²⁴ Using energies this close to the IP allows for a nearly soft ionization process, as

most of the excess energy is ejected with the photoelectron.²⁴ Although more selective methods of mass spectrometry is often desired, the use of single photon ionization had advantages of being easy to use, lacks the necessity for any fine tuning to spectral features, and most importantly there is no need for any previous spectral knowledge of the molecule in question.²⁵ Additionally, one photon ionization cross sections are much more consistent between organic molecules, allowing for much more quantitative analytical studies.^{26, 27}

Non-Resonant Two-Photon Ionization

Due to the difficulty of producing lasers with high enough energies for single photon ionization, the use of non-resonant multi-photon techniques was employed in many experiments. This method requires a molecule that has an intermediate electronic state to absorb the first photon, and must be stable enough to be ionized by a second photon.

Resonant Two-Photon Ionization (R2PI)

Perhaps the most selective method of ionization is R2PI, with the additional advantage of being several orders of magnitude more efficient than non-resonant ionization techniques. As discussed, the typical IP of an aromatic molecule is on the order of 8-9 eV. This threshold can be attained by combining two photons from an UV or visible light source, with the first photon exciting an electron from the ground state to the first electronic excited state and the second photon reaching the IP. The transition caused by the first photon occurs between two singlet states, and is so called the $S_0 \longrightarrow S_1$ transition. The lowest energy transition is referred to as the “origin”, and is a pure electronic transition from the ground state to the ground state of the first electronic excited state. Bands seen above the origin are attributed to transitions from the ground state into vibrational levels within the electronic excited state. These transitions are known as a vibronic (i.e. vibrational-

electronic) transitions, and are highly unique to structural, tautomeric and even conformational isomers.²⁴ Due mostly to the laser desorption and jet cooling of our gas-phase neutral molecules, these vibronic bands are often very well resolved and further details about the vibrational transitions can also be elucidated.

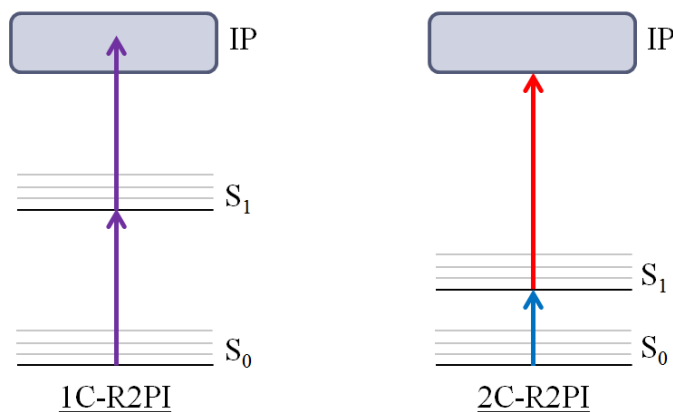


Figure 4: Schematic of ionization process for one color R2PI (1C-R2PI) and two color R2PI (2C-R2PI)

Often times the origin of aromatic molecules lies at or just below the half the IP, allowing for the photons associated with both the excitation and ionization steps to originate from the same laser. These experiments, referred to as 1-color R2PI (1C-R2PI), do not require the energy output for the ionization step to be resonant since any excess energy will be removed via the ejection of the photoelectron. It is common though, for the origin of these molecules to be much higher in energy than the halfway point to the IP. This requires separate lasers for excitation and ionization. Although these experiments are markedly more challenging since it demands two lasers overlapping both spatially and temporally, 2-color R2PI (2C-R2PI) has one distinct advantage: it allows for the fine optimization of the second photon, an advantage due to ionization efficiency being greatest at just above the IP.^{24, 28}

Another advantage of 2C-R2PI is the fact that the Frank-Condon region expands after the first absorption of a photon, $h\nu_1 + h\nu_2$ can in fact be less than the vertical ionization energy of the molecule in question. It can therefore be easy to saturate the excitation step in order to ionize the molecule with 1C-R2PI, whereas 2C-R2PI allows for laser flux to be optimized for both excitation and ionization. Figure 5 illustrates the advantages of 2C-R2PI.

R2PI spectroscopy was accomplished using the output of a frequency doubled (532 nm) or frequency tripled (355 nm) Nd:YAG laser (Quanta-Ray DCR 2A) to pump a tunable dye laser (Lumonics SpectrumMaster HD-500, linewidth 0.03cm^{-1}). This output was also, when necessary, frequency doubled using either monopotassium phosphate (KDP) or beta barium borate (BBO) crystals (linewidth 0.015cm^{-1}). The overall optical range of this system is 330 – 750 nm, with a typical energy output of around 0.75-1 mJ/pulse.

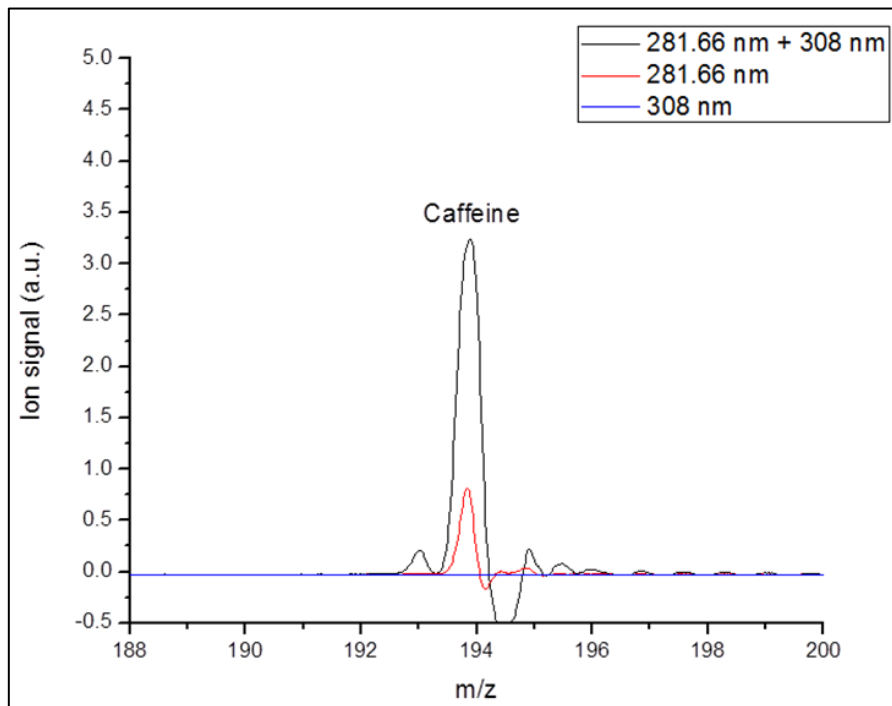


Figure 5: Comparison of mass spectra obtained from 1C-R2PI and 2C-R2PI

A.5. Time-of-Flight Mass Spectrometry

Perhaps the most elegantly simple method of analytical mass determination is the time-of-flight mass spectrometer (TOF-MS), as it is (1) relatively cheap, (2) fast, providing spectra in several microseconds and (3) has a mass range extending > 1 MDa.²⁹ It operates by accelerating a group of ions to a detector by imparting the same kinetic energy on each of the ions.³⁰ The TOF-MS was first developed in the late 1940s, and further advanced by Wiley and McLaren in the 1950's. It has also experienced a huge resurgence in the last decade, primarily due to improvements and modifications such as pulsed and continuous ionization sources, MALDI, faster electronics as well as R2PI techniques.³¹⁻³⁴ The TOF-MS comprises four parts (1) ion source (2) the flight tube (3) the reflectron and (4) the detector.

Ion Source

The beam machine uses an ion source developed by Wiley and McLaren known as a double-field source, which consists of three planar electrodes existing in the ion source (i.e. area where ionization laser intersects with molecules). As seen in Figure 6, these electrodes create two accelerating regions with a positive charge, repelling any ion that is formed out of the source and into the flight tube.³¹

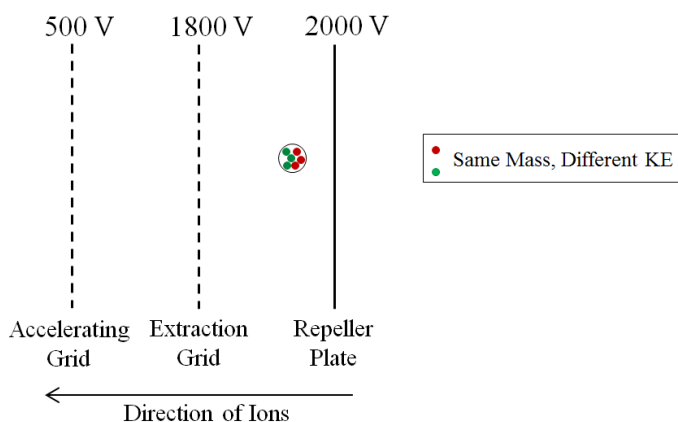


Figure 6: Ion source schematic, showing spatial distribution due to laser spot size

Flight Tube

The flight tube, or field-free region, is the site where mass separation occurs. If the kinetic energy of the ejected ions is assumed to be the same after the acceleration region of the ion source, they will have a kinetic energy of:

$$\frac{m\left(\frac{d}{t}\right)^2}{2} = zeE$$

$$m = \text{mass}$$

$$v = \text{distance/time} = \text{velocity}$$

$$z = \# \text{ charges on ion}$$

$$e = \text{charge of an electron}$$

$$E = \text{electric field}$$

Rearranging for t:

$$t = \sqrt{\frac{m}{z}} \left(d / \sqrt{2eE} \right)$$

Both d and E and e are constant throughout our experiments- showing us the flight time of the accelerated ions are proportional to the square root of mass over charge (i.e. heavier ions fly slower). To achieve a concurrent ejection of ions out of the ion source and into the drift tube requires the use of pulsed lasers. Note that a distribution both spatially and temporally occurs at the point of laser and molecule intersection- spatial spread as a result of laser spot creates ions with different potential energies, and temporal spread resulting from the width of the laser pulse. These are both factors that will affect the mass resolution of the TOF-MS, which is defined as:

$$\text{Resolution} = \frac{m}{\Delta m} = \frac{t}{\Delta t}$$

$$m = \frac{m}{z} \text{ value}$$

$\Delta m = \text{peak width at half maximum (FWHM)}$

$t = \text{arrival time of ion}$

$\Delta t = \text{FWHM of distribution of arrival times}$

This spatial and temporal distribution (see Figure 7) results in different initial velocities, and subsequently leads to ions of the same mass not reaching the detector at the same moment which greatly reduces the ability to distinguish between adjacent peaks. Mass resolution can therefore be improved by either increasing the time spent in the flight tube, or by extending the length of the flight tube. The beam machine has a flight tube measuring 150 cm.

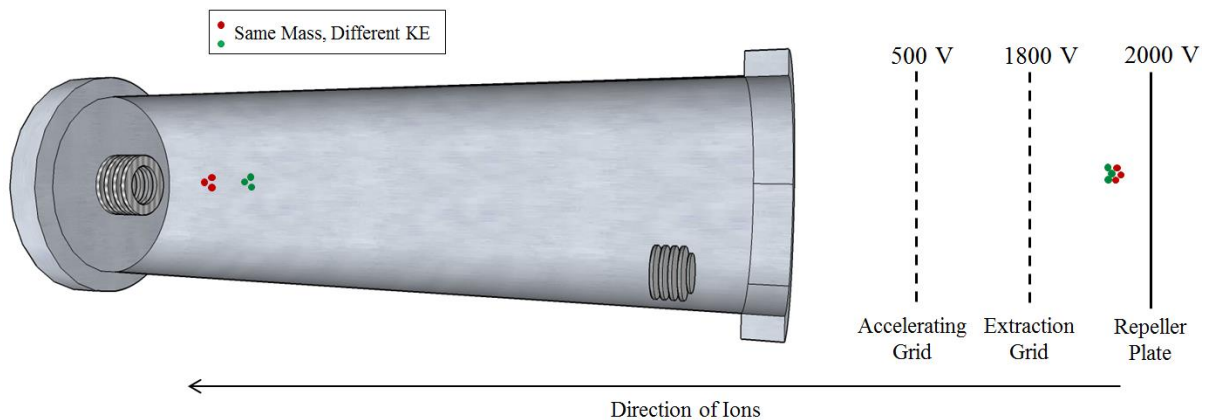


Figure 7: Schematic representation of the result of the spatial distribution. Ions on left have separated, regardless of the fact that they are the same mass

Reflectron

This early limitation of TOF-MS initiated by the spread of initial velocities of ions severely decreased the mass resolution of early systems. In the 1970s Mamyrin et al. corrected for the large velocity distribution by constructing an electrostatic ion mirror that ‘reflected’ the ions back towards the detector.³³ This also has the added benefit of extending the overall length of the instrument while maintaining a compact footprint. The correction in the velocity is the product of ions which have more energy (faster) penetrating deeper into the reflectron than do ions with comparatively less energy (slower), and therefore will take longer to re-emerge from the reflectron (Figure 8). This clever design does not actually lessen the energy spread of the ions, but rather corrects for the effect of the energy spread. The reflectron essentially allows the slower ions to catch up to the faster ones and reflectron voltages are optimized to achieve a focus at the point of the detector.³³ Typical mass resolution in the beam machine is 300 amu.

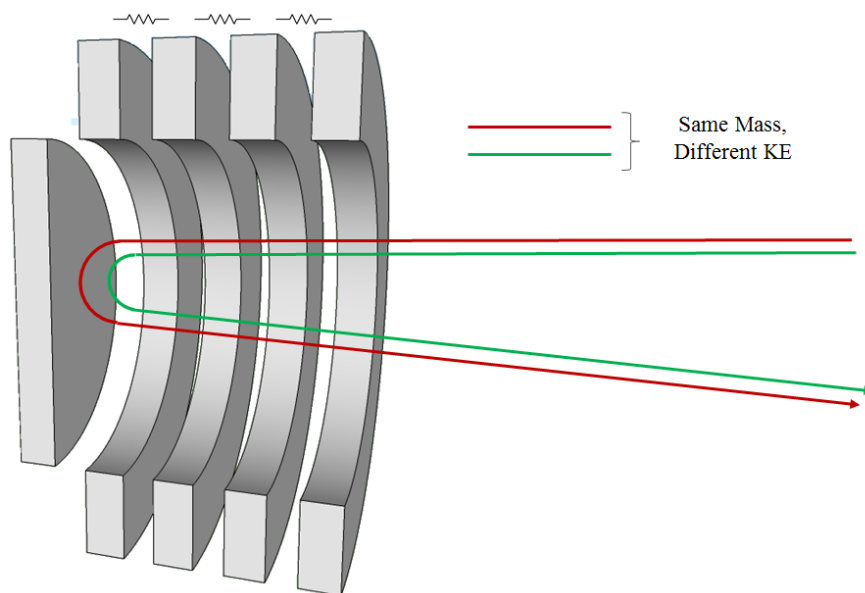


Figure 8: Reflectron, correcting for the KE distribution.

Detector

The ions slam into a 2” dual microchannel plate (MCP) detector (Figure 9), which is an array of 10^4 - 10^7 small electron multipliers oriented parallel to one another. Each channel is oriented at a small angle ($\approx 8^\circ$) relative to the incoming ions, allowing for a collision resulting in a large amplification of the ion signal (10^4 - 10^7) via electron cascades through the channels³⁵. The cascade then strikes an anode that measures the current, is further amplified by a fast pre-amplifier (10x) and then finally displayed on an oscilloscope or digitizer.

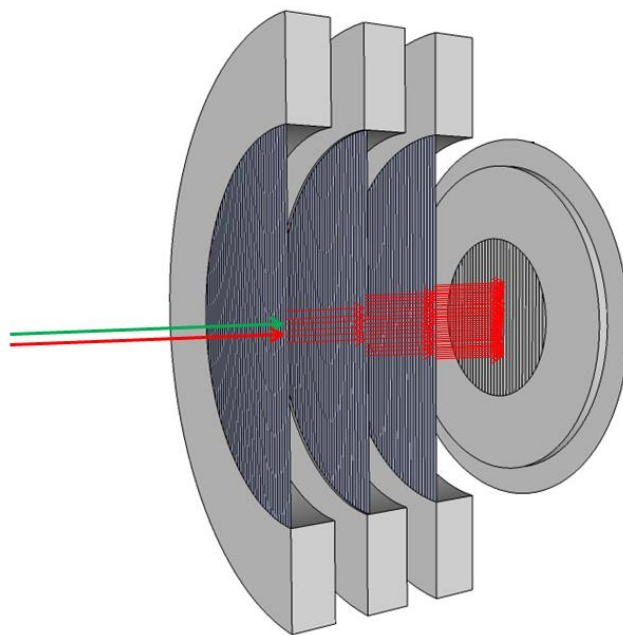


Figure 9: Microchannel plate detector, showing electron cascade as a result of ion impact.

A.6. Beam Machine Experimental Procedure

The graphite sample bar is roughed with 400 grit sandpaper, and sample is rubbed onto the abraded surface. The sample bar is mounted 0.5-1.0 mm below the axis of the molecular beam, within the vacuum chamber (height of sample bar can be adjusted). The desorption laser path is directed down onto the sample bar from above, and a lens is

commonly used to form a vertically focused desorption spot along the width of the sample bar and consequently increasing the amount of desorbed material. Timing of all aspects of the experiment are important and is synchronized by multi-channel digital delay generators.

Mass-Selected Spectroscopy

Mass-selected spectroscopy is performed with known standards. The wavelength of the excitation laser then is scanned while using a mass spectrometer to detect ions. A mass spectrum is produced for each laser pulse, and ‘mass gates’ can be set around peaks of interest which designates these peaks to be integrated (a total of 5 mass gates can be set). 10-30 mass spectra for each wavelength are taken, and the integrated mass gate values are averaged and plotted, and the resulting R2PI vibronic spectrum is shown on a PC. See below, in Figure 10.

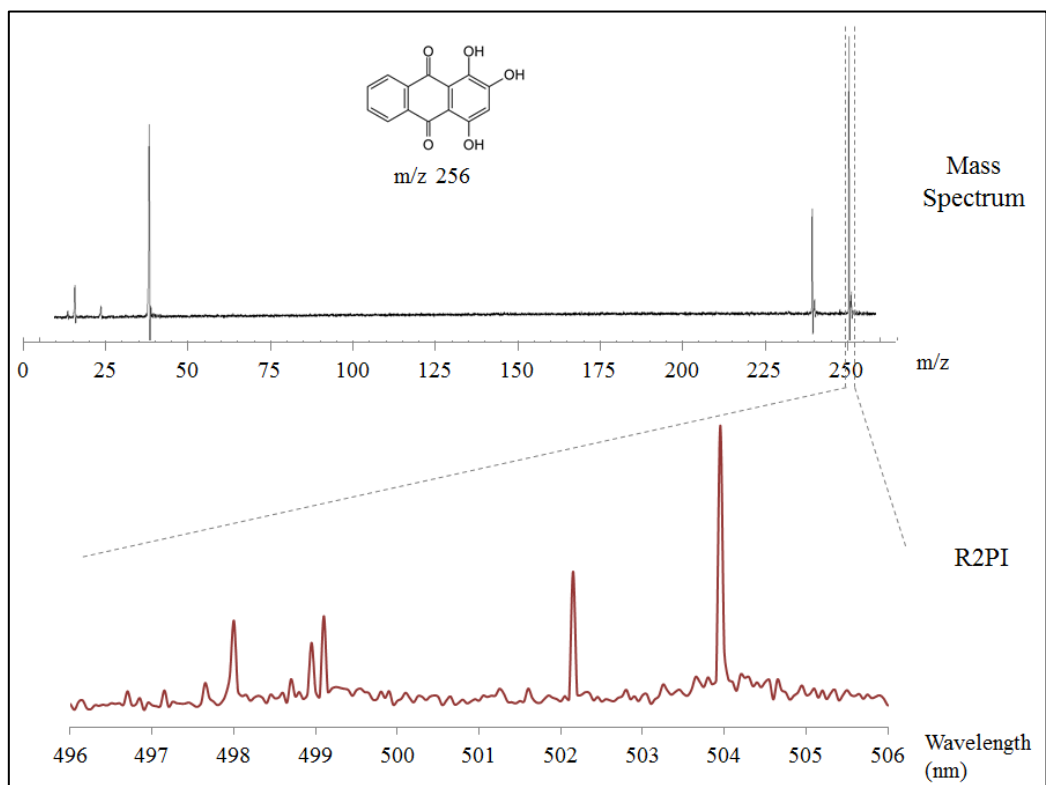


Figure 10: Mass-selected Spectroscopy.

Optically-Selected Mass Spectrometry

These experiments are often performed on ‘authentic’ analytical samples (e.g. pottery sherds), with the goal of identifying a specific molecule in the complex sample matrix. Therefore, the spectroscopy of the target molecule must be known. The ionization lasers are tuned to a strong resonance of the target molecule, and mass spectra are produced from the R2PI process. Due to the highly distinct nature of R2PI spectra- structural, tautomeric and conformational isomers can be distinguished from each other. See below in Figure 11.

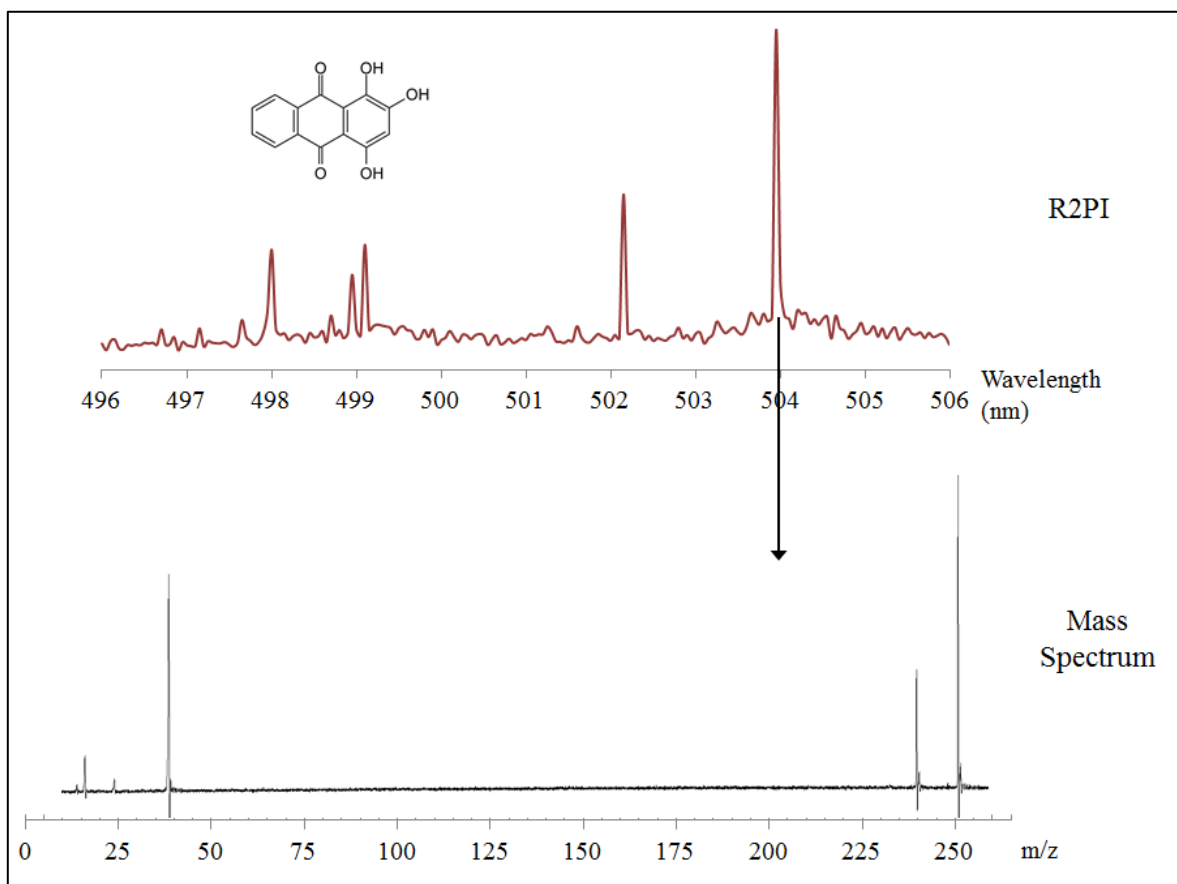


Figure 11: Optically-selected mass spectrometry.

B. Microscope Mass Spectrometer

While techniques for elemental analysis with high spatial resolution are common in several commercial instruments (e.g. SEM/EDS, SIMS), an analogous method for high spatial resolution detection of organic molecules is less common and much more difficult. One such method though, is a form of two-step microscope laser mass spectrometry as seen in Figure 12(μ MS). Samples are positioned underneath a microscope, and a desorption laser is focused onto the surface of the sample within the field of view of the microscope. Although there is no jet-cooling in the de Vries version of the μ MS, it does separate the desorption and ionization steps-allowing for independent optimization of each laser.³⁶⁻³⁸ Typically, a UV laser (e.g. excimer laser at 193 nm or frequency quadrupled Nd:YAG laser at 266 nm) is used for a desorption source to attain a diffraction limited spot size³⁹. Additionally, this is a system designed for sensitive analytical experimentation and is thus an extremely clean environment. The instrument is held at a pressure of 10^{-7} torr, and two turbo-molecular pumps (Balzers 500/333 L/s) are used rather than oil-diffusion pumps to eliminate any possibility of oil contamination. The load-lock is also pumped by clean sorption pumps.⁴⁰

B.1. Micron Stage Translation

Samples are loaded into the vacuum chamber through a load-lock, and locked into position on a special XYZ stage that is positioned directly under the microscope, previously having been driven by piezo inchworm motors. Due to technical difficulties with said motors, a new system was designed for manual micron-resolution control of the stages via vacuum feedthroughs.

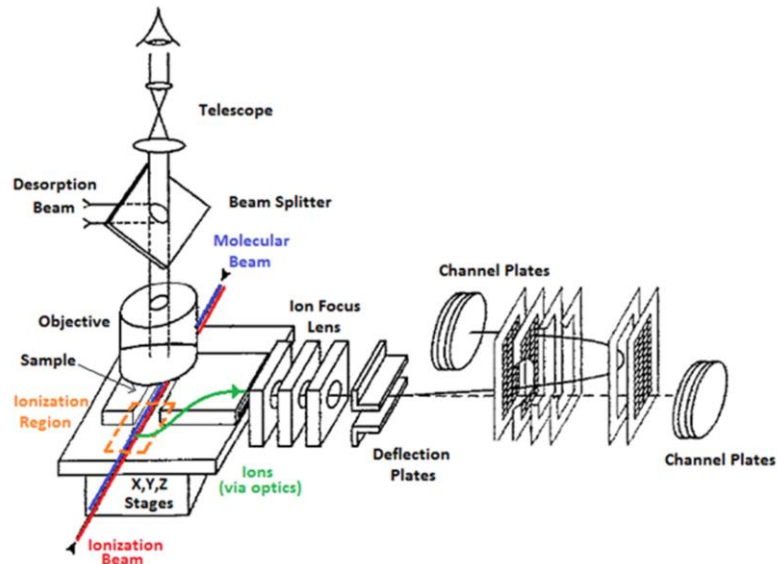


Figure 12: Microscope mass spectrometer instrument schematic.

B.2. Reflective Objective

In order to allow for simultaneous focusing of both the UV desorption laser in addition to visible light for the microscope image, an achromatic lens is needed. A reflective lens with Cassegrainian optics is used for this purpose, and is positioned within the vacuum chamber directly under the microscope. This particular optic was chosen both because it is achromatic, but also because it has a very high numerical aperture while maintaining a large working distance of 8 mm⁴⁰. A schematic of the reflective objective can be seen in Figure 13.

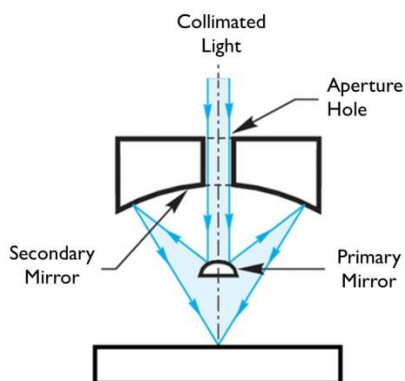


Figure 13: Optical path through a reflective objective.

The beam path of the desorption laser is directed onto a beam splitter directly above the reflective objective, with the beam splitter still allowing for transmission of light for visualization of the sample on the microscope. The beam splitter directs the desorption spot through the reflective objective, and eventually onto the sample itself with laser spot diameters between 4-8 μM . The desorbed plume of materials is immediately intersected with an ionization laser, normally 266 nm. The ions are then repelled down at TOF-MS.

1. R. Abbasi, M. Ackermann, J. Adams, M. Ahlers, J. Ahrens, K. Andeen, J. Auffenberg, X. Bai, M. Baker, B. Baret, S. W. Barwick, R. Bay, J. L. B. Alba, K. Beattie, T. Becka, J. K. Becker, K. H. Becker, P. Berghaus, D. Berley, E. Bernardini, D. Bertrand, D. Z. Besson, J. W. Bieber, E. Blaufuss, D. J. Boersma, C. Boehm, J. Bolmont, S. Boser, O. Botner, J. Braun, D. Breder, T. Burgess, T. Castermans, D. Chirkin, B. Christy, J. Clem, D. F. Cowen, M. V. D'Agostino, M. Danninger, A. Davour, C. T. Day, C. De Clercq, L. Demirors, O. Depaepe, F. Descamps, P. Desiati, G. de Vries-Uiterweerd, T. DeYoung, J. C. Diaz-Velez, J. Dreyer, J. P. Dumm, M. R. Duvoort, W. R. Edwards, R. Ehrlich, J. Eisch, R. W. Ellsworth, O. Engdegard, S. Euler, P. A. Evenson, O. Fadiran, A. R. Fazely, K. Filimonov, C. Finley, M. M. Foerster, B. D. Fox, A. Franckowiak, R. Franke, T. K. Gaisser, J. Gallagher, R. Ganugapati, L. Gerhardt, L. Gladstone, A. Goldschmidt, J. A. Goodman, R. Gozzini, D. Grant, T. Griesel, A. Gross, S. Grullon, R. M. Gunasingha, M. Gurtner, C. Ha, A. Hallgren, F. Halzen, K. Han, K. Hanson, D. Hardtke, R. Hardtke, Y. Hasegawa, J. Heise, K. Helbing, M. Hellwig, P. Herquet, S. Hickford, G. C. Hill, K. D. Hoffman, K. Hoshina, D. Hubert, J. P. Hulss, P. O. Hulth, K. Hultqvist, S. Hundertmark, R. L. Imlay, M. Inaba, A. Ishihara, J. Jacobsen, G. S. Japaridze, H. Johansson, J. M. Joseph, K. H. Kampert, A. Kappes, T. Karg, A. Karle, H. Kawai, J. L. Kelley, J. Kiryluk, F. Kislak, S. R. Klein, S. Klepser, G. Kohnen, H. Kolanoski, L. Kopke, M. Kowalski, T. Kowarik, M. Krasberg, K. Kuehn, T. Kuwabara, M. Labare, K. Laihem, H. Landsman, R. Lauer, H. Leich, D. Leier, A. Lucke, J. Lundberg, J. Lunemann, J. Madsen, R. Maruyama, K. Mase, H. S. Matis, C. P. McParland, K. Meagher, A. Meli, M. Merck, T. Messarius, P. Meszaros, H. Miyamoto, A. Mohr, T.

Montaruli, R. Morse, S. M. Movit, K. Munich, R. Nahnauer, J. W. Nam, P. Niessen, D. R. Nygren, S. Odrowski, A. Olivas, M. Olivo, M. Ono, S. Panknin, S. Patton, C. P. de Los Heros, J. Petrovic, A. Piegsa, D. Pieloth, A. C. Pohl, R. Porrata, N. Potthoff, J. Pretz, P. B. Price, G. T. Przybylski, R. Pyle, K. Rawlins, S. Razzaque, P. Redl, E. Resconi, W. Rhode, M. Ribordy, A. Rizzo, W. J. Robbins, J. Rodrigues, P. Roth, F. Rothmaier, C. Rott, C. Roucelle, D. Rutledge, D. Ryckbosch, H. G. Sander, S. Sarkar, K. Satalecka, S. Schlenstedt, T. Schmidt, D. Schneider, O. Schultz, D. Seckel, B. Semburg, S. H. Seo, Y. Sestayo, S. Seunarine, A. Silvestri, A. J. Smith, C. Song, G. M. Spiczak, C. Spiering, T. Stanev, T. Stezelberger, R. G. Stokstad, M. C. Stoufer, S. Stoyanov, E. A. Strahler, T. Straszheim, K. H. Sulanke, G. W. Sullivan, Q. Swillens, I. Taboada, O. Tarasova, A. Tepe, S. Ter-Antonyan, S. Tilav, M. Tluczykont, P. A. Toale, D. Tosi, D. Turcan, N. van Eijndhoven, J. Vandenbroucke, A. Van Overloop, V. Viscomi, C. Vogt, B. Voigt, C. Walck, T. Waldenmaier, H. Waldmann, M. Walter, C. Wendt, S. Westerhoff, N. Whitehorn, C. H. Wiebusch, C. Wiedemann, G. Wikstrom, D. R. Williams, R. Wischnewski, H. Wissing, K. Woschnagg, X. W. Xu, G. Yodh and S. Yoshida, *Astrophysical Journal Letters*, 2008, 689, L65-L68.

2. R. E. Honig and J. R. Woolston, *Appl Phys Lett*, 1963, 2, 138-139.
3. M. A. Posthumus, P. G. Kistemaker, H. L. C. Meuzelaar and M. C. Tennoeverdebrauw, *Anal Chem*, 1978, 50, 985-991.
4. M. Karas and F. Hillenkamp, *Anal Chem*, 1988, 60, 2299-2301.
5. J. B. Fenn, M. Mann, C. K. Meng, S. F. Wong and C. M. Whitehouse, *Science*, 1989, 246, 64-71.

6. C. D. Mowry and M. V. Johnston, *Rapid Commun Mass Sp*, 1993, 7, 569-575.
7. M. Karas and U. Bahr, *Trac-Trend Anal Chem*, 1986, 5, 90-93.
8. M. G. Sherman, J. R. Kingsley, J. C. Hemminger and R. T. Mciver, *Anal Chim Acta*, 1985, 178, 79-89.
9. G. J. Q. Vanderpeyl, K. Isa, J. Haverkamp and P. G. Kistemaker, *Nucl Instrum Methods*, 1982, 198, 125-130.
10. G. J. Q. Vanderpeyl, J. Haverkamp and P. G. Kistemaker, *Int J Mass Spectrom*, 1982, 42, 125-141.
11. R. B. Vanbreemen, M. Snow and R. J. Cotter, *Int J Mass Spectrom*, 1983, 49, 35-50.
12. R. B. Hall, *J Phys Chem-Us*, 1987, 91, 1007-1015.
13. F. Zaera and R. B. Hall, *J Phys Chem-Us*, 1987, 91, 4318-4323.
14. R. D. Macfarlane and D. F. Torgerson, *Science*, 1976, 191, 920-925.
15. R. N. Zare and R. D. Levine, *Chem Phys Lett*, 1987, 136, 593-599.
16. D. Burgess, R. Viswanathan, I. Hussla, P. C. Stair and E. Weitz, *J Chem Phys*, 1983, 79, 5200-5202.
17. M. Karas, D. Bachmann and F. Hillenkamp, *Anal Chem*, 1985, 57, 2935-2939.
18. G. Meijer, M. S. Devries, H. E. Hunziker and H. R. Wendt, *Appl Phys B-Photo*, 1990, 51, 395-403.
19. M. S. d. Vries, in *Challenges and Advances in Computational Chemistry and Physics*, ed. J. Leszczynski, Springer, Netherlands, 2008, vol. Radiation Induced Molecular Phenomena in Nucleic Acid, ch. 12, pp. 323-341.
20. R. E. Smalley, L. Wharton and D. H. Levy, *J Chem Phys*, 1975, 63, 4977-4989.
21. D. H. Levy, *Annual Review of Physical Chemistry*, 1980, 31, 197-225.

22. M. S. Devries, H. E. Hunziker, G. Meijer and H. R. Wendt, *Applied Spectroscopy in Material Science*, 1991, 1437, 129-137.
23. P. Arrowsmith, M. S. Devries, H. E. Hunziker and H. R. Wendt, *Appl Phys B-Photo*, 1988, 46, 165-173.
24. M. d. Vries, *Encyclopedia of Mass Spectrometry*, 2007.
25. J. B. Pallix, U. Schuhle, C. H. Becker and D. L. Huestis, *Anal Chem*, 1989, 61, 805-811.
26. J. Berkowitz and G. L. Goodman, *J Chem Phys*, 1979, 71, 1754-1760.
27. A. O. Nier, J. B. French and N. M. Reid, *Eos T Am Geophys Un*, 1971, 52, 875-&.
28. U. Boesl, H. J. Neusser and E. W. Schlag, *Chem Phys*, 1981, 55, 193-204.
29. R. J. Wenzel, U. Matter, L. Schultheis and R. Zenobi, *Anal Chem*, 2005, 77, 4329-4337.
30. B. Crews, PhD, UCSB, 2007.
31. W. C. Wiley and I. H. McLaren, *Rev Sci Instrum*, 1955, 26, 1150-1157.
32. M. Karas, D. Bachmann, U. Bahr and F. Hillenkamp, *Int J Mass Spectrom*, 1987, 78, 53-68.
33. M. Guilhaus, *Spectrochim Acta B*, 2000, 55, 1511-1525.
34. M. Guilhaus, D. Selby and V. Mlynski, *Mass Spectrom Rev*, 2000, 19, 65-107.
35. J. L. Wiza, *Nuclear Instruments & Methods*, 1979, 162, 587-601.
36. N. Winograd, J. P. Baxter and F. M. Kimock, *Chem Phys Lett*, 1982, 88, 581-584.
37. R. Tembreull and D. M. Lubman, *Anal Chem*, 1987, 59, 1082-1088.
38. R. Tembreull and D. M. Lubman, *Anal Chem*, 1987, 59, 1003-1006.

39. L. I. Grace, A. Abo-Riziq and M. S. deVries, *J Am Soc Mass Spectr*, 2005, 16, 437-440.
40. M. S. Devries, D. J. Elloway, H. R. Wendt and H. E. Hunziker, *Rev Sci Instrum*, 1992, 63, 3321-3325.

Chapter II. At the Interface of Chemistry and Art

A. High Spectral and Spatial Resolution

The analysis of cultural heritage materials presents a number of challenges that limit the range of analytical techniques available for use, these obstacles include: limited and extremely small samples, complexity of sample structure, the importance of maintaining spatial integrity and, most notably, the rarity of the samples. These limitations present unique challenges for the identification of organic dyes and pigments, particularly in paintings that may have multiple paint layers due to the artist's technique as well as subsequently applied restoration layers. These materials are often examined by analysis of microscopic painting cross-sections in which complex mixtures and thin (often only a few microns) layers of organic material are commonly encountered. Elucidating the nature of these organic compounds with high spatial resolution may help clarify aspects of a painting's history; and can assist in the painting's conservation since these molecules are often prone to degradation from moisture, light, or other environmental conditions. Therefore, there is a need for analytical techniques that can provide spatially resolved, molecularly-specific, and unambiguous identification of organic compounds in cultural heritage materials¹.

A.1. Current Analytical Techniques

A variety of spatially resolved spectroscopic and mass spectrometric techniques developed to identify elements and general functional groups are well established and extensively used in cultural heritage science,^{2,3} but they are not optimized for detailed analysis of molecular composition. For example, secondary ion mass spectrometry (SIMS) can attain spatial resolutions on the order of 10-50 nm for elemental analysis, and has also

been extended to some organic colorants as well.^{4,5} Due to the inherent fragmentation of organics with SIMS, many organic pigments that have similar molecular weights or structures can be difficult to distinguish from each other. Scanning electron microscopy/energy dispersive X-ray spectroscopy (SEM-EDS) provides high spatial resolution, but being an elemental analysis technique it is better suited to the identification of inorganic species than organic components.⁶ Micro X-ray fluorescence (μ -XRF) is a commonly used, often mobile, instrument capable of \sim 65-100 μ m spatial resolutions,^{7,8} but is also limited to elemental analysis. Molecular identification of organic molecules can be accomplished using spectroscopic techniques-such as a recent example combining laser ablation and surface-enhanced Raman spectroscopy (SERS)-⁹-but, relatively broad fluorescence signals masking organic bands in complex mixtures of natural organic colorants can often limit identification to broad classes of organic components. In addition, a spatial resolution of \sim 10 μ m limits its use in many paint cross-section applications. Raman microscopy and Raman mapping can also provide spatially resolved (\sim 1-2 μ m) molecularly specific identification, but still has difficulty to differentiate spectroscopically similar molecules that are common in organic colorants.^{10, 11} Fourier transform infrared spectroscopy (FTIR) microscopy can provide specific identification of both organic and inorganic compounds, and the continued development of attenuated total reflection (ATR) FTIR (\sim 6 μ m)¹², synchrotron-based FTIR ($<$ 1 μ m),^{13, 14} and FTIR imaging techniques (\sim 10-15 μ m)^{15, 16} have begun to address the challenges of thin layers and the need for spatial specificity. Still, FTIR either lacks the spatial or spectroscopic resolution for organic containing cross-sections, or requires the use of synchrotron facilities. An additional possibility is a form of laser desorption mass spectrometry (LDMS) that avoids many

problems associated with analyzing complex mixtures, and is a valuable tool in the identification of several organic pigments.¹⁷ However, fragmentation caused by LDMS can complicate categorical identification of certain pigments in addition to being limited by a spatial resolution of ~2-4 μm .¹⁸ Ultimately, none of these techniques has the ability to distinguish structurally similar molecular markers within complex matrices.

A.2. Organic Red Pigments

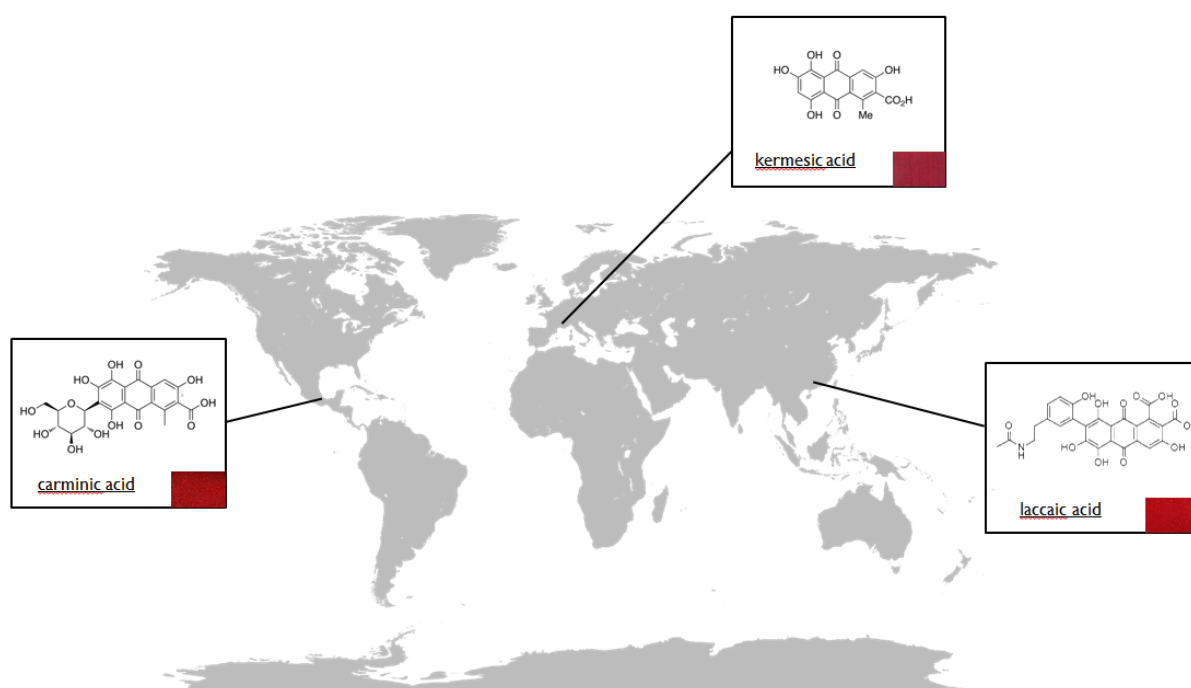


Figure 14: Geographical origins of three anthraquinone based dyes.

Works of cultural significance are constructed of an enormous collection of constituents and often will include a variety of both inorganic (e.g. ceramic, stone, glass, pigments, minerals, gemstones, or metal) and organic (e.g. wood, paper, canvas, organic colorants, glues, waxes, oils, resins, varnishes, polymers) components, often within a single complex object. Understanding the composition, properties and interactions of all of these

materials is paramount to the effective conservation of this work by shedding light on their compatibility with existing preservation techniques as well as their responses to environmental stresses such as temperature or moisture changes. It can also lead to a greater understanding of what types of molecules were used as coloring pigments, how and where they were manufactured, as well as aid in exposing new trade routes. Organic molecules also tend to be prone to degradation, so fugitive molecules can be identified and new preservation techniques can be developed. Art historians can also benefit greatly from understanding cultural heritage objects on a molecular level, as it can assist in their investigations between the historical environment in which they were created, as well as the artist's particular technique. For example, three similar organic red dyes (carminic acid, kermesic acid, and laccaic acid) have completely different geographical origins (see Figure 14). An unambiguous identification of each of these dyes can be a huge benefit in determining the provenance of the object, as well as the artist. Unfortunately, due mostly to the inherently complex nature of the substrate in which these molecules exist, identifying specific molecules has proven to be extremely difficult.

Natural organic colorants of plant or animal origin, derived from natural sources such as plants, lichens, insects and shellfish¹⁹, were important traditional sources of blue, yellow, and, importantly, red hues²⁰, and have therefore long been targets of investigation in cultural heritage research. Many organic colorants have a high tinting strength and, since very little material (as little as sub-nanogram concentrations) is required to achieve the desired color saturation, are present on artifacts in low concentration.^{21, 22} Organic colorants were transformed into paintable pigments – known as lake pigments – by the precipitation of the organic material onto inert substrates such as chalk, gypsum, or alum, further reducing

the mass percentage of the colored organic material present in an area (as compared to traditional inorganic mineral pigments) while simultaneously adding an inorganic matrix that may affect some analytical measurements of the chromophores.

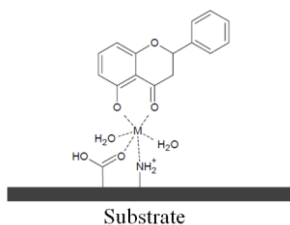


Figure 15: Lake pigment, created by precipitating a dye with an inert binder (usually a metallic salt).

Many traditional organic red colorants (including madder, alizarin, cochineal, lac dye, brazilwood, and dragonsblood) are compositionally similar: anthraquinones (see Figure 16) in particular have been used since prehistoric times as lake pigments²³ and contain primarily hydroxyl, carboxylic acid, and carbonyl moieties on an conjugated aromatic backbone . Several of these pigments are fugitive and therefore fade easily; the degradation of these pigments results in a very limited amount of the intended target chromophore being available for analysis. An example of this can be seen in Figure 17²⁴, illustrating the degradation of organic red dyes in Winslow Homer’s ‘For to Be a Farmer’s Boy’, painted in 1887.

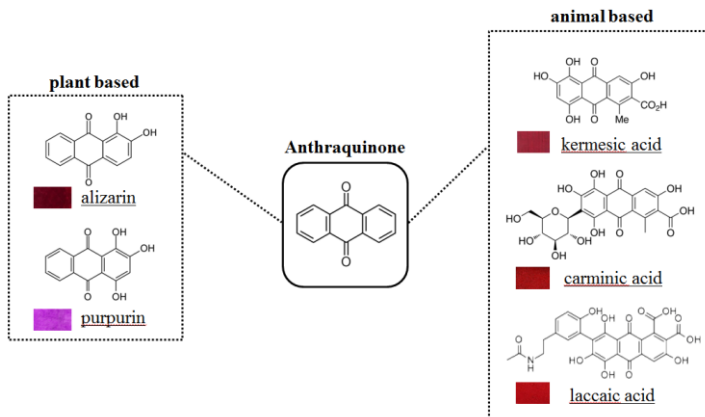


Figure 16: Several anthraquinone based dyes, and their natural source.

The chemical similarities between modern organic reds, along with the extremely low concentration in which they are found in lake pigments have long made their identification a thorn in the side of cultural heritage scientists. This is especially true concerning the unequivocal identification of single organic molecules or organic isomers within objects of cultural heritage. The fact that these molecules tend to degrade at a very fast rate has only made the need for a solution even more vital to their successful conservation.



Digital Restoration
(1887)

Current Condition
(2011)

Figure 17: Photodegradation of lake pigments within Winslow Homer's 'For to Be a Farmer's Boy'.

As discussed earlier, there are currently methods that are used to study organic red colorants in cultural heritage objects/samples has primarily utilized chromatography – both thin layer chromatography (TLC) ^{25, 26} and high pressure liquid chromatography (HPLC) ²⁰,

²⁷⁻³⁰ – though more recently successful applications of spectrofluorimetry ³¹, spectrophotometry ^{20, 27, 32, 33}, electrochemical methods ³⁴, dispersive Raman spectroscopy ³⁵, ³⁶, and surface enhanced Raman spectroscopy (SERS) ^{21, 22, 35, 37-41} have also been reported. Although each of these techniques has proven successful in particular circumstances, and will likely continue to do so, each also suffers from challenges that limit their use: chromatographic methods often require (and consume) more sample than can be safely collected from cultural heritage objects without causing visible damage; spectrophotometric, fluorimetric, and electrochemical methods often are not sufficiently molecularly specific for unambiguous identification; dispersive Raman spectroscopy is plagued by problems of interference from strong fluorescence; and disadvantages of SERS include the need for extracting colorants from complex sample matrices, spectral dependence on sample preparation conditions (including solution pH or chemical additives), the need to prepare specialized SERS substrates and the requirement that either samples be removed from, or metal nanoparticles deposited directly onto, the object of study. Additionally, the absorption efficiency of similar organic molecules can vary greatly in SERS, often resulting in masked bands and making correct identification difficult in complex mixtures. It is therefore essential that a method is developed aimed at identifying new methods appropriate for this type of sample. It must be compatible with complex substrates, and must be capable of unambiguous molecular identification.

A.3. Painting cross-sections

Over and above the intrinsic difficulty in the identification of compositionally similar organic materials, there arises the added complexity of the form in which the materials are present within an object. Organic materials may be present in heterogeneous mixtures (for

example, the binder in a layer of paint), or as a thin layer of pure material within a complex stratigraphy (for example, the presence of thin resin-containing varnish layers). In painted works of art multiple layers of materials – such as grounds, paints, sizing, glazes, and varnishes – are typically present, and the composition and stratigraphy of the individual layers can provide insight into the artists’ working practices and greatly inform our understanding of a work of art.⁴²

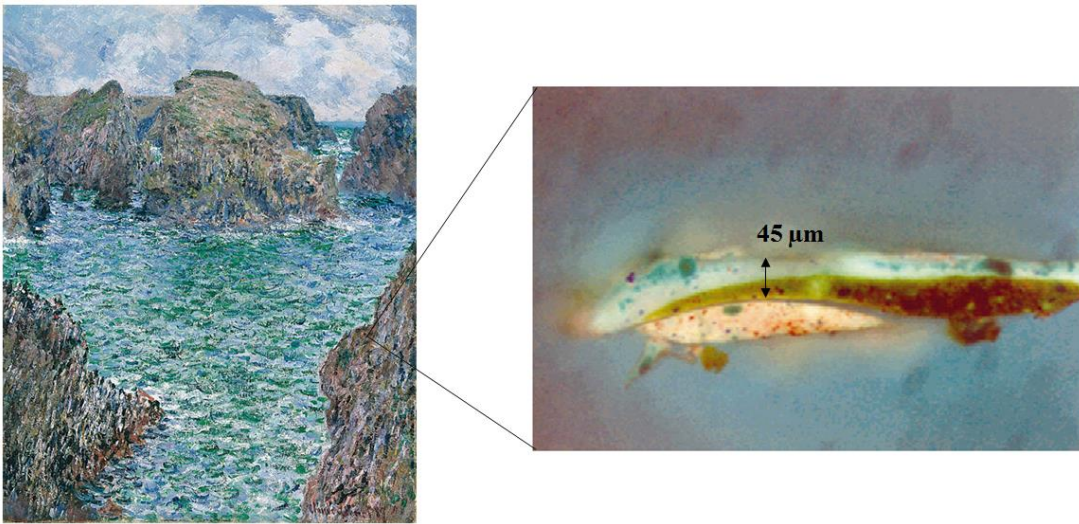


Figure 18: A cross section showing multiple layers of paint within Claude Monet’s ‘Port-Goulphar, Belle-Ile’.

A particularly powerful approach to understanding such details of paintings (whether executed on panel, canvas, or wall) and painted sculpture and decorative arts objects, therefore, is the study of microscopic cross sections. Small (<1mm³) samples removed from the object in collaboration with a conservator are mounted in resin or epoxy and either polished or sectioned using a microtome to reveal the layers of the painting’s structure (Figure 18).^{43, 44} The small sample size, the presence of both organic and inorganic materials in discrete strata that may only be on the order of a few microns thick, and the preciousness of the sample, which dictates that the sample should be recoverable following analysis whenever possible, all present challenges in the study of cross section samples.

In cultural heritage research, examination of paint cross sections utilizes primarily optical microscopy^{45, 46} and SEM-EDS^{46, 47} to provide elemental information, from which the presence of many inorganic pigments may be inferred. The high spatial resolution of Raman microscopy can provide specific identification of individual pigment particles, even within mixtures, but although inorganic pigments are readily detected, the number of organic materials directly detectable within a cross section is more limited.^{36, 48-50} ATR microspectroscopy^{44, 51}, and FTIR imaging^{16, 51-54} may also be employed, but often are limited by the lack of sufficient resolution to discriminate materials present in very thin (on the order of a few microns) layers or within mixtures. Ongoing research into the use of synchrotron-FTIR spectroscopy to generate chemical maps of organic materials in paint cross sections with high spatial resolution has shown promise⁵⁴, but similarly suffers from difficulties of differentiating compounds that share chemical moieties, inherent in any IR-based technique. Thus, the proposed development of REMPI- μ LMS, by providing a means of identifying organic materials *in situ* in cross sections with high spatial and chemical sensitivity will fill a gap in the existing suite of available analytical techniques.

B. Ancient Organic Dye R2PI Spectroscopy

B.1. Madder-Based Organics

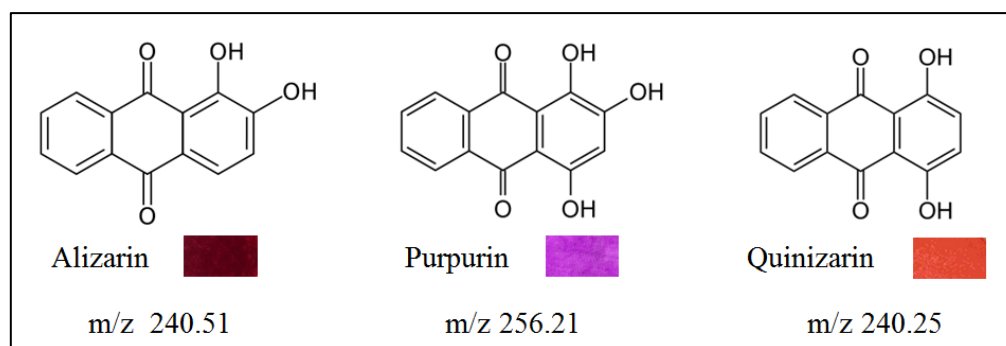
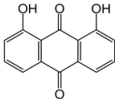
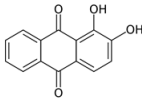
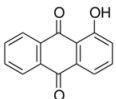
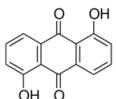
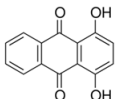
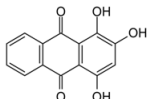


Figure 19: The three main chromophores within madder, from ordered from major to minor component.

Mass-selected R2PI spectroscopy was performed on three chromophores found within the madder root (*Rubia Tinctorum L*), all sharing the same anthraquinone double ring structure. Each molecule can be found in Figure 19, with alizarin being the main chromophore followed by purpurin and quinizarin. Note also, alizarin and quinizarin are structural isomers. The earliest known use of madder as a dye dates back over 4,000 years to an Egyptian painted leather quiver⁵⁵, and it was used extensively in both the Middle East and Europe up until the late 19th century when Graebe, Liebermann and Perkin industrialized the synthesis of alizarin dye.¹⁹ Natural madder dyes quickly became economically unfeasible, and so have largely been replaced both by synthetic alizarin as well as much more light resistant quinacridones (e.g. PV19). Unfortunately, alizarin tends to be very prone to photo-degradation and so the need for unambiguous identification is vital to understanding how to conserve and digitally reproduce the object.

To completely exploit the benefits of high resolution optically-selected mass spectrometry on objects of cultural heritage, the spectroscopy of the analyte in question must be known. In the case of anthraquinones, there was precedence for fluorescence excitation (FE) of bare alizarin (see Figure 20) provided by Huh et al.^{56, 57} The significant difference between R2PI spectroscopy and FE is the absence of any mass-selection in the latter. A photomultiplier tube is positioned near the interaction region between the excitation laser and the molecular beam, and a portion of the fluorescence is collected to take a fluorescence excitation spectra.⁵⁷

Table 1: Electronic origins of several related anthraquinone derivatives.

	1,8 DHAQ	Alizarin 1,2-DHAQ	1-HAQ	1,5 DHAQ	Quinizarin 1,4-DHAQ	Purpurin 1,2,4-THAQ
						
Electronic Origin	453.9		461.98	469.08	502.17	503.98
Relative Shift	-8.1		0	+7.1	+33.1	+42

Initially using 1-hydroxy-9,10-anthraquinone (1-HAQ), Huh found that the optical absorption of substituted anthraquinones progressively redshifted as more electron donating groups were added to the structure. The lowest electronic excited state of any substituted anthraquinone is of $\pi\text{-}\pi^*$ character, and such a redshift of this transition is commonly attributed to the electron transfer to the π ring from the electron donating substituent.^{58, 59} They also discovered that when an -OH group is substituted at a location that allows the formation of an intramolecular bond; the excited-state lifetime becomes considerably reduced. These compounds display a simple conversion of the incoming photon energy into heat, avoiding any generation of photochemically active molecules which inherently ensures they are photo-stable.⁵⁹ They suggest that an excited-state intramolecular proton transfer (ESIPT) greatly accelerates the rate of internal conversion by reducing the energy gap between the ground and excited state.⁶⁰ It is important to note though, that the existence of an intramolecular hydrogen bond does not automatically imply the occurrence of a fast excited-state lifetime, as seen with 1,4-HAQ. A list of common anthraquinone derivatives, as well as their electronic origin, is found in Table 1.

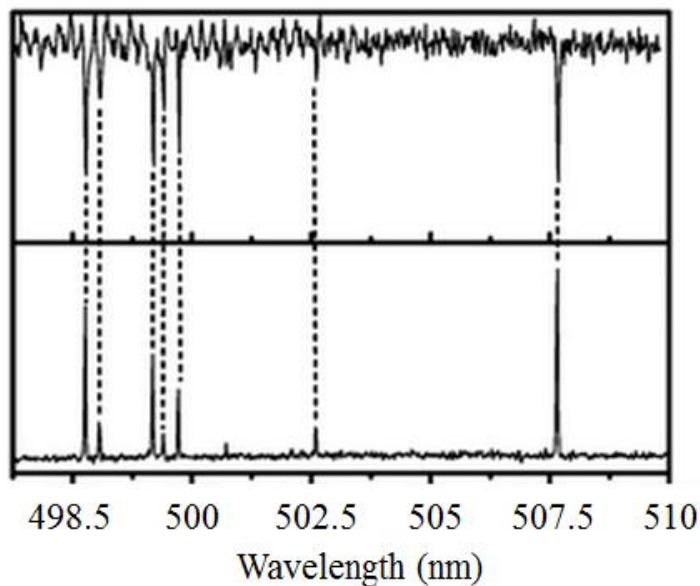


Figure 20: FE spectrum of alizarin standard.

Despite many attempts, an R2PI spectrum that correlated with the FE spectrum was never established. Instead, a very broad and structureless absorption was observed at ≈ 455 nm was seen (Figure 21). Both experiments were done on 97% pure alizarin purchased from Aldrich, and there was no further purification performed. Since the S_1 state is less than half the ionization energy, an excimer operating at 193 nm was used as an ionization source. Due to the lack of mass selection in FE, there is no way of guaranteeing that the observed fluorescence is in fact due to alizarin and not due to chemical impurities, thermal fragmentation, or clusters formed in the molecular beam.

The presence of a very fast excited state lifetime due to ESIPT in alizarin is likely the cause for the lack of any discernable R2PI spectrum. If the excited state lifetime is less than the pulse width of the lasers (8 ns), the decay rate will exceed the ionization rate and will consequently produce broad, featureless spectra. Specifically, there is a strong possibility of an excited state tautomerization that lowers the excited state lifetime of alizarin. As opposed to an anthraquinone with any 1,4 substitution pattern (e.g. purpurin and

quinizarin), molecules with just a 1,2 substitution similar to alizarin avoid any generation of photochemically active species by quickly converting incoming photon energy into heat, ensuring the photostability of these molecules.⁵⁹ In 1,4 substituted HAQS, the presence of two pseudoaromatic rings (formed through hydrogen bonds) that are formed in conjunction with the common anthraquinone ring stabilizes against excited state tautomerization. Supporting this theory is the fact that both purpurin (1,2,4-THAQ) and quinizarin displayed sharp vibronic peaks in the same frequency range, seen in Figures 22 and 23. To illustrate the high resolution of R2PI, Figure 24 has purpurin and quinizarin transposed on the same spectrum.

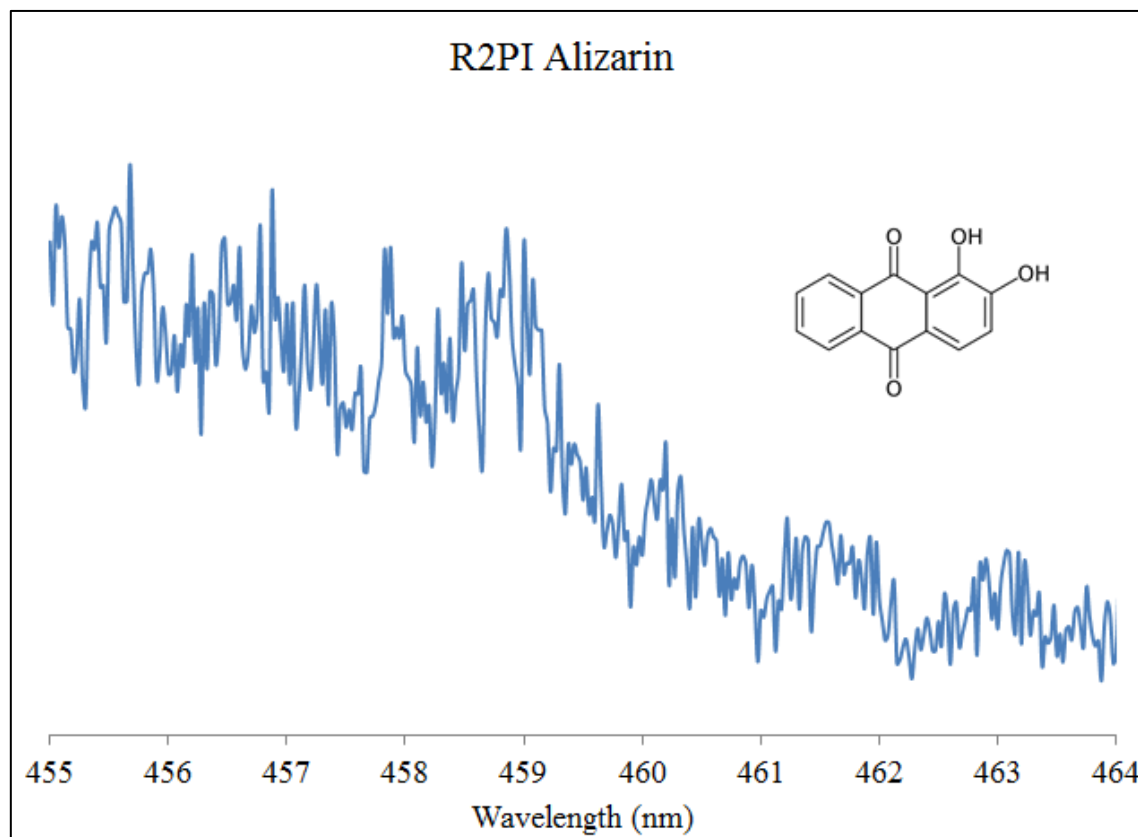


Figure 21: R2PI spectrum of alizarin standard.

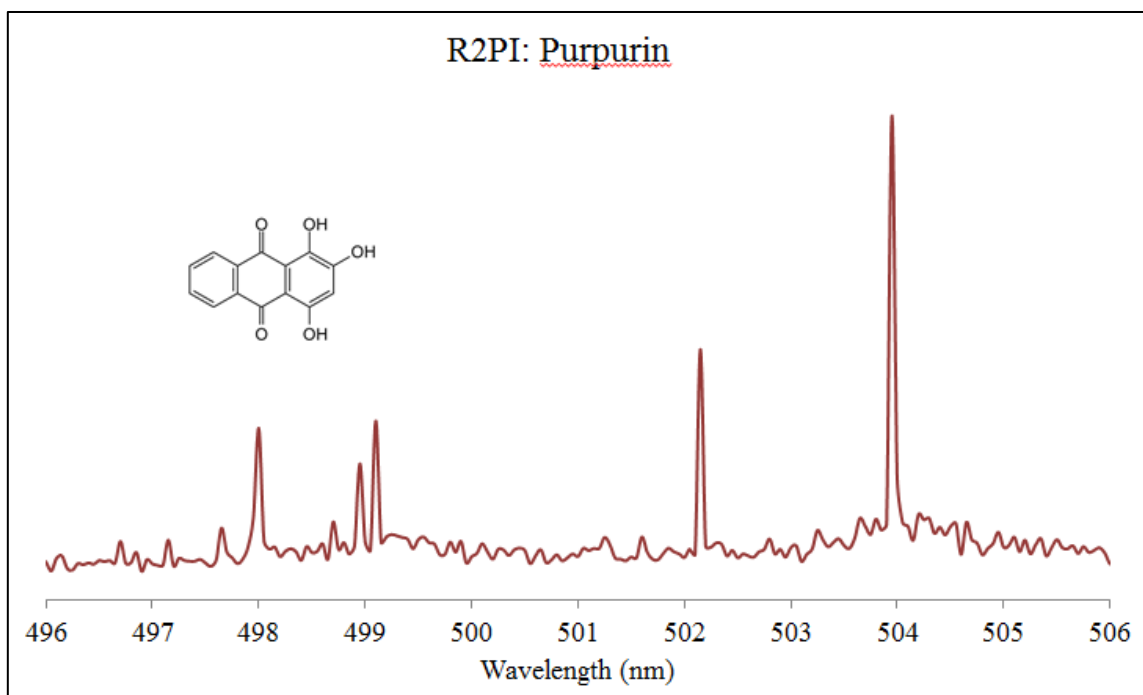


Figure 22: R2PI spectrum of purpurin standard.

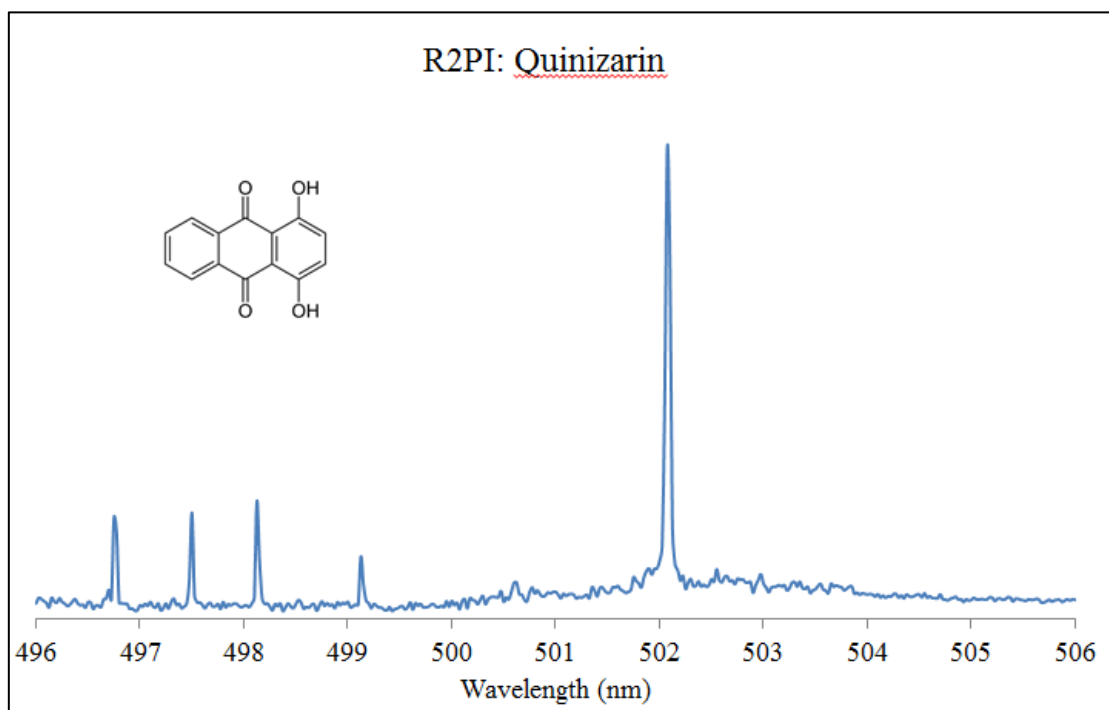


Figure 23: R2PI spectrum of quinizarin standard.

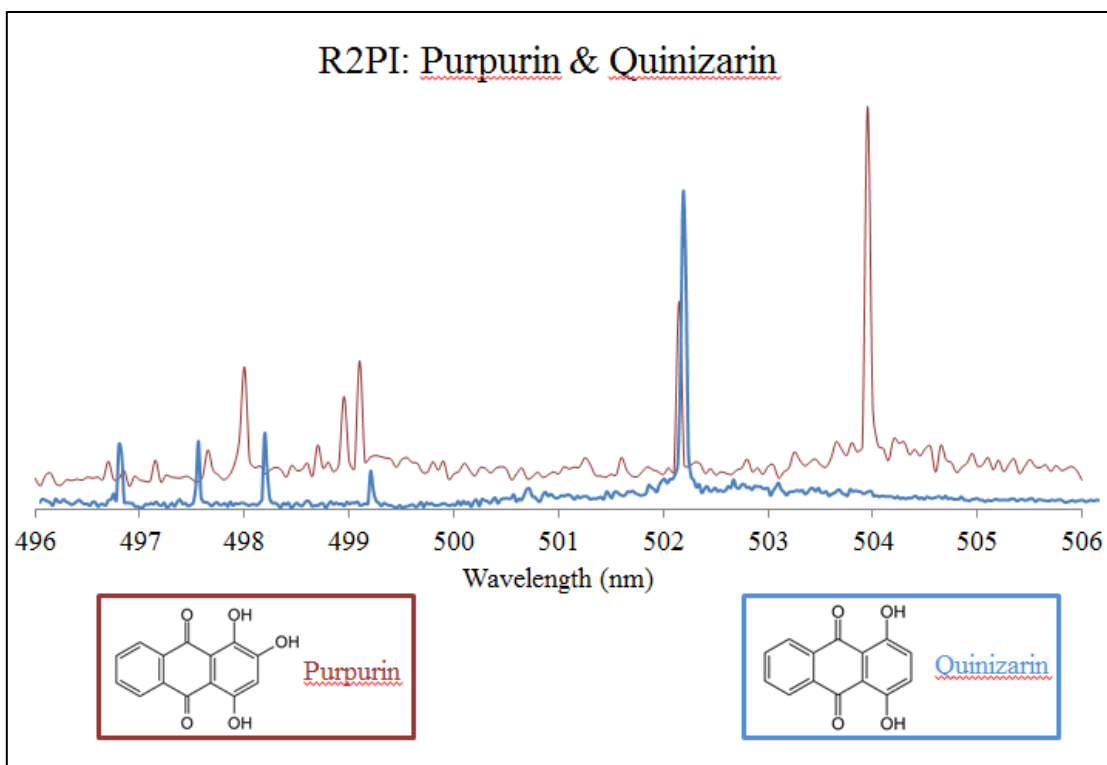


Figure 24: Representation of the high resolution afforded by R2PI in structurally similar molecules.

C. Modern Synthetic Organic Pigment R2PI Spectroscopy

Rhodamine Pigment

In order to probe the possibility of performing R2PI spectroscopy on lake pigments (insoluble salts, formed by precipitating an organic pigment with an inert metallic salt), rhodamine b pigment was used. In contrast to lake pigments, rhodamine b exists as a salt with a cationic organic portion, and so allows for experimentation without altering the field within the ion source. As can be seen in Figure 25, it was successfully desorbed as a neutral molecule, and also displayed a wavelength dependent fragmentation of rhodamine b. The fragment that is detected is the entire organic portion (m/z 443.6).

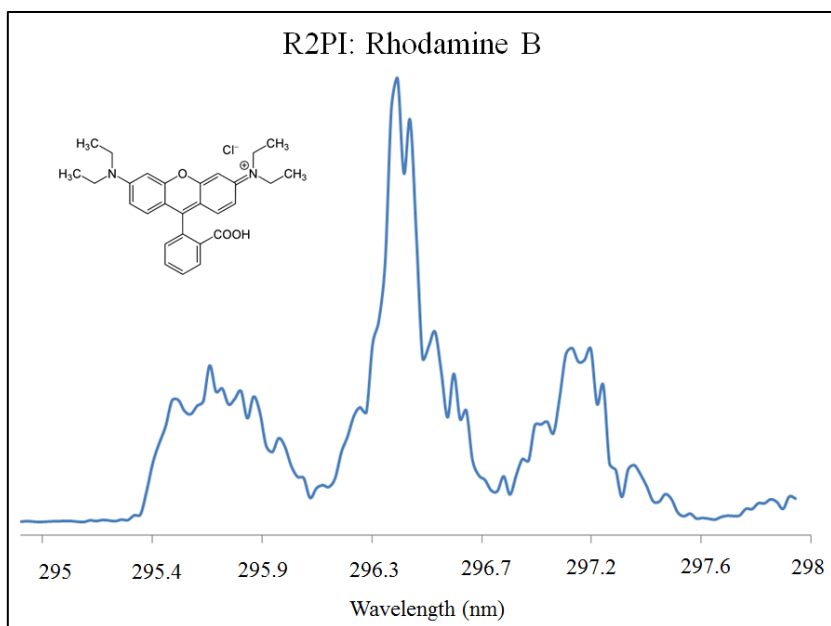


Figure 25: R2PI spectrum of rhodamine b standard.

Quinacridone (PV19)

With a yearly sales volume of over 100 million dollars, quinacridone is one of the most widely used synthetic pigments which is likely due to their exceptional color and light fastness.⁶¹ In addition, many other hues of reds and violets are simple R-group substitutions, and so mapping the R2PI spectroscopy (Figure 26) of this common backbone is important.

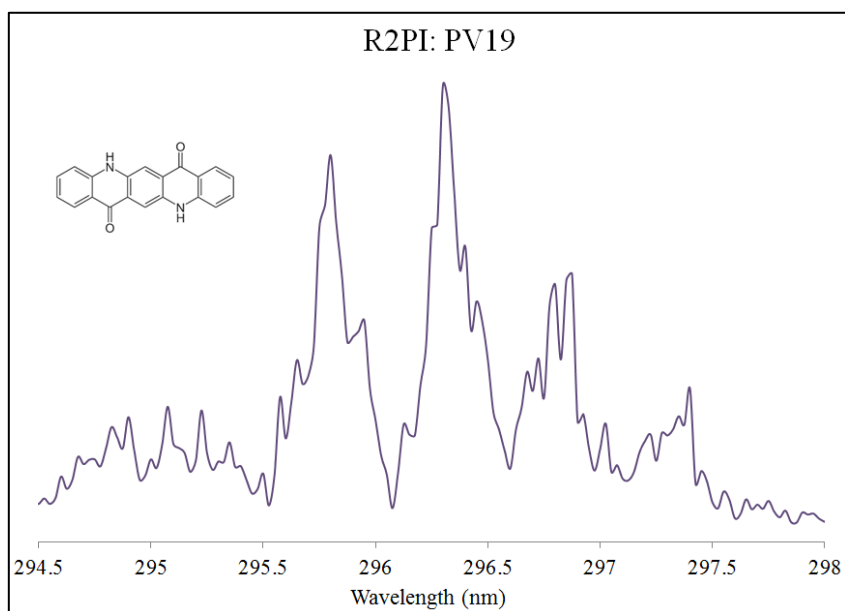


Figure 26: R2PI spectrum of pigment violet 19 (PV19) standard.

D. Non-Resonant 2-Photon Ionization Mass Spectrometry

To explore the possibility of performing quantitative analysis studies, non-resonant 2-photon ionization methods were completed on the two main madder chromophores, as well as a small selection of modern organic pigments. As is apparent in the mass spectra below, non-resonant techniques lead to much more fragmentation than R2PI. Still, the fragmentation is relatively limited compared to more traditional methods of mass spectrometry due to the presence of supersonic jet-cooling. An excimer laser was used as the ionization laser for the following experiments, operated at 193 nm.

Alizarin and Purpurin

The non-resonant 2 photon ionization of purpurin repeatedly led to mass fragments at m/z 240.21, which is identical to the parent mass peak of alizarin. This is greatly significant in terms of how effective current methods, such as laser ionization mass spectrometry (LIMS), can be in determining the presence of purpurin and alizarin. As previously discussed, the large scale manufacturing of pure alizarin in the later 19th century caused the relatively expensive process of madder dye extraction essentially obsolete. This is in fact, very beneficial to scientists as it has allowed the use of purpurin and other madder derivatives to be used as molecular markers to aid in such things as authentication and greatly helps in determining the paintings provenance. Alizarin can be seen in Figure 27, and purpurin in Figure 28.

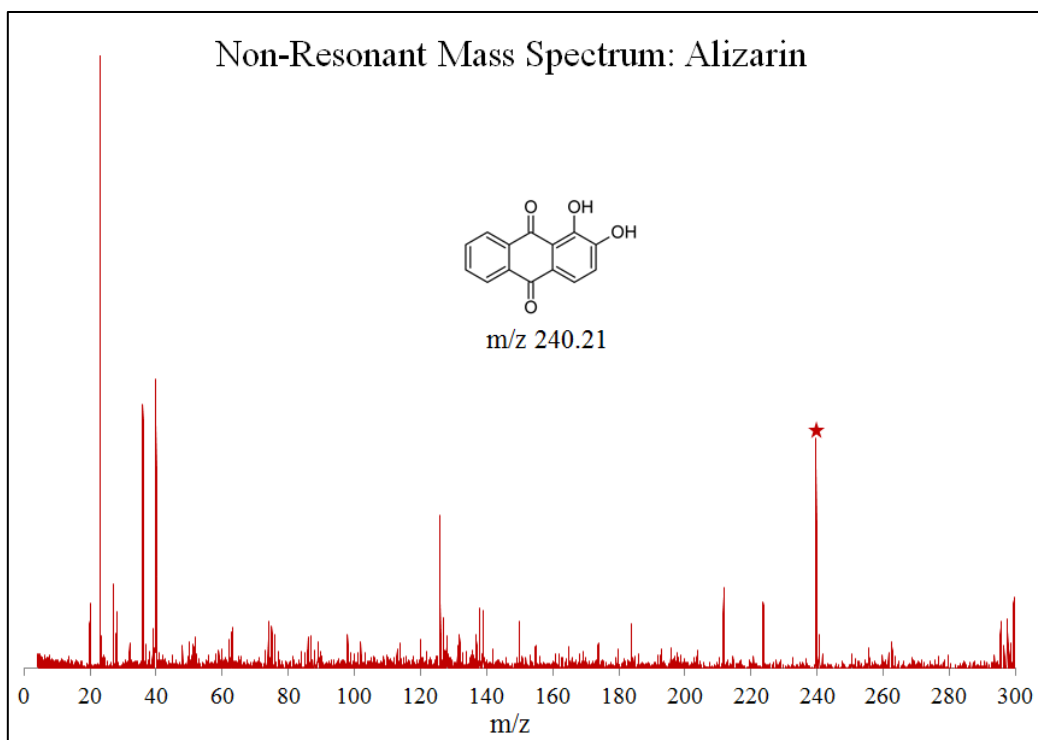


Figure 27: Non-resonant mass spectrum of alizarin standard.

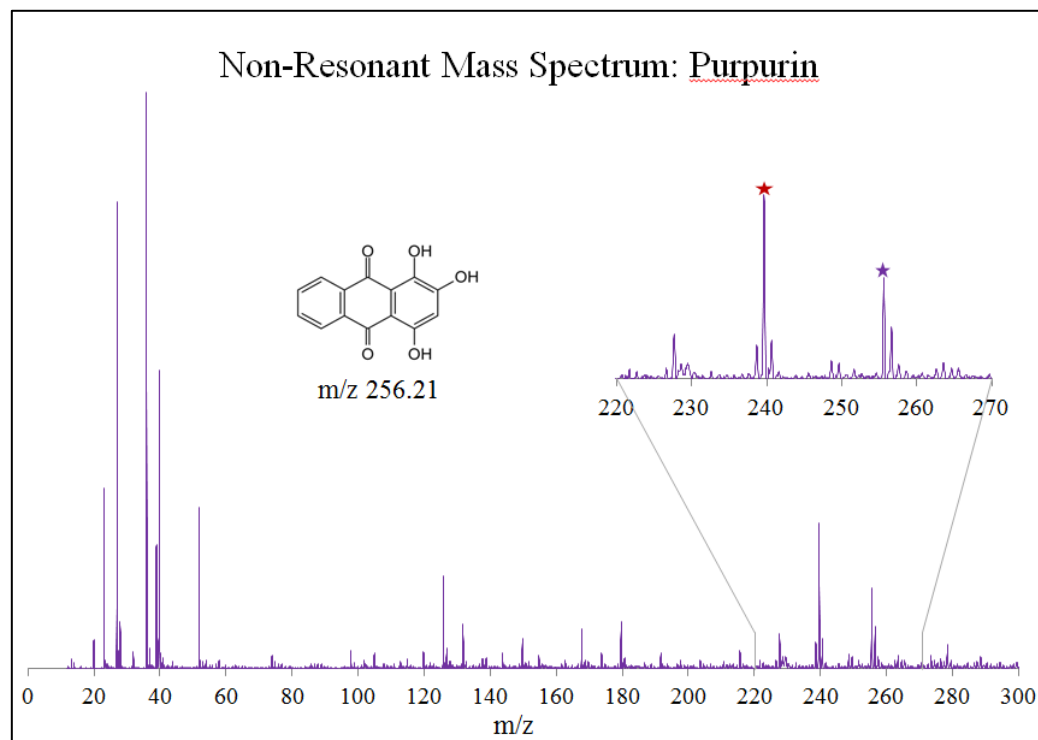


Figure 28: Non-resonant mass spectrum of purpurin standard.

Modern Synthetics

Non-resonant 2-photon ionization on modern synthetic dyes was also explored using PV19, Pigment Red 254 (PR254) and Pigment Orange 43 (PO43). The spectra can be seen in Figures 29, 30 and 31.

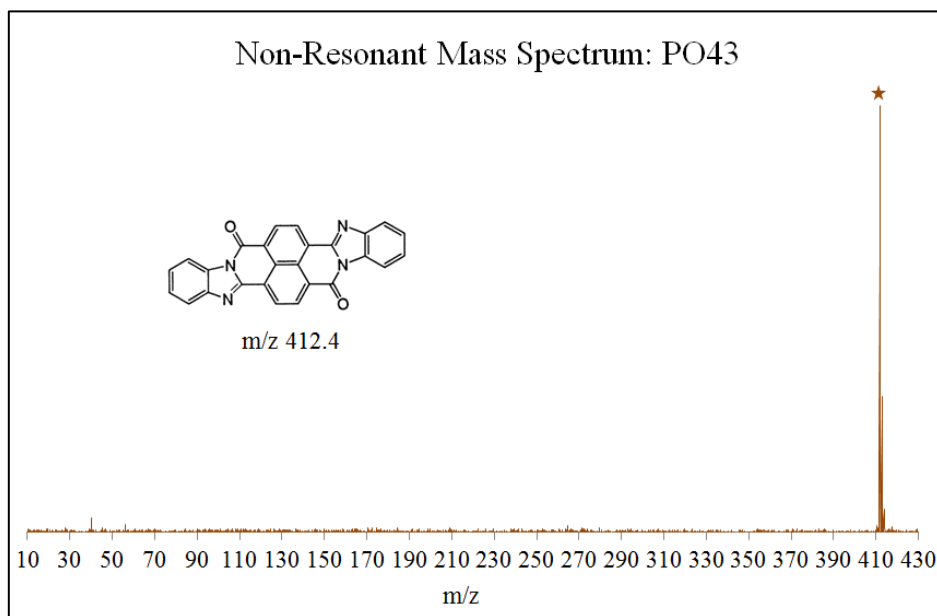


Figure 29: Non-resonant mass spectrum of pigment orange 43 (PO43).

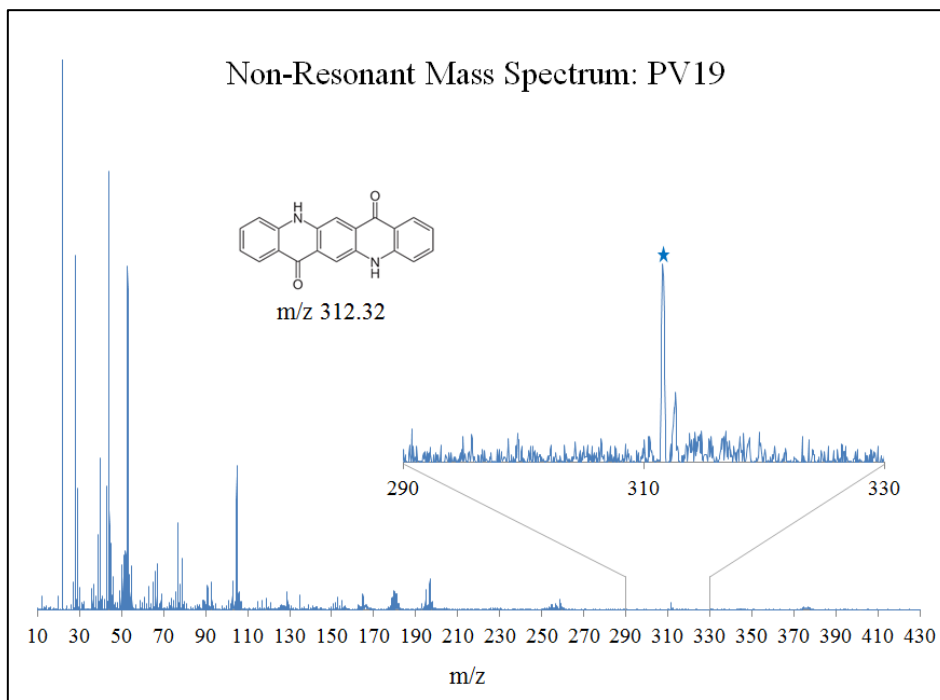


Figure 30: Non-resonant mass spectrum of pigment violet 19 (PV19).

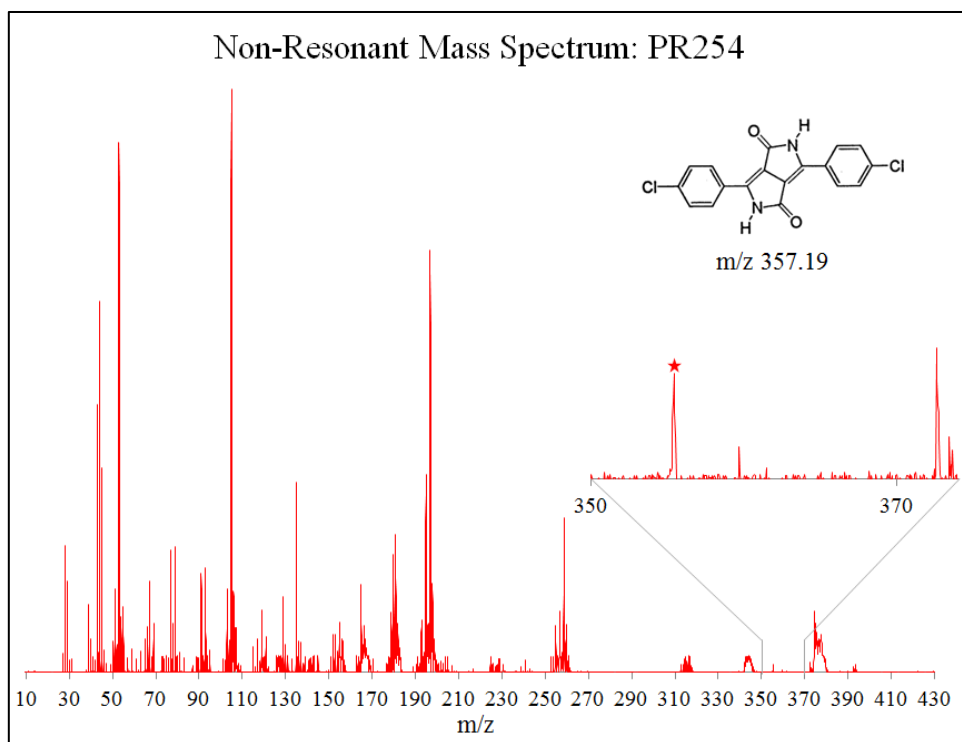


Figure 31: Non-resonant mass spectrum of pigment red 254 (PR254).

1. S. C. Owens, J. A. Berenbeim, C. S. Patterson, E. P. Dillon and M. S. de Vries, *Anal Methods-Uk*, 2014, 6, 8940-8945.
2. G. Spoto, A. Torrisi and A. Contino, *Chem Soc Rev*, 2000, 29, 429-439.
3. G. Spoto and G. Grasso, *Trac-Trend Anal Chem*, 2011, 30, 856-863.
4. A. Adriaens and M. G. Dowsett, *Appl Surf Sci*, 2006, 252, 7096-7101.
5. C. S. Deroo and R. A. Armitage, *Anal Chem*, 2011, 83, 6924-6928.
6. C. Genestar and C. Pons, *Anal Bioanal Chem*, 2005, 382, 269-274.
7. G. Vittiglio, S. Bichlmeier, P. Klinger, J. Heckel, W. Fuzhong, L. Vincze, K. Janssens, P. Engström, A. Rindby, K. Dietrich, D. Jembrih-Simbürger, M. Schreiner, D. Denis, A. Lakdar and A. Lamotte, *Nuclear Instruments and Methods in Physics Research Section B: Beam Interactions with Materials and Atoms*, 2004, 213, 693-698.
8. K. Trentelman, M. Bouchard, M. Ganio, C. Namowicz, C. Schmidt and M. Walton, *X-Ray Spectrom.*, 2010.
9. P. S. Londero, J. R. Lombardi and M. Leona, *Anal Chem*, 2013, 85, 5463-5467.
10. G. Paternoster, R. Rinzivillo, F. Nunziata, E. M. Castellucci, C. Lofrumento, A. Zoppi, A. C. Felici, G. Fronterotta, C. Nicolais, M. Piacentini, S. Sciuti and M. Vendittelli, *Journal of Cultural Heritage*, 2005, 6, 21-28.
11. P. Vandenabeele, B. Wehling, L. Moens, H. Edwards, M. De Reu and G. Van Hooydonk, *Anal Chim Acta*, 2000, 407, 261-274.
12. S. Prati, E. Joseph, G. Sciutto and R. Mazzeo, *Accounts of Chemical Research*, 2010, 43, 792-801.
13. G. D. Smith, *J Am Inst Conserv*, 2003, 42, 399-+.

14. J. Mass, J. Sedlmair, C. S. Patterson, D. Carson, B. Buckley and C. Hirschmugl, *Analyst*, 2013, 138, 6032-6043.
15. E. Joseph, S. Prati, G. Sciutto, M. Ioele, P. Santopadre and R. Mazzeo, *Anal Bioanal Chem*, 2010, 396, 899-910.
16. E. Joseph, C. Ricci, S. G. Kazarian, R. Mazzeo, S. Prati and M. Ioele, *Vib. Spectrosc.*, 2010, 53, 274-278.
17. D. P. Kirby, N. Khandekar, K. Sutherland and B. A. Price, *Int. J. Mass spectrom.*, 2009, 284, 115-122.
18. L. I. Grace, A. Abo-Riziq and M. S. deVries, *J Am Soc Mass Spectr*, 2005, 16, 437-440.
19. E. S. B. Ferreira, A. N. Hulme, H. McNab and A. Quye, *Chem Soc Rev*, 2004, 33, 329-336.
20. G. G. Balakina, V. G. Vasillev, E. V. Karpova and V. I. Mamatyuk, *Dyes Pigment.*, 2006, 71, 54-60.
21. M. Leona, J. Stenger and E. Ferloni, *J. Raman Spectrosc.*, 2006, 37, 981-992.
22. A. V. Whitney, R. P. Van Duyne and F. Casadio, *J. Raman Spectrosc.*, 2006, 37, 993-1002.
23. M. J. Melo and A. Claro, *Accounts of Chemical Research*, 2010, 43, 857-866.
24. C. L. Brosseau, F. Casadio and R. P. Van Duyne, *Journal of Raman Spectroscopy*, 2011, 42, 1305-1310.
25. L. Masschelein-Kleinler, *Mikrochim. Acta*, 1967, 6, 1080-1085.
26. J. Hofenk de Graaff and W. G. T. Roelofs, presented in part at the ICOM Committee for Conservation 3rd Triennial Meeting Madrid, 1973.

27. C. Clementi, W. Nowik, A. Romani, F. Cibir and G. Favaro, *Anal. Chim. Acta*, 2007, 596, 46-54.
28. J. Wouters, *Stud. Conserv.*, 1985, 30, 119-128.
29. J. Wouters and N. Rosario-Chirinos, *J. Am. Inst. Conserv.*, 1992, 31, 237-255.
30. I. Karapanagiotis, Daniffia, A. Tsakalof and Y. Chryssoulakis, *J. Liq. Chromatogr. Relat. Technol.*, 2005, 28, 739-749.
31. A. Wallert, *Stud. Conserv.*, 1986, 31, 145-155.
32. G. W. Taylor, *Stud. Conserv.*, 1983, 28, 153-160.
33. M. Leona and J. Winter, *Stud. Conserv.*, 2001, 46, 153-162.
34. T. Grygar, S. Kuckova, D. Hradil and J. Hradilova, *J. Solid State Electrochem.*, 2003, 7, 706-713.
35. S. Murcia-Mascaros, C. Domingo, S. Sanchez-Cortes, M. V. Canamares and J. V. Garcia-Ramos, *J. Raman Spectrosc.*, 2005, 36, 420-426.
36. C. M. Schmidt and K. A. Trentelman, *e-Preservation Science*, 2009, 6, 10-21.
37. M. V. Canamares, J. V. Garcia-Ramos, C. Domingo and S. Sanchez-Cortes, *J. Raman Spectrosc.*, 2004, 35, 921-927.
38. M. V. Canamares, J. V. Garcia-Ramos, C. Domingo and S. Sanchez-Cortes, *Vib. Spectrosc.*, 2006, 40, 161-167.
39. K. Chen, M. Leona, K. C. Vo-Dinh, F. Yan, M. B. Wabuyele and T. Vo-Dinh, *J. Raman Spectrosc.*, 2006, 37, 520-527.
40. Q. T. Shadi, B. Z. Chowdhry, M. J. Snowden and R. Withnall, *J. Raman Spectrosc.*, 2004, 35, 800-807.

41. A. V. Whitney, F. Casadio and R. P. Van Duyne, *Appl. Spectrosc.*, 2007, 61, 994-1000.
42. F. Rosi, A. Burnstock, K. J. Van den Berg, C. Miliani, B. G. Brunetti and A. Sgamellotti, *Spectrochim. Acta A:Mol. Biomol. Spectrosc.*, 2009, 71, 1655-1662.
43. C. Miliani, F. Rosi, A. Burnstock, B. G. Brunetti and A. Sgamellotti, *Appl. Phys. A:Mater. Sci. Process.*, 2007, 89, 849-856.
44. S. Prati, E. Joseph, G. Sciutto and R. Mazzeo, *Acc. Chem. Res.*, 2010, 43, 792-801.
45. W. C. McCrone, *Journal of the International Institute for Conservation (J.IIC-CG)*. 1982, 7, 11-34.
46. D. Pinna, M. Galeotti and R. Mazzeo, eds., *Scientific Examination for the Investigation of Paintings. A Handbook for Conservator-restorers*, Centro Di della Edifimi srl, Florence, 2009.
47. N. W. Bower, D. C. Stulik and E. Doehne, *Fresenius' Journal of Analytical Chemistry*, 1994, 348, 402-410.
48. M. V. Cañamares, M. Leona, M. Bouchard, C. M. Grzywacz, J. Wouters and K. Trentelman, *J. Raman Spectrosc.*, 2010, 41, 391-397.
49. P. Vandenabeele, B. Wehling, L. Moens, H. Edwards, M. D. Reu and G. V. Hooydonk, *Anal. Chim. Acta*, 2000, 407 261-274.
50. H. G. M. Edwards, L. F. C. de Oliveira and H. D. V. Prendergast, *The Analyst*, 2004, 129, 134-138.
51. E. Joseph, S. Prati, G. Sciutto, M. Ioele, P. Santopadre and R. Mazzeo, *Anal. Bioanal. Chem.*, 2010, 396, 899-910.
52. C. Ricci, S. Bloxham and S. G. Kazarian, *J. Cult. Herit.*, 2007, 8, 387-395.

53. M. Spring, C. Ricci, D. A. Peggie and S. G. Kazarian, *Anal. Bioanal. Chem.*, 2008, 392, 37-45.
54. M. J. Nasse, B. Bellehumeur, S. Ratti, C. Olivieri, D. Buschke, J. Squirrell, K. Eliceiri, B. Ogle, C. S. Patterson, M. Giordano and C. J. Hirschmugl, *Vib. Spectrosc.*, IN PRESS, DOI: 10.1016/j.vibspec.2011.11.016.
55. M. Leona, *P Natl Acad Sci USA*, 2009, 106, 14757-14762.
56. H. Huh, S. H. Cho, J. Heo, N. J. Kim and S. K. Kim, *Phys Chem Chem Phys*, 2012, 14, 8919-8924.
57. S. H. Cho, M. H. Yoon and S. K. Kim, *Chem Phys Lett*, 2000, 326, 65-72.
58. S. Jiang and D. H. Levy, *J Phys Chem A*, 2002, 106, 8590-8598.
59. S. H. Cho, H. Huh, H. M. Kim, C. I. Kim, N. J. Kim and S. K. Kim, *J Chem Phys*, 2005, 122, 34304.
60. M. H. Vanbenthen, G. D. Gillispie and R. C. Haddon, *J Phys Chem-Us*, 1982, 86, 4281-4283.
61. E. F. Paulus, F. J. J. Leusen and M. U. Schmidt, *Crystengcomm*, 2007, 9, 131-143.

Chapter IV. Nanometer Scale Thermal Desorption

A. Chemical Analysis with High Spatial Resolution

The need for surface sampling and chemical imaging that goes beyond the limits of diffraction is an area of research that has seen continuing and steadily advancing research for the past decade.¹⁻⁴ Proximal probe thermal desorption (TD) is one such method that has been developed from atomic force microscopy (AFM), one of the most powerful tools for sub-micron characterization in applications ranging from bacterial imaging to analysis of degradation processes within organic thin films.⁵⁻¹⁰ While there is a plethora of different methods of characterization can be used with traditional AFM methods, unambiguous identification of organic molecules within complex mixtures has proven very challenging.¹¹ Originally, heated AFM cantilevers were developed with the intent of focusing on the thermal properties of materials on a nanometer scale, but their applications have now been extended to include high spatial resolution atmospheric pressure thermal desorption, as well as phase change detection on a sub-micron scale.^{11, 12}

Recently, Berkel and coworkers reported nanometer scale atomic force microscopy (AFM) proximal probe thermal desorption (AFM-TD) (Anasys Instruments, Santa Barbara) of organic molecules, and subsequent detection via electrospray ionization mass spectrometry (ESI-MS).^{12, 13} Additionally, the Zenobi group developed an active plasma source allowing for ambient pressure ionization mass spectrometry on direct analysis of desorbed material.¹⁴ We further extend this combination of AFM proximal probe AFM-TD and MS by decoupling the AFM step from the MS step. In our approach we collect sub-micron size samples through AFM proximal probe AFM-TD, followed by separate analysis with resonant two photon ionization (R2PI) coupled with mass spectrometry. While ESI-MS

is well suited for mass spectrometry of unknown compounds, R2PI can identify and selectively ionize specific molecules. So, when particular compounds can be targeted, R2PI is well suited for the complicated samples typically present in cultural heritage artifacts. We note that the inherent optical resolution in low temperature laser spectroscopy such as R2PI can often be much higher than the mass resolution in a typical mass spectrometer (MS).¹⁵ We also employ non-resonant LDMS to demonstrate the flexibility created by decoupling AFM-TD and MS. Our approach consists of a two-step process: (1) Sample collection, in which an AFM-mounted microscope is used to identify features, proximal probe AFM-TD is performed at selected locations and desorbed material is transferred to a sample bar through a capillary, and (2) Sample analysis, in which the bar with desorbed material is transferred to the laser mass spectrometer for laser desorption of molecules, followed by jet cooling of the desorbed molecules, R2PI and finally detection in a time-of-flight MS. While normally the spatial resolution of laser desorption is limited by the laser spot size of approximately 1 μm ¹⁶, the combination with the preceding AFM-TD sampling step makes it possible to reach a spatial resolution of $\sim 0.5 \mu\text{m}$.

The advantages of this new approach are two pronged; it allows for atmospheric pressure sampling, but more importantly avoids the limits of other high spatial resolution desorption techniques. For example, one of the most commonly used methods for high spatial resolution sampling is through focused laser techniques. While these techniques do have the advantage of a very high heating rate (avoiding thermal fragmentation), it is inherently limited by the limits of diffraction and in the best case will allow for spot sizes on the order of 1 micron.^{16, 17}

This unparalleled spatial resolution, if combined with a highly accurate analytical technique, would allow the imaging of the special spatial distribution of specific chemical species- essentially a chemical map on a nanoscale. Several applications can benefit from this new technique, including atmospheric work in explosives, pharmaceuticals, herbicides and dyes. Previous work undertaken by Berkel et al combining proximal probe TD with electrospray ionization demonstrated the technique was capable of desorption craters as small as 250 nm in diameter and 100 nm deep.¹⁸⁻²¹

B. Experimental

Instrumentation

All proximal probe TD experiments described in this thesis were carried out using an Anasys Instruments afm+®. The system allows for high spatial resolution nanothermal analysis (nanoTA), achieved by the use of Thermalever™ AFM probes. They are fabricated with silicon in order to maximize the temperature distribution in the cantilever, and a resistive heater element is integrated into the end of the cantilever allowing for the controlled heating of the probe. The cantilevers are u-shaped, permitting the current to flow through the resistive element which induces heating. The thermal conductance of a silicon heated cantilever is around 1 $\mu\text{W/K}$, when in contact with a surface.^{22, 23} Silicon fabricated cantilevers allow for a temperature maximum of approximately 1000°C, but more importantly have a thermal time constant as low as 10 microseconds^{24, 25}. This time constant will determine the response time of the heater, and will directly affect the efficiency of the thermal desorption.²⁶⁻³¹

The heat transferred to the substrate is primarily via conduction, either through the solid contact between the tip and the substrate or through the liquid meniscus formed

through melting (see Figure 32).³² Approximately 30% of the heat generated by the heater in the cantilever is transferred to the substrate via the air gap, and nearly all of the remaining heat is transferred to the substrate.²² The geometry of the tip, and most specifically the portion of the tip that is in contact with the surface, heavily influences the desorption characteristics and needs to be explored further.

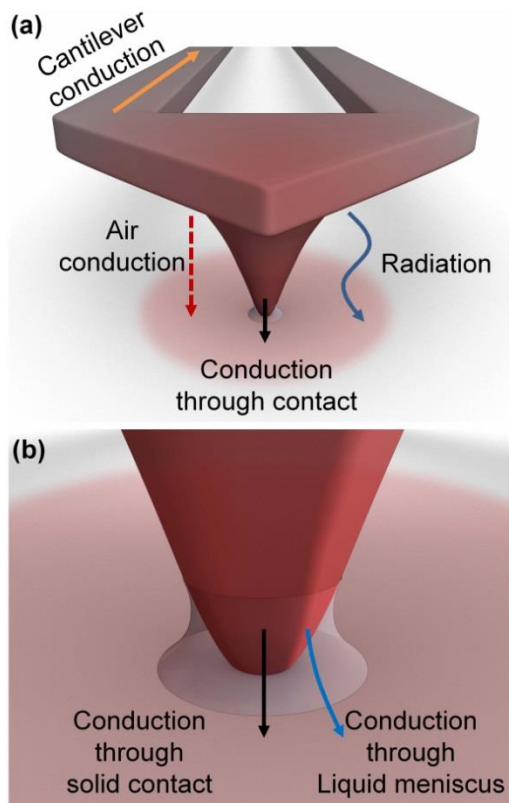


Figure 32: Heat transfer through proximal probe to sample.

nanoTA voltage profiles were performed within each potential sampling layer to define the bulk phase transition, which is used to determine heating rates and maximum temperatures for each respective substrate. The particular probe used for the studies described here have a maximum heating rate of 10 000 °C/s, which often corresponded to a maximum desorption temperature of 400°C in tens of μ s. Each probe is calibrated by increasing the voltage on the probe using three polymeric materials with known melting

temperatures: PCL, PE and PET. Figure 33 shows an example of this ‘deflection curve’. As the phase change of each material is reached during the voltage ramp, the probe penetrates into the sample surface and the voltage value can then be converted to °C.

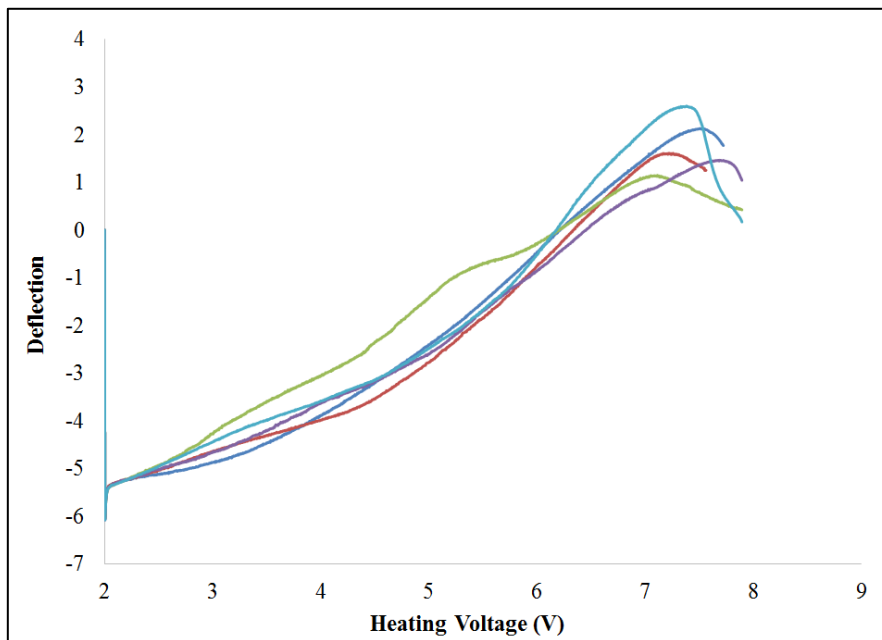


Figure 33: Deflection curve, used for calibrating temperature of probe.

Solvents and Chemicals

The dye alizarin crimson dark (Kremer Pigment 2361), and the synthetic organic pigments PV19 (Pigment Violet 19, Ciba) and PO43 (Pigment Orange 43, Clariant) were obtained from the Getty Conservation Institute's Reference Collection. Alizarin 97% pure was obtained from ACROS Organics. Binding media used for paint samples were egg yolk for alizarin crimson, and multi-purpose white glue (Elmer's Glue) for the synthetic organic pigments. Egg yolks were taken from whole chicken eggs obtained indiscriminately from the grocery store. Technovit 2000 LC light curing resin (Heraeus Kulzer GmbH & Co. KG) was used for the preparation of painting cross-section samples. Caffeine (anhydrous) was obtained from Sigma Aldrich to prepare a sample to test the analytical method prior to cross-section analysis. HPLC grade methanol was obtained from Fischer Chemical.

Sample Preparation

Two methods are employed to make samples; thin film deposition on a silica wafer and resin embedding of painting cross-sections. Using a home-built spin coater, a 0.3–0.5 mL aliquot of 0.02 M caffeine in methanol is deposited onto a silica substrate by a syringe and spun off at 5000 rpm for 1 s. To prepare samples from which a cross-section could be made, individual layers of paint (arbitrary thickness) are applied to a modern gesso-prepared board (Ampersand gesso board, acrylic gesso surface) and allowed to dry. Incisions are made using a scalpel in the dried paint to reveal and remove a piece of the painted surface in cross-section, before embedding in resin and curing under blue light. These samples are dry-polished iteratively by hand (Micro-Mesh, Micro Surface Finishing Products, Inc). The process is shown in Figure 34.

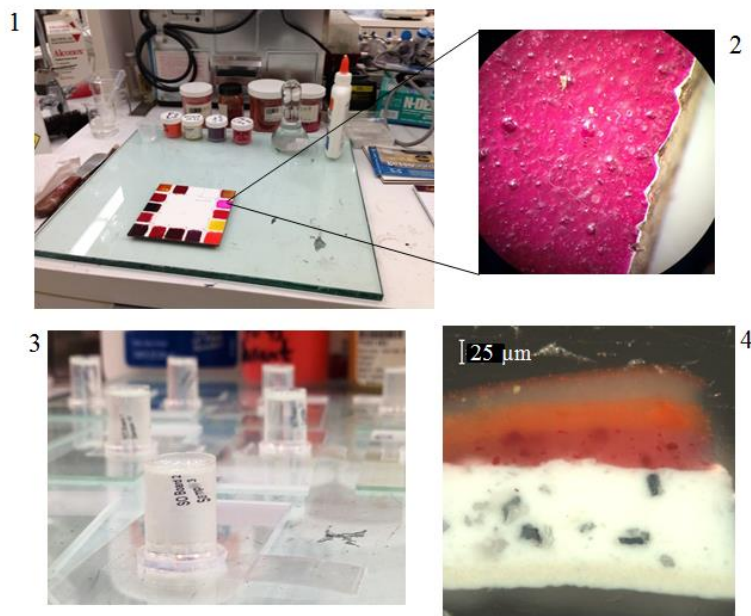


Figure 34: (1) Natural dyes were prepared, painted and left to dry. (2) Microscopic incisions were made to expose cross sections, and (3) cross sections were mounted in resin and cured. (4) Shows the final, polished cross section within resin.

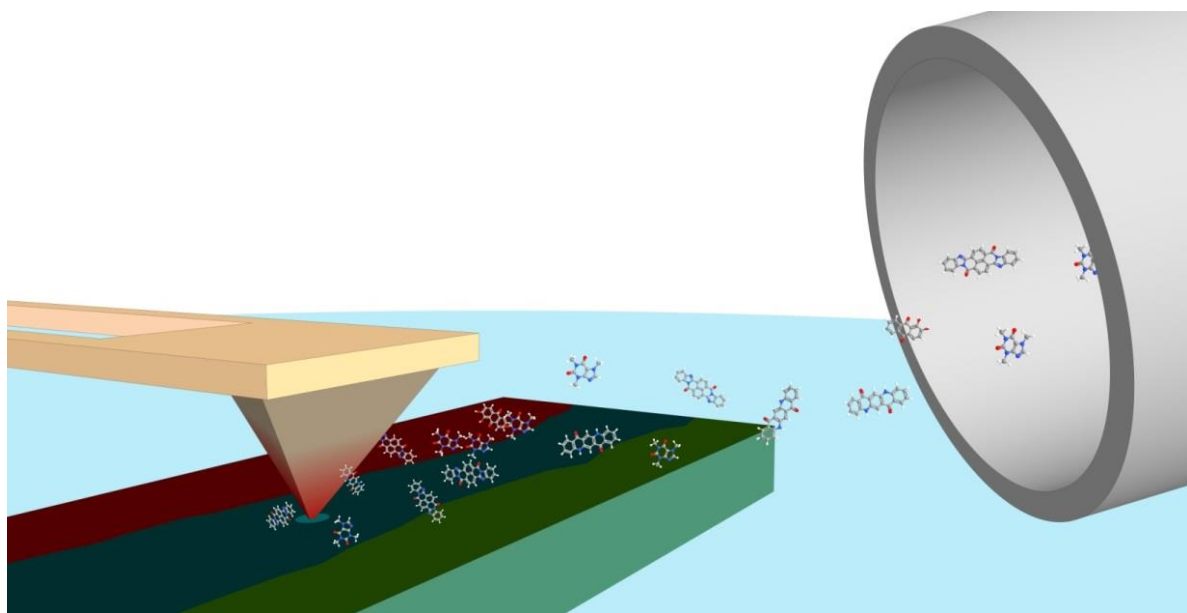


Figure 35: Schematic of proximal probe desorption, and transfer via capillary.

The plume thermally desorbed material is drawn via vacuum through a stainless steel capillary (Figure 35) and into an isolated sample collection box, where it deposits onto a graphite sample bar. For caffeine sampling a SS 6" \times 0.05" OD \times 0.03" ID capillary is pumped at a flow rate of \sim 150 mL/s. For pigments, a SS 6" \times 0.05" OD \times 0.033" ID capillary is pumped at a flow rate of \sim 215 mL/s. The larger diameter capillary served to increase the flow rate. The capillary is heated to 90 °C to reduce condensation of the desorbed material during the transfer. The capillary is positioned approximately 200-500 μ m from the AFM tip in order to maximize the amount of desorbed material drawn through the capillary and onto the graphite sample bar; limiting this distance avoids interference from mechanical vibrations caused by the continuous pumping of the sample collection box. Since the analysis step is separated from the analysis step, it is possible to optimize the sampling geometry and conditions for maximum collection. In real time direct inlet mass spectrometry, for example, this is harder to achieve because the flow rate affects the ionization efficiency. Numerous desorption spots from the same local area (e.g. paint layer)

are deposited additively onto the graphite bar in order to maximize sample material transfer ensuring enough material for subsequent mass spectral analysis. The graphite bar can be translated allowing deposition of different spots across the bar. The entire sample collection box is on a 3-axis stage to give full movement for positioning the capillary nearest the AFM tip. Figure 36 shows an overall instrument schematic of the AFM setup.

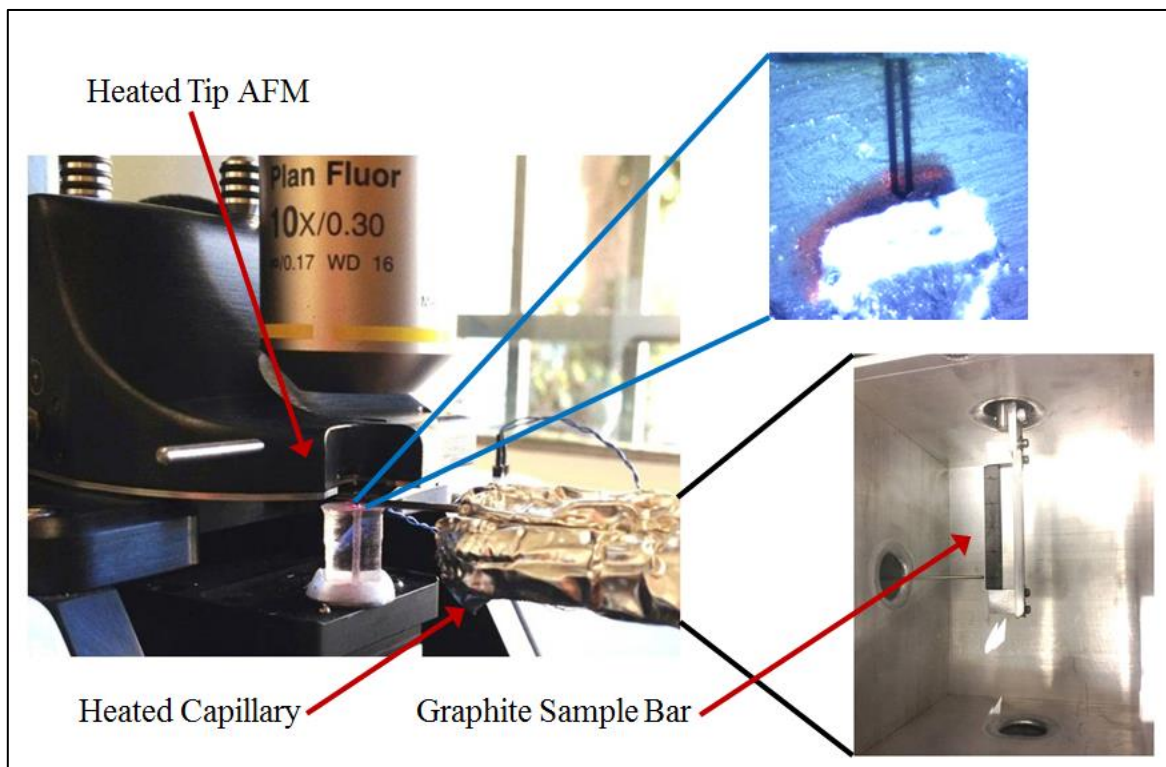


Figure 36: Instrument setup, showing proximal probe extending over cross section in upper right, in addition to the capillary output next to the graphite sample bar in lower right corner.

The experimental setup for the beam machine has been described earlier. The sample bar containing material from the AFM desorption is loaded into a high vacuum chamber, where it is positioned directly in front of a pulsed nozzle. The sample bar can be translated for successive laser shots on different locations. Material is laser desorbed from the sample bar by light from a Continuum MiniLite 1064 nm Nd:YAG laser, which is attenuated to minimize fragmentation and focused to a slit approximately 1×5 mm, within 5 mm of the

nozzle. The desorbed material is entrained in a pulsed supersonic argon stream controlled by an ACPV2 pulsed cantilever piezovalve³³ with an opening diameter of 300 μm and an concave conical shape with a full angle of 40° , at a backing pressure of 6 bar. The Ar molecular beam is skimmed before entering a source region where it is intersected by laser beam(s) and photo-ionized.

Two ionization techniques are employed: resonance enhanced two photon ionization (R2PI) and non-resonant ionization. R2PI uses a first photon from a Lumonics tunable dye laser to resonantly excite a molecule to an electronic excited state, followed immediately by a second photon from either the same or a different dye laser which ionizes the molecule. We have previously reported the spectroscopy of caffeine³⁴, which allows tuning the dye laser to a specific resonance in order to selectively ionize it and record the mass spectrum. The R2PI of caffeine was carried out with a set wavelength of 281.635 nm (1.1 mJ/pulse). Non-resonant ionization was carried out for all pigments using a 193 nm excimer laser (~4 mJ/pulse). All ions are characterized in a reflectron time-of-flight mass spectrometer.

A topographic image was taken before and after each experiment to investigate the AFM-TD depression sizes as well as any other changes to the morphology of the sample. Table 2 lists the complete set of molecules that were successfully transferred and identified, along with the number of times the tip was heated to induce desorption (AFM-TD Events) for each sample, as well as desorption depression characteristics. Successful AFM-TD appeared to be dependent on the thermal characteristics of the binding medium, as opposed to the pigment within that binding medium.

C. Results and Discussion

Table 2: Proximal probe desorption characteristics.

Molecule	Molecular Weight (g/mol)	TD Events	Crater Diameter (nm)	Crater Depth (nm)	Crater Volume (nm ³)
Caffeine	194.19	55 - 100	360	20 - 200	$6.8 \times 10^5 - 6.8 \times 10^6$
Alizarin	240.21	15	750	700	1.0×10^8
PV19	312.32	10	750 - 1500	800 - 1000	$1.2 \times 10^8 - 5.9 \times 10^8$
PO43	412.41	10	800 - 1000	200-400	$3.4 \times 10^7 - 1.0 \times 10^8$

Caffeine

Initial proof of concept experiments were conducted using caffeine, as Berkel et al had demonstrated the feasibility of proximal probe TD on this molecule. Using a home-built spin coater, a 0.3 – 0.5 mL aliquot of 0.02 M caffeine in methanol is deposited onto a silica substrate by a syringe and spun off at 5000 rpm for 1 s.

To determine the viability of separate AFM-TD and mass spectrometric steps, caffeine served for initial experiments as we have previously reported laser desorption jet-cooling R2PI-MS of caffeine, and the R2PI spectroscopy of this molecule is well known³⁴. Generally R2PI mass spectral analysis is only possible with prior knowledge of the R2PI spectrum for the jet-cooled molecule. Since the spectroscopic peaks are dependent on, and extremely sensitive to, structure this technique allows for indisputable identification of molecules by simultaneous spectroscopic and fragment-free mass spectrometric characterization. Figure 37a shows the R2PI spectrum of caffeine obtained by scanning the

tunable excitation laser³⁴. The photo-ionization step adds significantly to the molecular selectivity of the analysis, the strong absorption at 281.635 nm was used for R2PI-MS experiments.

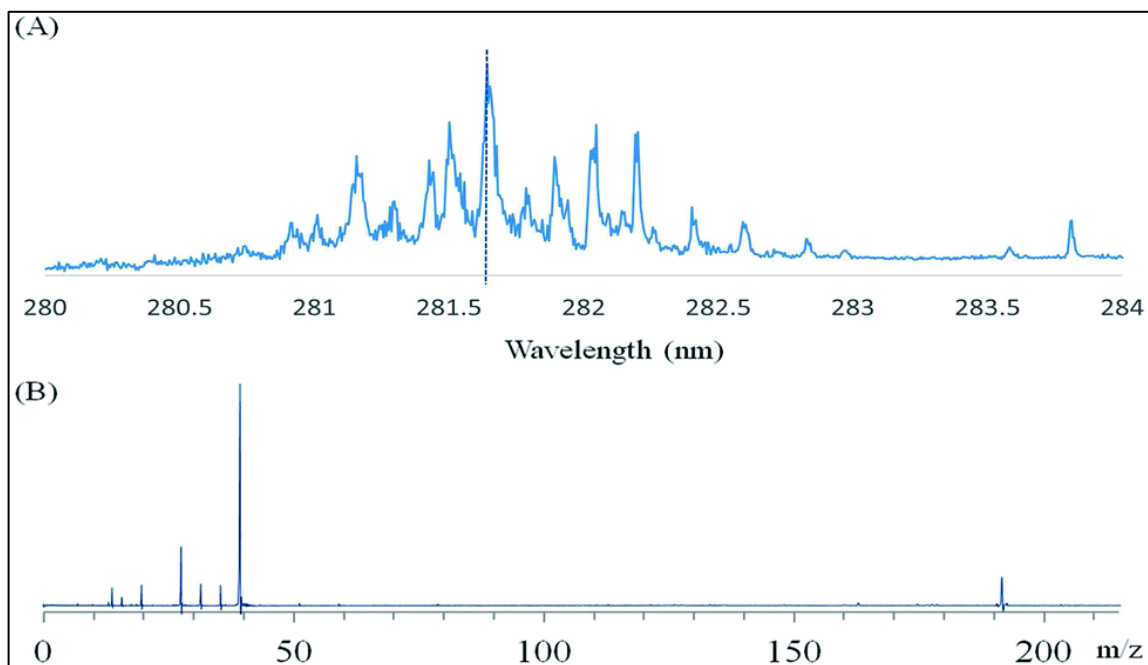


Figure 37: (A) Caffeine R2PI spectrum and (B) optically-selected mass spectrum, taken at wavelength depicted by dotted line in R2PI spectrum.

A number of AFM-TD events from a caffeine-coated silica wafer were transferred to a graphite sample bar as 3 separate spots (AFM-TD events on each spot: (1)55 (2)75 (3)85). Figure 37b illustrates the R2PI-MS corresponding to material from spot 1 on the sample bar. The parent peak of caffeine is seen at m/z 194, indicating a successful transfer of the sample following AFM-TD (Ar, the carrier gas, can be seen at m/z 40). Note the absence of unrelated peaks observed from either AFM-TD fragmentation or the laser desorption of the graphite matrix, illustrating the highly selective nature of R2PI-MS. To verify caffeine was present in each spot on the sample bar, the signal of caffeine (i.e. the intensity at m/z 194.19) was monitored as the sample bar was translated, in order to laser desorb from each of the 3

spots. Figure 38 shows a back and forth scan. After spot 3 was analyzed, the direction of the bar was reversed in order to laser desorb again from same spots 2 and 1. The signal spike seen in spot 3 is due to an increase in the bar speed reversing directions, exposing fresh sample at a faster rate and resulting in a slight signal increase. The rate was returned to a slower speed after the increased signal seen in spot 3.

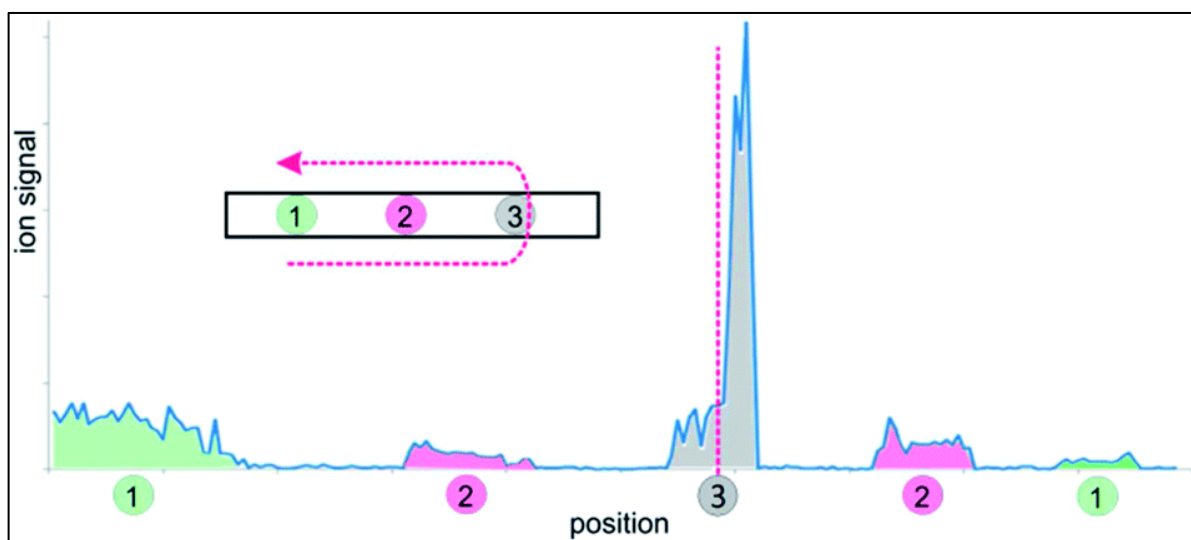


Figure 38: Caffeine ‘distance scan’. Labeled peaks correspond to deposited spots on sample bar, after desorption and transfer through capillary.

The fact that signal from spots 2 and 1 can be detected on the second pass demonstrates that complementary analytical techniques can be performed on the same sample spot more than once.

Organic Paint Analysis

Following successful application to the well-characterized caffeine system, the AFM-TD technique was next applied to more challenging samples – a traditional organic colorant and modern synthetic pigments prepared as mounted cross-sections – in order to determine whether the overall approach is reasonable for samples of these types.

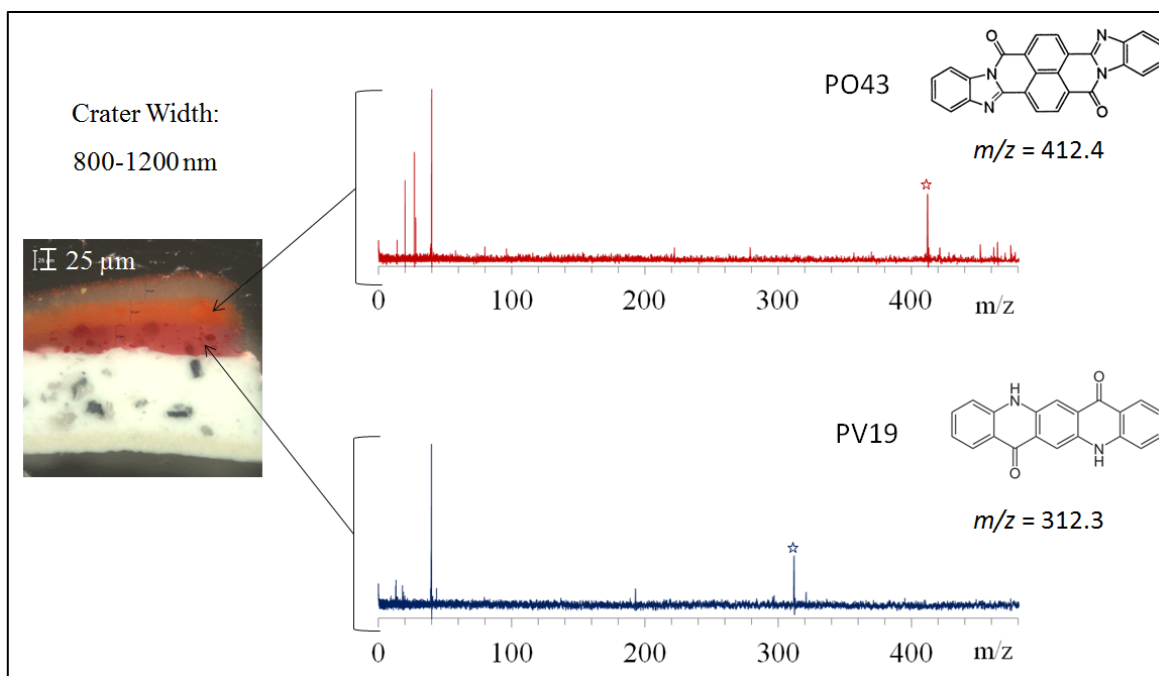


Figure 39: Non-resonant mass spectra of PO43 and PV19, after proximal probe TD.

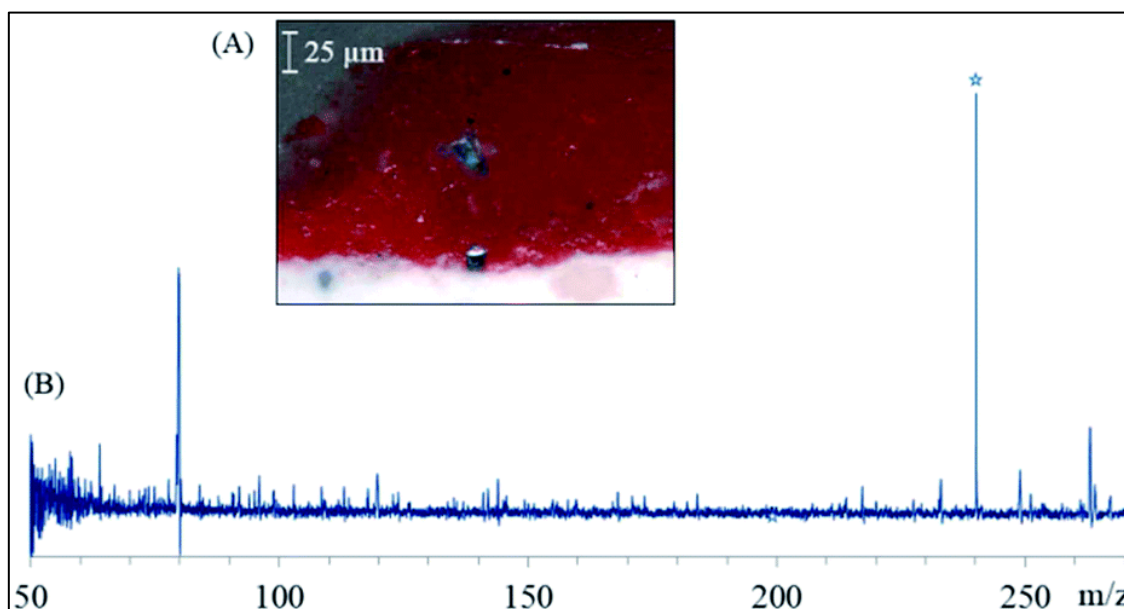


Figure 40: Non-resonant spectrum of alizarin, after proximal probe TD.

We performed additional experiments using modern synthetic pigments PV19 and PO43. Figure 39 shows a microscope image of a cross-section consisting of a sequence of layers (from bottom to top: titanium white, PV19, PO43, PY151, PR254). Figure 5b shows the mass spectrum produced from the layer of PV19, where the parent peak is visible at m/z

312.32. Figure 5c shows the mass spectrum of the PO43 layer. The parent peak of PO43 can be seen at m/z 412.41. There was little indication of any fragmentation in the modern synthetic pigments, although it is worth noting these were pure standards. In contrast, traditional colorants such as alizarin crimson are complex mixtures of molecules because they are often obtained through plant and animal matter, and consequently have complex spectra. Desorption depression sizes in the modern synthetics ranged from 750-2500 μm , likely due to melting of the paint medium (Elmer's Glue) by the radiant heat from the probe tip. There was no indication of any PV19 desorption or detection in the PO43 layer, nor vice-versa, demonstrating the absence of cross contamination and confirming the high spatial resolution.

To complement work done on the natural organic dye, a cross-section containing the traditional red organic colorant alizarin crimson was used. Fig. 40 shows a microscope image of this cross section. Following AFM-TD of the alizarin layer, we performed laser desorption mass spectrometry using a 193 nm excimer laser for ionization. The parent peak corresponding to the alizarin chromophore can be seen at m/z 240.21. Several other species also appear, indicative of the complex nature of these natural organic dyes. Analogous non-resonant laser ionization experiments with standard alizarin crimson dye (without the AFM-TD step) were performed to determine whether additional fragments were created in the AFM-TD heating step. The results indicated that though some additional fragmentation did occur, the vast majority of the mass peaks were identical. The limited additional fragmentation was likely due to thermal fragmentation during the relatively slow heating rate of the AFM-TD process. Nonetheless, in each case, intact molecules were successfully thermally desorbed, transferred, and detected in a mass spectrometer. As evident by the

small size of the sampling depressions (750 nm diameter), several samples within even the thinnest paint layers could be obtained while maintaining the bulk of the cross-sections for further analytical work. Figure 41 show the typical topography of a layer of paint both before and after thermal desorption.

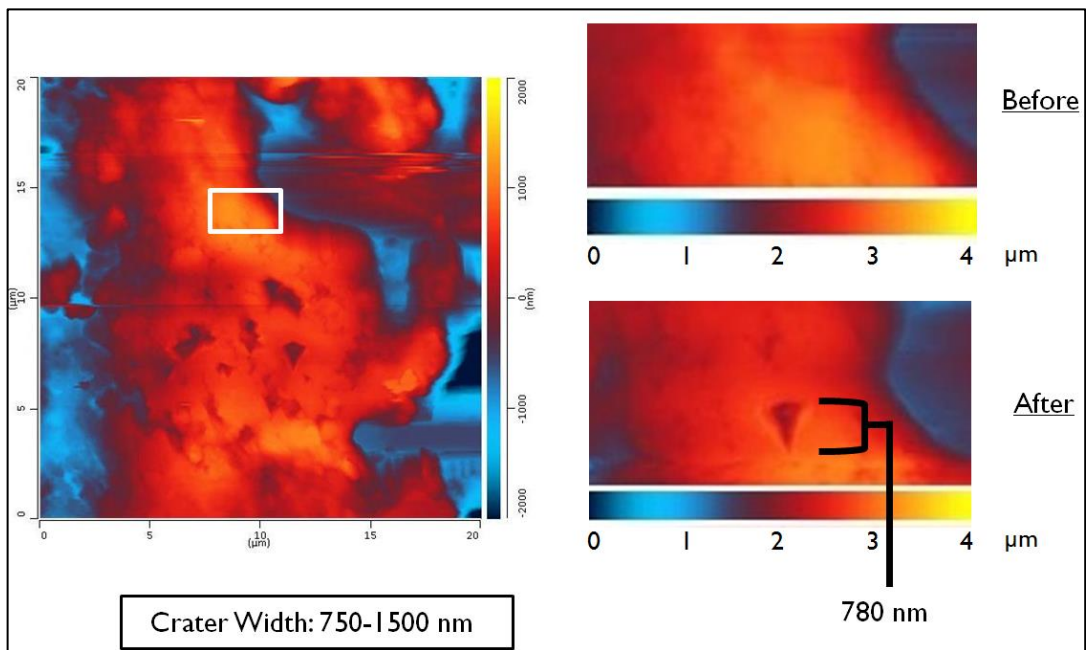


Figure 41: AFM topographical image of painting cross section on left. Images on right represent enlarged area within white rectangle, both before (upper) and after (lower) proximal probe TD.

D. Summary

We have demonstrated a new approach for coupling proximal probe AFM-TD and subsequent chemical analysis in separate steps. This approach allows the use of a diverse set of techniques adapted to the characteristics of each individual sample on a case by case basis. By using R2PI mass spectrometry for the separate analysis step, this new sample collection method provides a format for unambiguously identifying specific organic colorants. This approach should be particularly well-suited for samples in which the spatial resolution of other available analytical techniques is insufficient to probe, such as thin layers

or small inclusions of an unknown organic material. Further work is needed to catalogue the response of different target compounds of interest in the sampling step as well as their spectra for R2PI analysis. Forthcoming work will be extended to identify different binding media, including oil, gum, varnishes and more complex mixtures of organic and inorganic pigments, as these are more representative of authentic cultural heritage artifacts. This method can also be extended to other fields of research which face similar challenges in spatially resolved organic analysis.

1. C. L. Evans, E. O. Potma, M. Puoris'haag, D. Cote, C. P. Lin and X. S. Xie, *P Natl Acad Sci USA*, 2005, 102, 16807-16812.
2. D. A. Muller, L. F. Kourkoutis, M. Murfitt, J. H. Song, H. Y. Hwang, J. Silcox, N. Dellby and O. L. Krivanek, *Science*, 2008, 319, 1073-1076.
3. G. J. Van Berkel, S. P. Pasilis and O. Ovchinnikova, *J Mass Spectrom*, 2008, 43, 1161-1180.
4. D. R. Ifa, N. E. Manicke, A. L. Dill and G. Cooks, *Science*, 2008, 321, 805-805.
5. F. Dinelli, M. Murgia, P. Levy, M. Cavallini, F. Biscarini and D. M. de Leeuw, *Phys Rev Lett*, 2004, 92.
6. H. C. Yang, T. J. Shin, M. M. Ling, K. Cho, C. Y. Ryu and Z. N. Bao, *J Am Chem Soc*, 2005, 127, 11542-11543.
7. R. M. Overney, E. Meyer, J. Frommer, H. J. Guntherodt, M. Fujihira, H. Takano and Y. Gotoh, *Langmuir*, 1994, 10, 1281-1286.
8. L. M. Do, E. M. Han, Y. Niidome, M. Fujihira, T. Kanno, S. Yoshida, A. Maeda and A. J. Ikushima, *J Appl Phys*, 1994, 76, 5118-5121.
9. M. J. Doktycz, C. J. Sullivan, P. R. Hoyt, D. A. Pelletier, S. Wu and D. P. Allison, *Ultramicroscopy*, 2003, 97, 209-216.
10. P. Schaer-Zammaretti and J. Ubbink, *Ultramicroscopy*, 2003, 97, 199-208.
11. O. S. Ovchinnikova, V. Kertesz and G. J. Van Berkel, *Anal Chem*, 2011, 83, 598-603.

12. O. S. Ovchinnikova, M. P. Nikiforov, J. A. Bradshaw, S. Jesse and G. J. Van Berkel, *Acs Nano*, 2011, 5, 5526-5531.
13. J. A. Bradshaw, O. S. Ovchinnikova, K. A. Meyer and D. E. Goeringer, *Rapid Commun Mass Sp*, 2009, 23, 3781-3786.
14. M. M. Nudnova, L. Zhu and R. Zenobi, *Rapid Commun Mass Sp*, 2012, 26, 1447-1452.
15. G. Meijer, M. S. Devries, H. E. Hunziker and H. R. Wendt, *Applied Physics B-Photophysics and Laser Chemistry*, 1990, 51, 395-403.
16. L. I. Grace, A. Abo-Riziq and M. S. deVries, *J Am Soc Mass Spectr*, 2005, 16, 437-440.
17. M. S. Devries, D. J. Elloway, H. R. Wendt and H. E. Hunziker, *Rev Sci Instrum*, 1992, 63, 3321-3325.
18. D. M. Price, M. Reading, A. Hammiche and H. M. Pollock, *Int J Pharm*, 1999, 192, 85-96.
19. D. M. Price, M. Reading, A. Hammiche and H. M. Pollock, *J Therm Anal Calorim*, 2000, 60, 723-733.
20. D. M. Price, M. Reading, T. J. Lever, A. Hammiche and H. M. Pollock, *Thermochim Acta*, 2001, 367, 195-202.
21. O. S. Ovchinnikova, K. Kjoller, G. B. Hurst, D. A. Pelletier and G. J. Van Berkel, *Anal Chem*, 2014, 86, 1083-1090.
22. J. Lee, T. L. Wright, M. R. Abel, E. O. Sunden, A. Marchenkov, S. Graham and W. P. King, *J Appl Phys*, 2007, 101.
23. B. Lee, C. B. Prater and A. P. King, *Nanotechnology*, 2012, 23.

24. W. P. King, T. W. Kenny, K. E. Goodson, G. L. W. Cross, M. Despont, U. T. Durig, H. Rothuizen, G. Binnig and P. Vettiger, *J Microelectromech S*, 2002, 11, 765-774.
25. J. Lee, T. Beechem, T. L. Wright, B. A. Nelson, S. Graham and W. P. King, *J Microelectromech S*, 2006, 15, 1644-1655.
26. R. J. Cannara, A. Sebastian, B. Gotsmann and H. Rothuizen, *2009 9th Ieee Conference on Nanotechnology (Ieee-Nano)*, 2009, 781-783.
27. J. H. Bae, T. Ono and M. Esashi, *Appl Phys Lett*, 2003, 82, 814-816.
28. D. W. Lee, M. Despont, U. Drechsler, C. Gerber, P. Vettiger, A. Wetzel, R. Bennewitz and E. Meyer, *Microelectron Eng*, 2003, 67-8, 635-643.
29. U. Drechsler, N. Burer, M. Despont, U. Durig, B. Gotsmann, F. Robin and P. Vettiger, *Microelectron Eng*, 2003, 67-8, 397-404.
30. B. W. Chui, T. D. Stowe, T. W. Kenny, H. J. Mamin, B. D. Terris and D. Rugar, *Appl Phys Lett*, 1996, 69, 2767-2769.
31. B. D. Terris, H. J. Mamin, M. E. Best, J. A. Logan, D. Rugar and S. A. Rishton, *Appl Phys Lett*, 1996, 69, 4262-4264.
32. W. P. King, Bhatia, B., Felts, J., Kim, H.J., Kwon, B., Lee, B., Somnath, S, Rosenberger, M, *Annual Review of Heat Transfer*, 2013, 287-326.
33. D. Irimia, D. Dobrikov, R. Kortekaas, H. Voet, D. A. van den Ende, W. A. Groen and M. H. M. Janssen, *Rev Sci Instrum*, 2009, 80.
34. M. P. Callahan, Z. Gengeliczki, N. Svadlenak, H. Valdes, P. Hobza and M. S. de Vries, *PCCP*, 2008, 10, 2819-2826.

Chapter V. Organic Residue Analysis in Ancient Pottery

A. Chemistry, Archaeology, Archaeometry and Anthropology

Archaeology, or more specifically archaeometry, is a discipline that relies on physical evidence to draw conclusions about the history of humanity from culturally significant objects such as ancient tools, metalwork, bones, pottery and a vast array of other materials. It is a science based primarily on the unbiased interpretation of the most clearly defined data available. Conversely, an anthropologist's knowledge is often based ultimately on interpersonal and intersubjective ideas and characterizations of cultures.¹ Clifford Geertz, a well-respected and influential anthropologist, once remarked on “the oddity of constructing texts ostensibly scientific out of experiences broadly biographical.”² A general consensus within the field can often be agreed upon without clear and indisputable evidence, and it can be a difficult task to challenge what is often a deeply entrenched theory or concept.

The molecular analysis of both inorganic and organic compounds within an archaeological artifact can be paramount in determining the manufacturing process of the item, exposing new trade routes, or shedding light on resources and diets within different regions of the world. Due mostly to the very durable nature of inorganic based artifacts (e.g. glass, ceramic, metals), most early research focused on inorganic elemental identification, but a variety of recent technological enhancements has made organic residue analysis a much more practical option. One of the most common sources of organic residues is within pottery, usually found in the form of broken fragments or ‘sherds’ due to their high affinity for long-term storage of these compounds.

The earliest evidence of pottery use by humans is attributed to hunter-gatherers from East Asia, dating to between 12,000 and 20,000 years ago and was most likely developed as a means to stock food, beverage, and most likely a surplus of other products.³ Fortunately, pottery sherds are found in relatively large abundances compared to other objects of cultural heritage allowing for in depth characterization studies. Slipped pottery is particularly common, and has the additional advantage of being water permeable which allows for long term storage of organic residues within the structure of the sherds.

A.1. Current Analytical Methods

Analysis of organic compounds in pottery sherds has long relied on the use of infrared spectroscopy⁴⁻⁶, separation techniques such as gas chromatography-mass spectrometry (GC-MS) and liquid chromatography-mass spectrometry (LC-MS)^{5, 7-15}, and optical microscopy (including polarized light microscopy and ultraviolet (UV) imaging).^{5, 16, 17} Chromatographic techniques, while providing a wealth of information, often cannot be routinely applied due to the relatively large (microgram) sample-size, and sample consumption, requirements of most GC and LC techniques. Optical and fluorescence microscopy, while informative, does not directly provide *chemical* information.¹⁸ Fourier transform infrared (FTIR) microscopy of samples from works of art can provide specific identification of organic (as well as some inorganic) compounds, but can be challenging since the organic materials often are present as part of an extremely complex mixture.¹⁹ The continued development of attenuated total reflection (ATR) FTIR²⁰⁻²² has begun to address these challenges. Still, FTIR spectroscopy is limited by the inability to reliably differentiate between compounds that share chemical moieties, and thus often can only identify the class of material present, rather than the specific individual chemical species. Therefore, there remains a need for the development of

complementary techniques that can provide molecularly-specific and unambiguous identification of organic residues within objects of cultural heritage, specifically pottery sherds.

A.2. Methylxanthine Plants

Many of these ceramic containers were used to store mind-altering ingredients; some of the most commonly seen constituents found in pottery are caffeine, theobromine and theophylline (Figure 43). The Mesoamerican region, extending from central Mexico down to northern Costa Rica, is a particularly common carrier of these molecules. These compounds are found within a class of purine bases known as methylxanthines, and in fact are still enormously popular today in drinks such as coffee, tea, and more recently yerba mate. Caffeine in particular acts on humans by binding to receptor sites for the neurotransmitter adenosine, increasing neuronal activity and stimulating the secretion of epinephrine-leading to a stimulating effect.²³ Serving as natural pest deterrents, these three methylxanthines are found in over 13 orders of plants, comprising well over 100 different plant species (this number is expected to be much higher, as there are close to 250 different species of tea, and over 80 species of coffee which have not been confirmed to contain the methylxanthines but most likely do) and are often used as molecular markers to identify geo-cultural origins of pottery sherds.²⁴ Furthermore, each plant species has a characteristic concentration of each methylxanthine, which is commonly used to determine the precise species of plant serving as the source of the organic residues in question (Table 3). The following studies focus on species originating in North and South America, as these were considered the most likely sources of methylxanthines found in Maya pottery sherds under investigation. Figure 42 shows a map depicting the geographical origins of each relevant plant species.

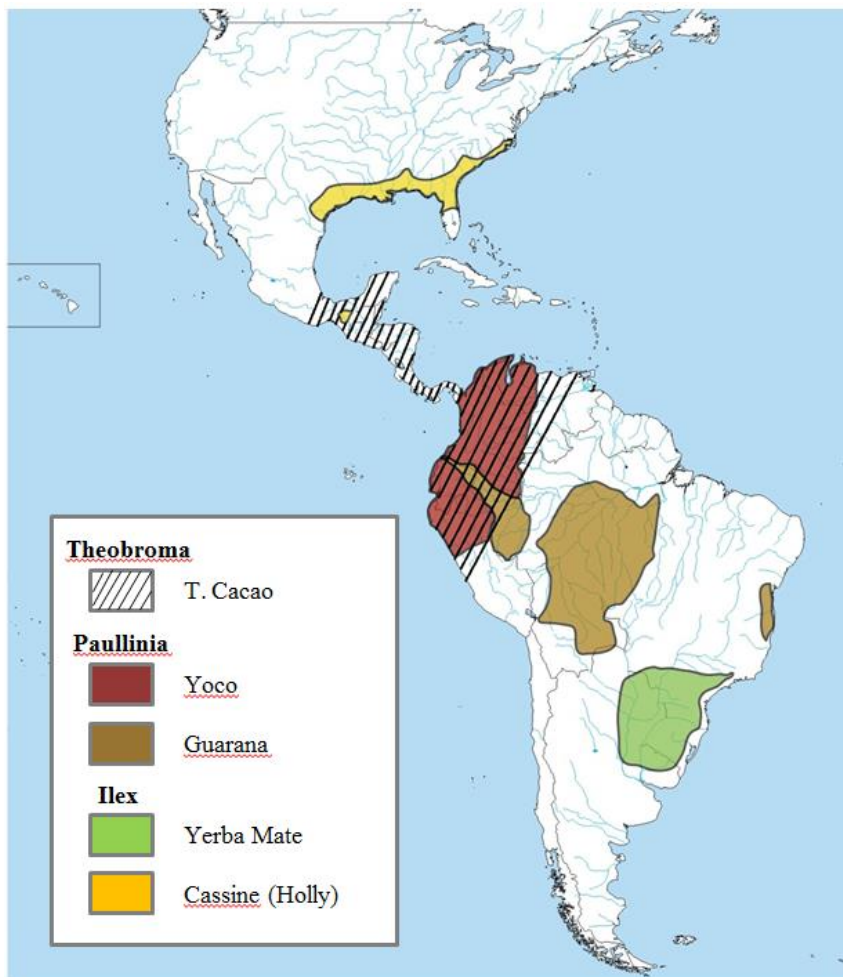


Figure 42: Geographical origins of methylxanthine containing plants.

Table 3: Methylxanthine quantities within plants of interest.

Genus	Species	Theobromine	Theophylline	Caffeine
		(mass % of dry weight)		
Theobroma	<i>T. cacao</i>	1.4% - 2%	0.3% - 0.4%	0.2% - 0.9%
Ilex	<i>I. paraguariensis</i> (yerba mate)	0.3% - 0.9%	trace	1% - 2%
	<i>I. cassine</i> (holly)	0.22%	ND	0.12%
	<i>I. vomitoria</i> (holly)	0.11%	ND	0.56%
Paullinia	<i>P. yoco</i>	0.05%	ND	0.3% - 0.4%
	<i>P. cupana</i> (guarana fruit)	0.015%	0.01%	4.28%

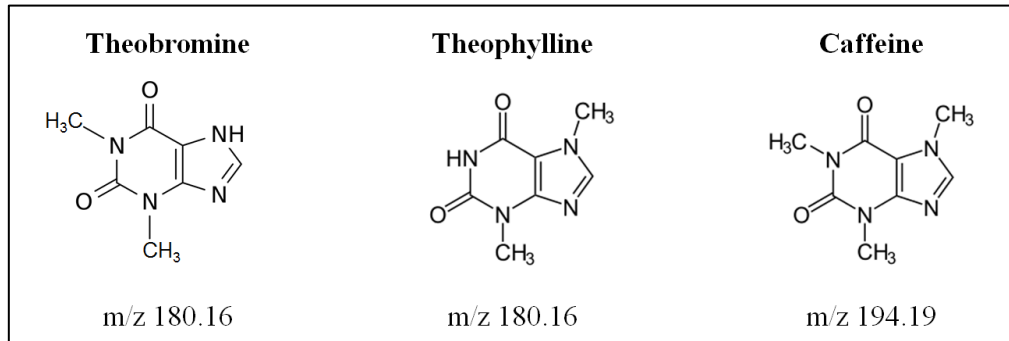


Figure 43: The three methylxanthine molecular markers.

Theobroma

As a member of the theobroma genus, the cacao bean (*Theobroma cacao*) originates from a tree confined to within the tropical regions of South America and Mesoamerica.²⁵ The ground seeds, or pods (Figure 44), produced by the tree were ground up and mixed with other ingredients (water, maize, honey) to make a drink that had a mild stimulating effect.³ It was a particularly important cultural icon in Mesoamerican society, and has been consumed by the Maya as early as 600 BC³ in addition to being the precursor to modern day chocolate.



Figure 44: Cacao beans from *Theobroma Cacao*.

Although cacao does contain more than 500 different molecules, the vast majority of which are not exclusive to cacao and consequently cannot be used as unique molecular markers. This complexity often instead makes the unambiguous identification of molecular markers very difficult. Methylxanthines such as theobromine, theophylline and caffeine are

comparatively restricted to a handful of different species and are thus used as unique molecular fingerprints allowing for their use as indicators for several different plant species. An additional advantage these methylxanthines possess is the fact that they are easily extracted using organic solvents. With respect to cacao, the presence of theobromine as the dominant methylxanthine is commonly accepted as indisputable proof that sherds did contain a cacao based beverage. This is due to the fact that the cacao plant is believed to be the only Mesoamerican plant whose primary methylxanthine derivative is theobromine.^{3, 26}

For instance, Hester et al. used high-performance liquid chromatography (HPLC) coupled to atmospheric-pressure chemical-ionization mass spectrometry (APCI MS) to analyze pottery sherds from Colha, located in Northern Belize. The presence of both caffeine and theobromine led to the conclusion that the sherds, dating back over 2600 years, were direct evidence of cacao use.³ Powis et al. also used a combination of liquid chromatography and mass spectrometry to identify theobromine in sherds from southern Mexico, and established that cacao products did play a role in rituals for sacrificial victims, based analysis of related artifacts.²⁷ McGovern et al. analyzed sherds for theobromine originating from the Ulua Valley in modern day Honduras with LC-MS as well, showing that the use of cacao stretched back to 1000 BC, which is in fact the earliest evidence of cacao use by in any part of the world.²⁸

Ilex

Similar to cacao in Mesoamerican cultures, people from regions around modern day American gulf coast prepared a black tea made from the yaupon holly (*I. vomitoria*) and the dahoon holly (*I. cassine*). Both species contain caffeine and theobromine, but is not believed

to contain theophylline.^{24, 29} The primary methylxanthine in yaupon holly is caffeine followed by theobromine, while dahoon holly has higher concentrations of theobromine.²⁹



Figure 45: Holly berries from *Ilex Vomitoria*.

Recent and highly controversial research has suggested the existence of an extensive trade between the people of Mesoamerica and those from the American Southwest, based on the existence of theobromine residue in sherds in northwestern New Mexico.³⁰ This is in conflict with most widely accepted concepts, in which there was little or no commerce between these peoples. It was reported that plant databases do suggest there is not a plant native to the American Southwest that contains theobromine.³⁰ Theobromine found in these sherds was attributed to cacao, supposedly revealing a previously unknown trade route, despite the fact that a methylxanthine containing plant (*I. vomitoria*) found along the American Gulf Coast contains a significant amount of theobromine.³¹

Another plant belonging to the same *I. vomitoria* genus as holly, is a species most commonly known as yerba mate (*I. paraguariensis*), seen in Figure 46. It originates from South America, specifically regions of Brazil, Paraguay and Argentina³² and has historically been prepared by infusing the leaves and twigs³³. Mate does and does indeed contain all three methylxanthines of interest, with the concentration of caffeine being the highest, followed closely by theobromine, while theophylline is present in only small quantities.³⁴⁻³⁷



Figure 46: Yerba mata, or *Ilex paraguariensis*.

Paullinia

Undeniably, the least examined genus of methylxanthine containing plants is Paullinia, most commonly found in the central Amazon region.³⁸ Though it contains over 180 species, there are only two that have been reported to contain methylxanthines: Paullinia cupana (*P. cupana*) and Paullinia yoco (*P. yoco*). The bark of *P. yoco* (Figure 47, left) is used to prepare a beverage, while the fruit serves as the source of the stimulants in *P. cupana* (Figure 47, right), more commonly known as guarana fruit.³⁹ Both are dominated by the presence of caffeine, but also contain trace amounts of theobromine and theophylline as well.^{38, 40}



Figure 47: Paullinia yoco (left), and guarana fruit (right).

A.3. Organic Residues as Molecular Markers

When choosing a molecular marker, one must take huge cautions in confirming that the molecule in question is exclusive to the object of interest. Food and beverage residue analysis are particular problems because finding truly unique compounds is difficult. High amounts of theobromine relative to theophylline and caffeine, as discussed above, are used as conclusive evidence of cacao usage despite evidence that they commonly found in several other sources in South, Central, and North America. While high concentrations of theobromine, theophylline and caffeine are primarily restricted to the genera *Camellia*, *Coffea*, *Cola*, *Paullinia*, *Ilex* and *Theobroma*. And of these genera, only *Theobroma*, *Ilex*, and *Paullinia* are found in North and South America. Archaeometry scientists therefore, must take extra precautions when determining the origins of organic residues.

To complicate matters further, there are an abundance of other factors that can heavily influence ratios of methylxanthines within pottery sherds. It is important to know how the samples were handled in the field (e.g. cross contamination), what types of solutions were used to wash the samples, how water soluble each marker is, or whether the sherds are prone to absorbing compounds dissolved in surrounding groundwater. Additionally, just as is common now, these vessels likely contained an assortment of diverse substances as opposed to one. The exact method that these drinks were prepared, as well as which part of the plant was harvested, can also have a significant impact on the level of methylxanthines. Reber et al. have also shown that there can be considerable interaction between buried sherds and their surrounding soil, and therefore advise local soils to be sampled concurrently with sherds to help account for any influence the soil may have.²⁴

Figure 48 shows the specific stratigraphy found around the sherds that were analyzed in this

dissertation⁴¹, and illustrates the difficulty of indisputably establishing the origins of molecular markers without taking many other factors into account.

Contamination of methylxanthines within sherds by microbes can also be significant factor, as reported by D.K. Washburn et al.³¹ One pathway for such bacterial metabolism of caffeine involves the conversion to theobromine and paraxanthine, and eventually to 7-methylxanthine and xanthine³¹. The presence of paraxanthine can therefore be used to decrease the likelihood that caffeine metabolism contributed to the presence of theobromine. Environmental contamination tends to be a large problem as well, particularly in this class of methylxanthines because of their large presence in the contemporary world. Washburn insightfully examined dust that had settled in various areas throughout six different museums in six different cities, and each sample revealed low levels of both theobromine and theophylline with higher and more variable levels of caffeine³¹.

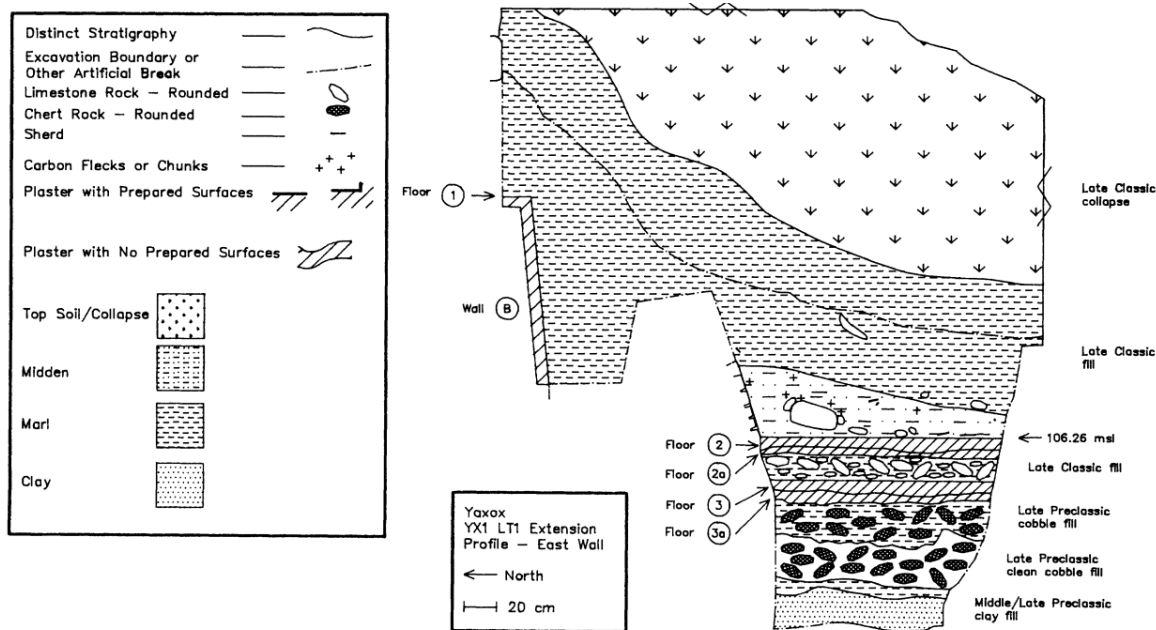


Figure 48: Soil topography in El Pilar.

Unambiguous identification of beverage residues, especially using methyl xanthines, is a highly complex problem that requires scrutiny based not only on scientific evidence and

knowledge of the ethnobotanical history of an area, but also how these objects have interacted with their environment over thousands of years. It is therefore very difficult to unambiguously identify the source of the organic residues in pottery, as it is often quite difficult to determine the degree to which the objects have been altered. Ultimately, researchers must go to great lengths to consider only scientific evidence, rather than attempt to fit the evidence to accepted anthropological theories.

Clearly, the ability to use several molecular markers is hugely advantageous in correctly identifying geo-cultural origins of organic residues. There are indeed several other methylxanthine derivatives that are present in very small quantities that have yet to be extensively explored, particularly theacrine, liberine and methyliberine.

B. El Pilar Pottery

Pottery sherds dating to 600-900 CE were generously donated by Dr. Anabel Ford, who discovered the Belize River Archeological Settlement Survey (BRASS), located on the modern day border of Guatemala and Belize. The entirety of the collection studies was found in the El Pilar settlement, shown in Figure 49.^{27, 41} This was a logistically advantageous area, as it was on the furthest upstream portion of the region's most important navigable river. The sherds were collected, washed extensively with water to clear any debris from the surface, and then stored together in plastic bags. A photo of several sherds is shown in Figure 50.

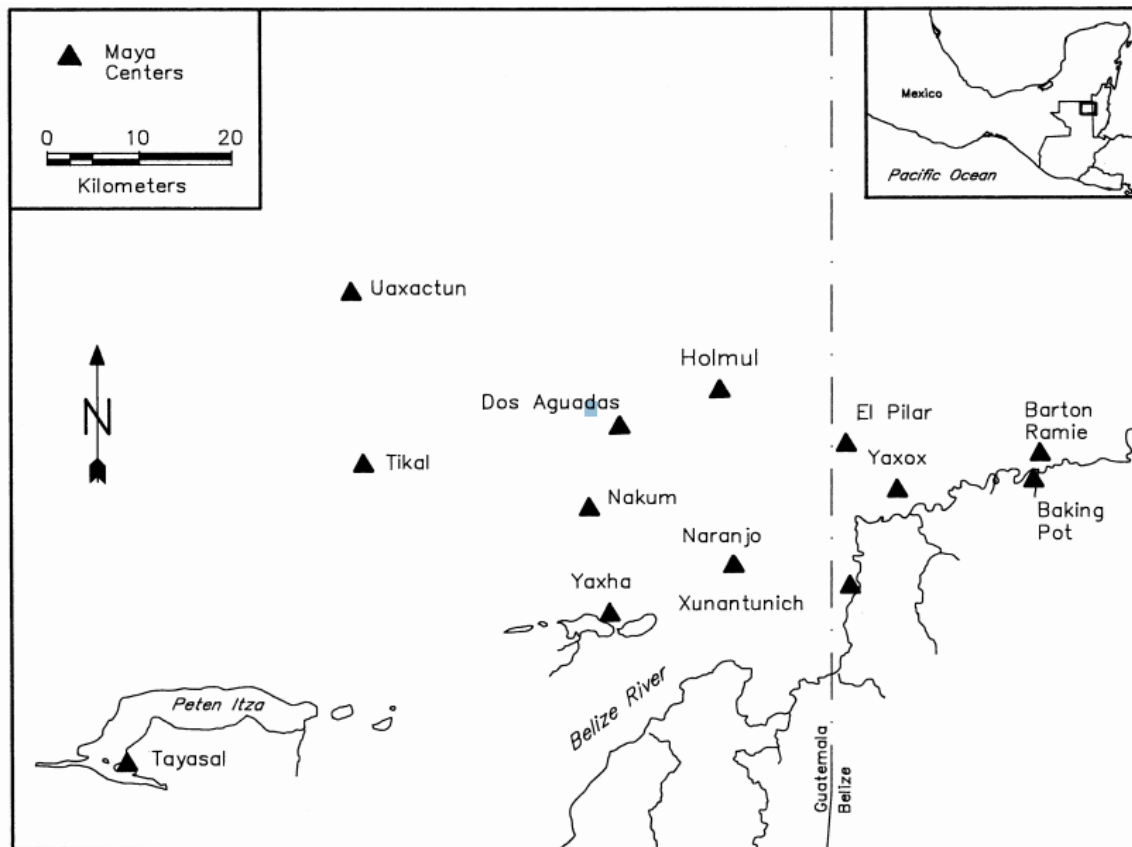


Figure 49: Location of El Pilar, on the border of Belize and Guatemala.

B.1. R2PI Spectroscopy

The R2PI spectroscopy of several methylxanthines is known and has been extensively studied by Callahan et al.⁴² Further, R2PI spectroscopy is easily able to distinguish between the isomers theobromine and theophylline, as can be seen in Figure 51. Despite differing only by the placement of a methyl group, theobromine and theophylline have significantly different R2PI spectra, allowing for their selective ionization and unmistakable identification. Moreover, while methods commonly used for organic residue analysis in pottery such as HPLC-MS⁴¹ require highly invasive extractions involving organic solvents, the de Vries laboratory has demonstrated the remarkable advantage of directly laser desorbing from the sherd material.

B.2. Experimental

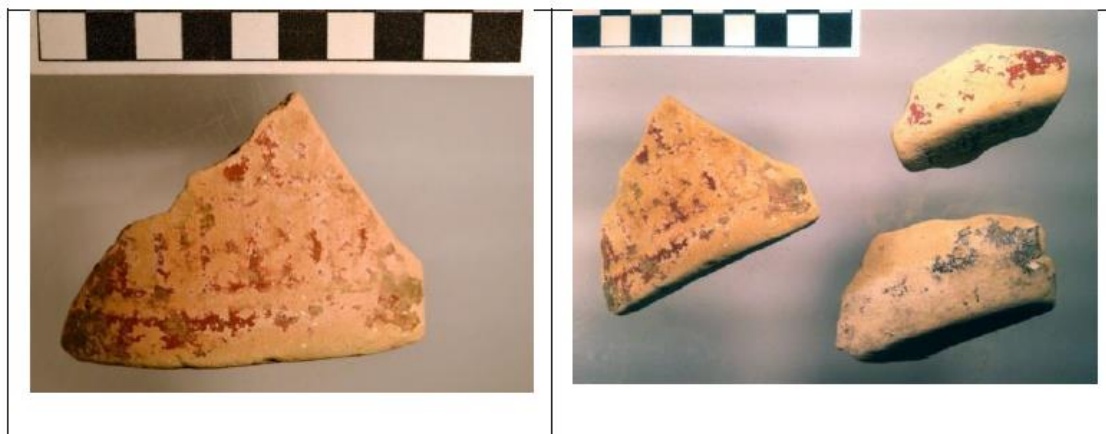


Figure 50: Maya pottery sherds.

Caffeine, theophylline and theobromine pure standards were obtained, and the R2PI spectroscopy was re-established on each prior to receiving the pottery sherds to serve as a control. A total of 13 sherds were analyzed for each of these three methylxanthines.

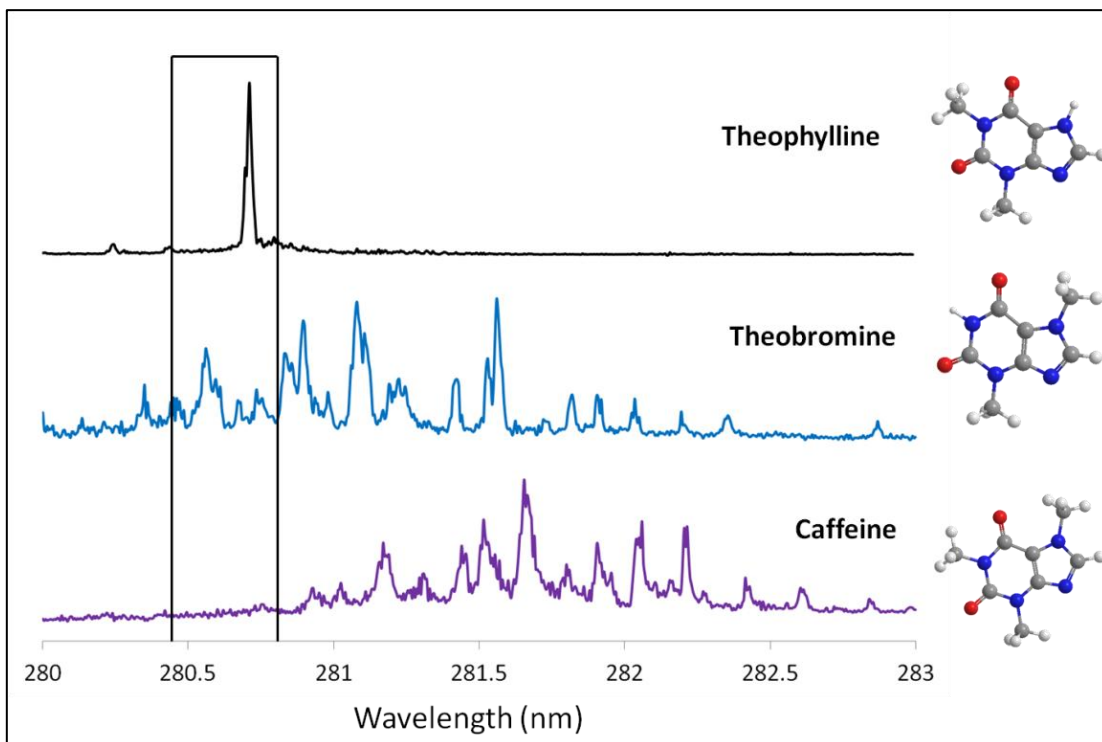


Figure 51: R2PI spectra of target methylxanthines. Rectangle represents an area with shared optical activity.

Sherds were each independently scraped to obtain material in a powder form (≈ 400 mg), and the powder was either extracted (72 hrs, 3mL 3:1 acetone:water) or placed on double sided tape on top of the graphite sample bar, prior to being loaded into the beam machine. Extracted samples were filtered and drop-cast with an automatic syringe (2-3 mL) onto gold plated sample bars, and allowed to evaporate under mild heating (65-75 °C). Gold bars required a desorption wavelength of 266 nm, while 1064 nm was used for the crushed sherd on graphite (wavelengths chosen according to substrate, not adsorbate). Two methods were performed to verify the presence of the target methylxanthines: (1) mass-selected spectroscopy and (2) optically-selected mass spectrometry. Mass-selected spectroscopy was achieved by scanning the wavelength of the excitation laser within spectroscopically active windows of each molecule, and was completed on both the extract in addition to a direct desorption from the sherd powder. Optically-selected mass spectrometry was accomplished by identifying a strong R2PI signal for each methylxanthine, but more importantly a signal that was unique to each target molecule (this was especially important for theophylline and theobromine, as they have an identical mass). The excitation laser was then tuned to this wavelength rather than being scanned, and mass spectra were collected from the selective ionization of each target molecule.

B.2. Results and Discussion

Table 4 shows a summary of the results gathered from all experiments. The data from the analysis of extract revealed some levels of all three methylxanthines in each sherd, excluding sherd 11. Possible explanations for this will be discussed later. R2PI analysis of extracts seems to suggest much lower levels of theobromine than theophylline, with caffeine

being easiest of the group to identify within the sherds. This is based on the amount of signal seen for each molecule.

Table 4

#	Site Origin	Zone	<u>Desorption from Extract</u>			<u>Direct Desorption from Sherd Scrapings</u>		
			Theobromine	Theophylline	Caffeine	Theobromine	Theophylline	Caffeine
1	Med Rank House	Valley	Positive	Positive	Positive	Positive	Positive	Positive
2	High Rank House	Ridgeland	Positive	Positive	Positive	Not Tested	Positive	Positive
3	Small Rank House	Foothills	Positive	Positive	Positive	Not Tested	Positive	Positive
4	Minor Center	Foothills	Positive	Positive	Positive	Positive	Positive	Positive
5	High Rank House	Ridgeland	Positive	Positive	Positive	Not Tested	Positive	Positive
6	High Rank House	Ridgeland	Positive	Positive	Positive	Not Tested	Positive	Positive
7	Med Rank House	Valley	Positive	Positive	Positive	Positive	Positive	Positive
8	Small Rank House	Valley	Positive	Positive	Positive	Not Tested	Positive	Positive
9	Small Rank House	Valley	Positive	Positive	Positive	Not Tested	Positive	Positive
10	Small Rank House	Valley	Positive	Positive	Positive	Not Tested	Positive	Positive
11	Small Rank House	Valley	Negative	Negative	Negative	Not Tested	Negative	Negative
12	Small Rank House	Valley	Positive	Positive	Positive	Not Tested	Positive	Positive
13	Small Rank House	Valley	Positive	Positive	Positive	Not Tested	Positive	Positive

Extract Analysis

Figure 52 shows the R2PI spectrum for pure theobromine and theophylline standards, in comparison to the equivalent spectrum from the extract of sherd 7. Note also the ability of R2PI to distinguish between theobromine and theophylline standards, molecules that differ only by the placement of a methyl group. While the observation of theophylline within the sherd is indisputable, the presence of theobromine was much less clear. A similar scan was performed for sherd 7 within a spectroscopically active window

for caffeine (281.4 nm – 282.0 nm), and can be seen in Figure 53. As discussed, caffeine was the most readily observable methylxanthine in when desorbing from an extract.

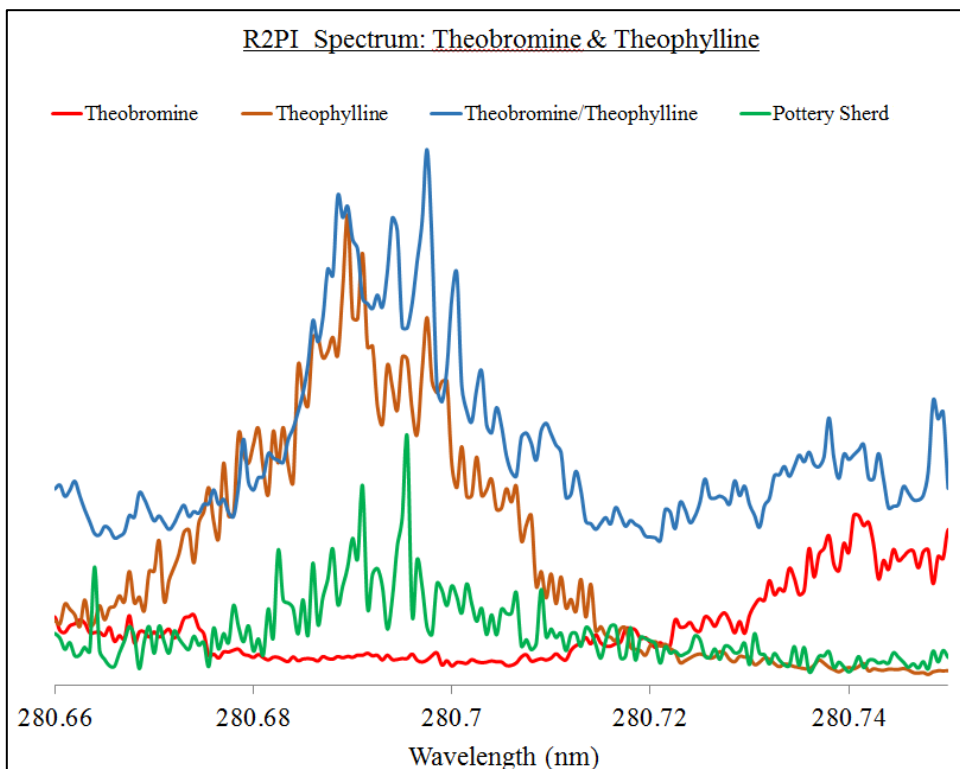


Figure 52: R2PI spectra of theobromine/theophylline standards, in addition to pottery sherd extract.

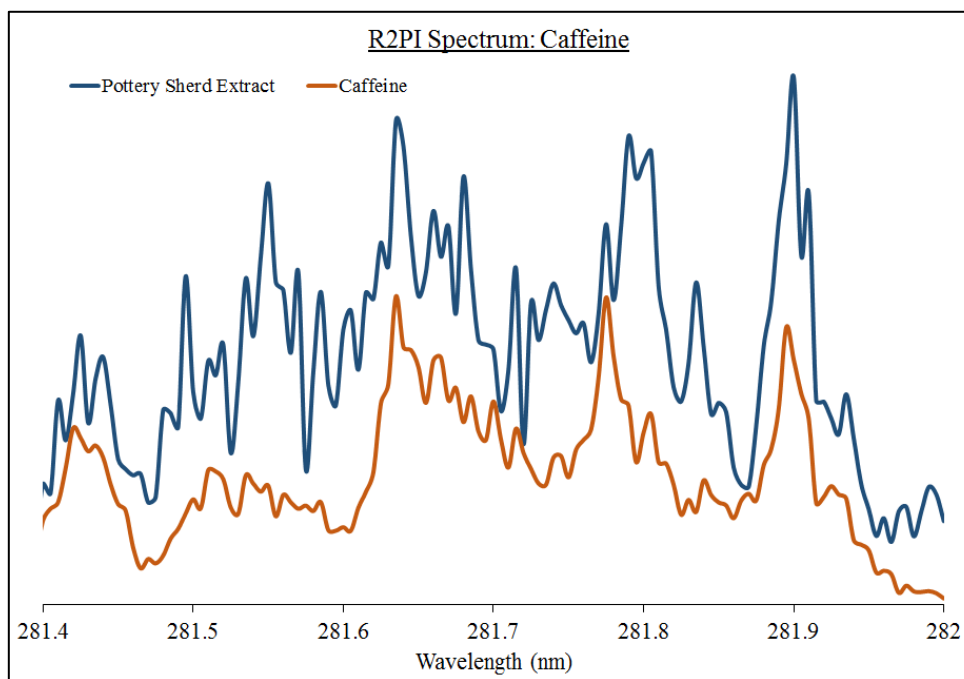


Figure 53: R2PI spectra of caffeine, in addition to pottery sherd extract.

In order to optimize conditions for each target methylxanthine, a wavelength correlating to a strong R2PI transition and unique to each methylxanthine was chosen to perform optically-selected mass spectrometry. The wavelengths chosen for each molecule can be seen in below in Figure 54, and Figures 56, 57 and 58 show the corresponding optically selected mass spectra of each methylxanthine. Reiterating an earlier point, all methylxanthines were detected within the extracts of all sherds except sherd 11.

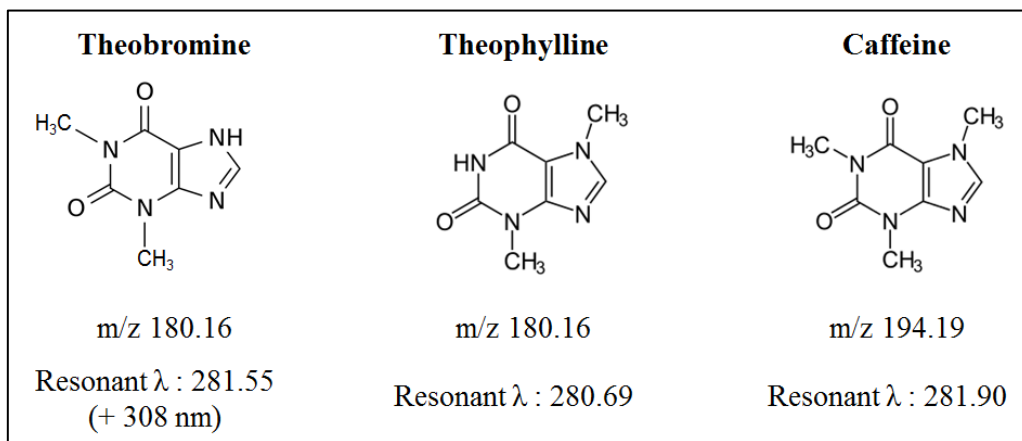


Figure 54: Target methylxanthines, along with respective wavelengths chosen for optically selected mass spectrometry.

Contrary to theophylline and caffeine, theobromine required the use of 2C-R2PI, with the first laser tuned to 281.55 nm and the ionization laser at 308 nm. Figure 55 is an illustration of the selective ionization of the target molecules within the extract, as ionization only occurs when the lasers are tuned to a highly specific resonance unique to each target molecule. Note also the nearly complete absence of any fragmentation, regardless of the fact that this is desorbed from the highly complex nature of an extract.

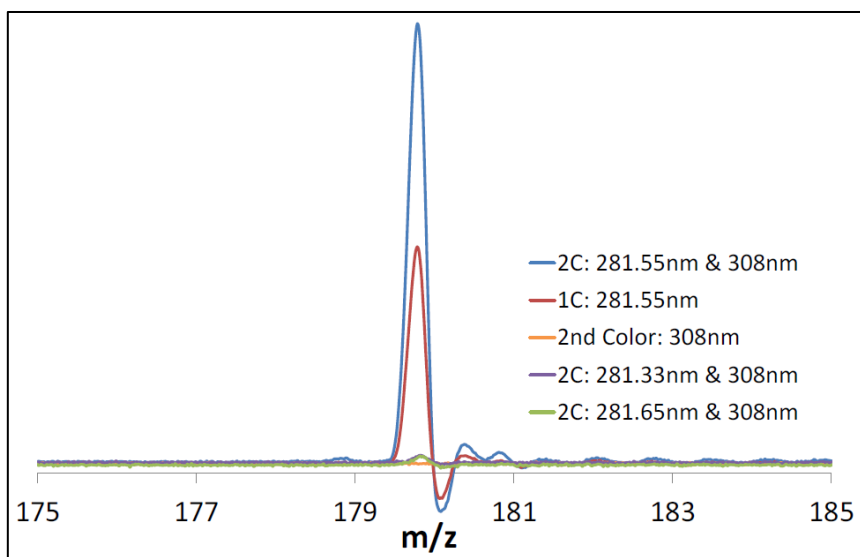


Figure 55: Advantages of 2C-R2PI seen in theobromine.

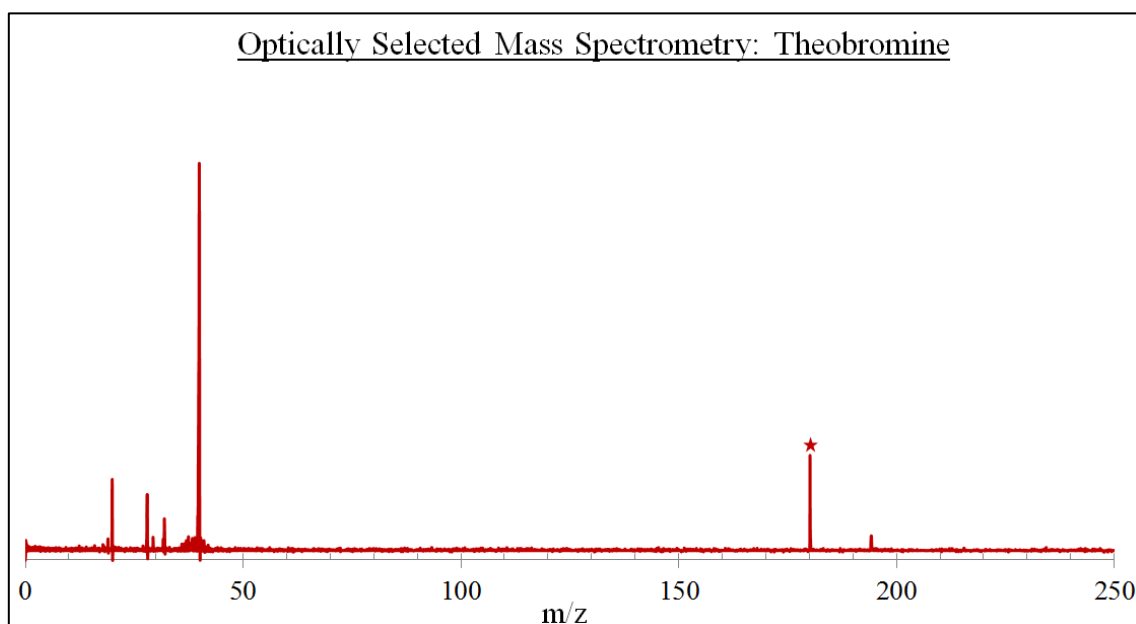


Figure 56: Optically-selected mass spectrum within pottery sherd. Asterisk represents theobromine parent peak.

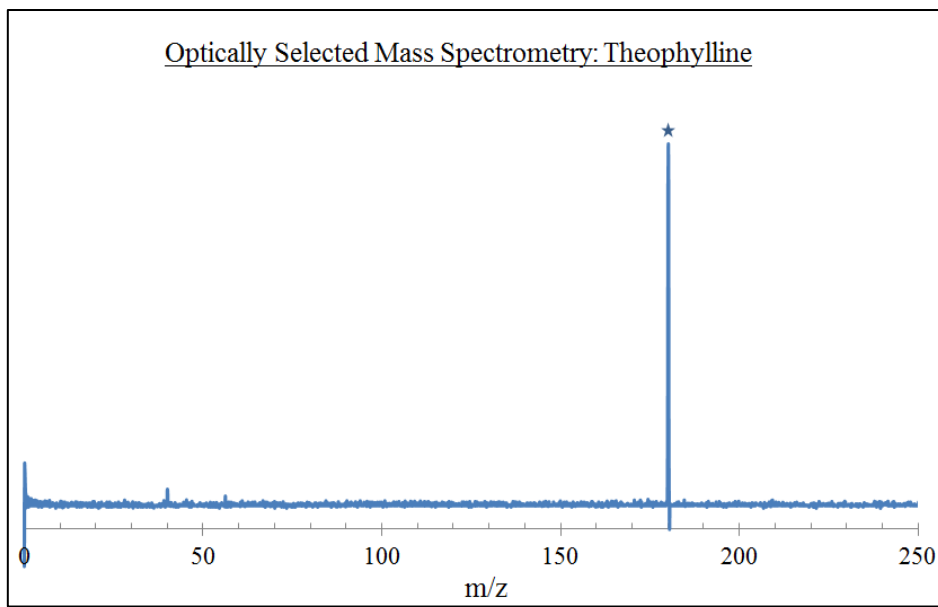


Figure 57: Optically-selected mass spectrum within pottery sherd. Asterisk represents theophylline parent peak.

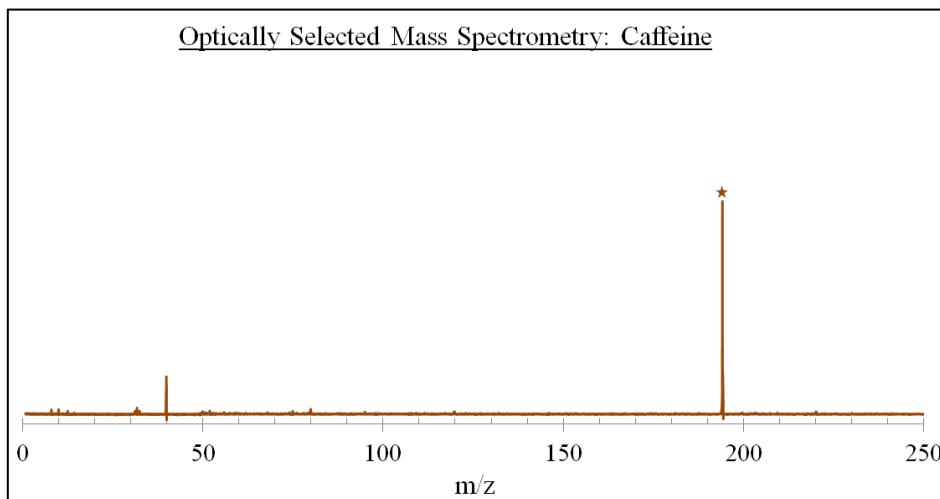


Figure 58: Optically-selected mass spectrum within pottery sherd. Asterisk represents caffeine parent peak.

Direct Sherd Analysis

In order to investigate the potential of directly desorbing from sherd material, scrapings of the sherds were also examined for methylxanthines. The large amount of material required for extraction (≈ 400 mg) often prevents any analysis of pottery sherds, as many of these items are essentially priceless. We have show that direct desorption from

pottery sherd material is indeed possible, and have successfully combined it with high resolution R2PI spectroscopy. Figure 59 shows the R2PI spectrum obtained from sherds 4 and 7, two different shaped vessels. This data suggested more theobromine residue in the pedestal base vessel, perhaps because it had a particularly unique usage.

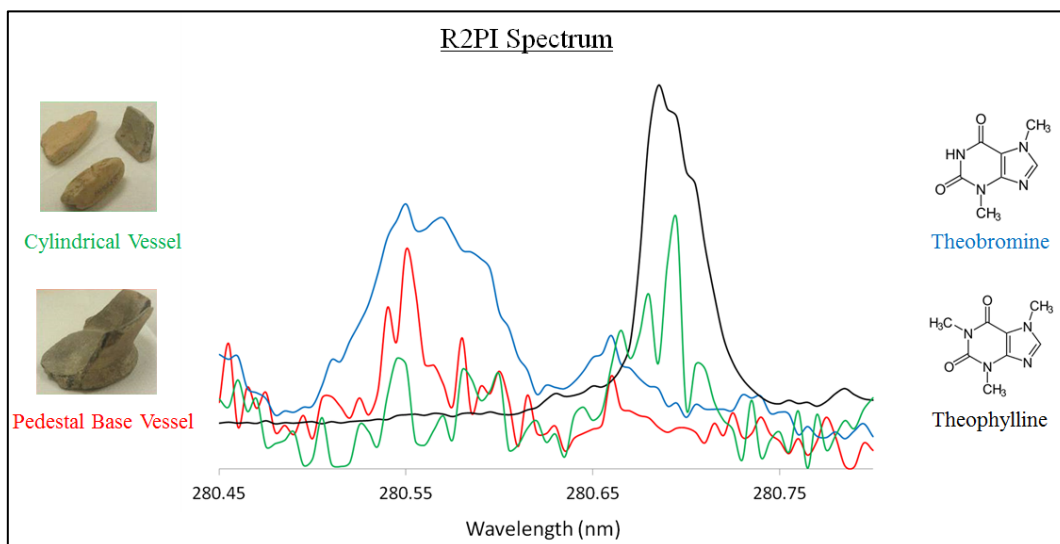


Figure 59: R2PI spectra of two different vessels, performed directly on sherd material.

C. Illinois River Sherds



Figure 60: Origin of Illinois river sherds.

Professor Greg Wilson, from the Department of Anthropology at the University of California Santa Barbara, donated 7 sherds from what is present day Fulton County, Illinois- collected from bluff tops on the western side of the Central Illinois River Valley flood plain denoted by red outline in Figure 60. The sherds originated from a Mississippian culture, and date back to between 1100-1200 CE. They were analyzed using the same procedures established with the Maya sherds. See TABLE for results indicating the presence or absence of each methylxanthine for each respective sherd. In total, five of these samples showed a strong presence of caffeine and theobromine, while just four displayed the presence of theophylline.

D. Summary

As discussed, the attribution of the geocultural origins of pottery sherds is a very complex task, requiring a deep understanding of numerous factors that can have a huge impact on the presence of certain organic residues. Some of these are out of the control of scientists (e.g. environmental impacts, solubility differences leading to different leaching rates, various clays impacting the affinity for long term storage of organic molecules), but many are certainly manageable. The initial washing and storage process for example, must be more tightly controlled. If possible, the use of water should be avoided at all costs and sherds should be collected in individual containers.

Great care must also be taken to distinguish between methylxanthines present as a result of airborne or any other contamination, and those existing as a result of definite prehistoric usage of the vessel. The possibility of these containers being used for multiple beverages containing our target methylxanthines must also be considered, and more unique

set of molecular markers therefore must be used in order to unambiguously identify specific plant sources.

Although the presence of all three methylxanthines in these Mesoamerican sherds does suggest that cacao is the likely source, it is irresponsible not to investigate other possible origins. This is specifically true after observing almost identical levels of each methylxanthine within the Illinois River sherds, originating over 200 miles northeast of any previously known evidence of cacao. Yet, if objectively analyzed, both sets of data do support the presence of cacao residue. If cacao is indeed the source of the methylxanthines found in the Illinois River sherds, it strongly suggest a previously unknown trade network between Mesoamerican and North American cultures.

It must also be pointed out, as earlier discussed, that there are currently well over 100 species of plants that contain these target methylxanthines. It would thus also be careless to not consider any of those sources. This is particularly true considering the fact that two of those sources have historically been amongst the widely consumed beverages, coffee and tea. Both contain the target methylxanthines in similar proportions to cacao, but are largely ignored as sources due to their geographical origins, as well as pre-conceived notions of when these plants arrived to the Americas. Coffee is believed to have originated in Africa and arrived in the Americas in 1720, while tea was first imported by the Dutch in the 17th century. It must at least be considered that coffee and tea could be the sources of these methylxanthines, as we don't have any evidence to suggest otherwise.

1. M. Carrithers, *Curr Anthropol*, 1990, 31, 263-282.
2. C. Geertz, *Works and lives : the anthropologist as author*, Stanford University Press, Stanford, Calif., 1988.
3. W. J. Hurst, S. M. Tarka, T. G. Powis, F. Valdez and T. R. Hester, *Nature*, 2002, 418, 289-290.
4. M. R. Derrick, J. M. Landry and D. C. Stulik, *Methods in scientific examination of works of art : infrared microspectroscopy*, Getty Conservation Institute Los Angeles, 1991.
5. D. Pinna, M. Galeotti and R. Mazzeo, eds., *Scientific Examination for the Investigation of Paintings. A Handbook for Conservator-restorers*, Centro Di della Edifimi srl, Florence, 2009.
6. R. H. Michel, P. E. Mcgovern and V. R. Badler, *Anal Chem*, 1993, 65, A408-A413.
7. J. S. Mills and R. White, *The Organic Chemistry of Museum Objects*, Butterworth-Heinemann, Oxford, Second edn., 1994.
8. M. P. Colombini and F. Modugno, eds., *Organic Mass Spectrometry in Art and Archaeology*, John Wiley & Sons, West Sussex, 2009.
9. J. Wouters and A. Verhecken, *Studies in Conservation*, , 1989, 34 189-200.
10. J. Wouters, *Stud. Conserv.*, 1985, 30, 119-128.
11. J. Wouters, C. M. Grzywacz and A. Claro, *Stud. Conserv.*, 2010, 55, 186-203.
12. J. Wouters, C. M. Grzywacz and A. Claro, *Stud. Conserv.*, 2011, 56, 231-249.
13. S. Charters, R. P. Evershed, L. J. Goad, A. Leyden, P. W. Blinkhorn and V. Denham, *Archaeometry*, 1993, 35, 211-223.
14. K. L. Olson and S. J. Swarin, *Abstr Pap Am Chem S*, 1985, 189, 85-Anyl.

15. H. Barnard, A. N. Dooley, G. Areshian, B. Gasparyan and K. F. Faull, *J Archaeol Sci*, 2011, 38, 977-984.
16. W. C. McCrone, *Journal of the International Institute for Conservation (J.IIC-CG)*, 1982, 7, 11-34.
17. J. Riederer, *Hyperfine Interact*, 2004, 154, 143-158.
18. M. Toffolo, A. M. Maeir, J. R. Chadwick and E. Boaretto, *Radiocarbon*, 2012, 54, 371-390.
19. L. M. Shillito, M. J. Almond, K. Wicks, L. J. R. Marshall and W. Matthews, *Spectrochim Acta A*, 2009, 72, 120-125.
20. S. Prati, E. Joseph, G. Sciutto and R. Mazzeo, *Acc. Chem. Res.*, 2010, 43, 792-801.
21. E. Joseph, S. Prati, G. Sciutto, M. Ioele, P. Santopadre and R. Mazzeo, *Anal. Bioanal. Chem.*, 2010, 396, 899-910.
22. P. Nel, C. Lonetti, D. Lau, K. Tam, A. Sagona and R. S. Sloggett, *Vib Spectrosc*, 2010, 53, 64-70.
23. S. M. Rafferty, *British Archaeological Reports International Series*, 2007, 1650, 179-180.
24. E. A. Reber and M. T. Kerr, *J Archaeol Sci*, 2012, 39, 2312-2319.
25. N. Ogata, *Lowland Maya Area: Three Millennia at the Human-Wildland Interface*, 2003, 415-438.
26. W. J. Hurst, R. A. Martin, S. M. Tarka and G. D. Hall, *J Chromatogr*, 1989, 466, 279-289.
27. T. G. Powis, A. Cyphers, N. W. Gaikwad, L. Grivetti and K. Cheong, *P Natl Acad Sci USA*, 2011, 108, 8595-8600.

28. J. S. Henderson, R. A. Joyce, G. R. Hall, W. J. Hurst and P. E. McGovern, *P Natl Acad Sci USA*, 2007, 104, 18937-18940.
29. A. L. Edwards and B. C. Bennett, *Econ Bot*, 2005, 59, 275-285.
30. D. K. Washburn, W. N. Washburn and P. A. Shipkova, *J Archaeol Sci*, 2011, 38, 1634-1640.
31. D. K. Washburn, W. N. Washburn, P. A. Shipkova and M. A. Pelleymounter, *J Archaeol Sci*, 2014, 50, 191-207.
32. A. D. Meinhart, C. S. Bizzotto, C. A. Ballus, A. C. P. Rybka, M. R. Sobrinho, R. S. Cerro-Quintana, J. Teixeira and H. T. Godoy, *J Agr Food Chem*, 2010, 58, 2188-2193.
33. F. H. Reginatto, M. L. Athayde, G. Gosmann and E. P. Schenkel, *J Brazil Chem Soc*, 1999, 10, 443-446.
34. H. Ashihara, T. Yokota and A. Crozier, *Adv Bot Res*, 2013, 68, 111-138.
35. G. Pereira-Caro, G. Borges, C. Nagai, M. C. Jackson, T. Yokota, A. Crozier and H. Ashihara, *J Agr Food Chem*, 2013, 61, 427-434.
36. C. I. Heck and E. G. De Mejia, *J Food Sci*, 2007, 72, R138-R151.
37. C. M. Pagliosa, M. A. Vieira, R. Podesta, M. Maraschin, A. L. B. Zeni, E. R. Amante and R. D. D. C. Amboni, *Food Chem*, 2010, 122, 173-178.
38. A. R. Henman, *J Ethnopharmacol*, 1982, 6, 311-338.
39. C. S. Weckerle, M. A. Stutz and T. W. Baumann, *Phytochemistry*, 2003, 64, 735-742.
40. T. W. Baumann, B. H. Schulthess and K. Hanni, *Phytochemistry*, 1995, 39, 1063-&.
41. A. Ford and S. Fedick, *J Field Archaeol*, 1992, 19, 35-49.

42. M. P. Callahan, Z. Gengeliczki, N. Svadlenak, H. Valdes, P. Hobza and M. S. de Vries, *Phys Chem Chem Phys*, 2008, 10, 2819-2826.